Low Power Wireless Sensor Applications

Yuen Chi Lap

A Thesis Submitted in Partial Fulfillment
of the Requirements for the Degree of
Master of Philosophy
in
Department of Computer Science & Engineering

June, 2004

Low Power Wireless Sensor Applications

submitted by

Yuen Chi Lap

for the degree of Master of Philosophy
at the Chinese University of Hong Hong

Abstract

Energy harvesting is becoming a popular technique for pervasive computing. It is possible to extract ambient power from sunshine, wind, waves, vibrations, etc. Although vibrational to electrical power conversion is a well-studied topic, recent advances in low power electronics make it possible to miniaturize vibration powered systems to sizes that were previously intractable.

In this work, two key areas related to vibration powered systems were studied, namely improving the efficiency of the energy conversion process, and the development of applications which can use this type of energy source.

A micro power generator (MPG) resulted in this project generates 120 μW with maximum output voltage 2.4 V. A voltage multiplier (part of the power management circuit) incorporated in the MPG was estimated to be 53 % efficient for input power around 100 μW. The converted energy is stored in storage capacitor (1 mF) and can be used as required.

A long-term temperature monitoring system was implemented. In this system, data is transmitted via radio frequency to a host computer. The time taken for one temperature measurement is roughly 1.4 s and the system energy consumption was 212.62 μJ. For first time activation, the MPG takes 32 seconds to produce sufficient energy to drive the wireless RF thermometer with input acceleration 4.63 m/s^2 and frequency 80 Hz. 18 seconds are required

for later measurements.

A battery powered 2D input ring was also implemented. It illustrated how one could control electronic devices using finger motion and wireless technology. Based on this technology, gesture-based inputs from a small wearable device can be used to control almost any electronic system including computers, portable digital assistants (PDAs), mobile phones, televisions and air conditioners. Future research could lead to vibration based versions of this ring.

低功率無線傳感器應用

袁志立

香港中文大學
計算機科學與工程學課程
哲學碩士論文

2004年6月

摘要

能量收集是瀰漫計算中一項普遍的技術。這項技術可於四周環境中，如：陽光、風力、海浪、震動等提取能量。雖然，把震動力轉換成電能已是廣泛研習的課題，但是在如何縮小震動力發電系統的題目上，一直沒有方案。然而，除著近期低功耗電子學的發展，以上問題可望解決。

本文對於震動力發電系統研習了兩個主要的地方，即改進能量轉換過程的效率和發展應用這類型能源的用途。

在計畫中，我們製成了一台微型發電機 (MPG)，它能產生 120微瓦 電力，最大輸出電壓爲 2.4伏特。這個微型發電機拼入了一個電壓增益器(電力管理電路的一部份)。當輸入能量爲 100微瓦 時，此電壓增益器的效能爲 53%。而轉換所得的能量均存於存貯電容器 (1毫法拉)，以供有需要時使用。

我們實現了一個長時期溫度監測系統作爲微型發電機的應用例子。這個系統透過射頻傳送數據到主計算機。單一次的測量，系統耗時約 1.4秒 ，耗電 212.62微焦耳。在輸入加速率爲 每平方秒4.63米 與輸入頻率爲 80赫茲 下，微型發電機首次啓動耗時 32秒，用以產生足夠能量來推動無線射頻溫度計。其後每次激活間距爲 18秒。

我們亦實現了一個電池推動的二維空間輸入指環。它說明了如何利用手指的動作和無線技術來操控電子裝置。基於此項技術，一個細小、可佩帶的裝置能夠透過手的姿勢與動作來操控大部份的電子裝置，包括：電子計算機、便攜式數字助理 (PDAs)、流動電話、電視和空氣調節器。未來的研究將可達成以震動力推動的輸入指環。

Acknowledgments

This thesis would not be completed without the help of many people.

I would like to thank my final year project and Master Degree supervisor, Professor Leong Heng Wai Philip, for his guidance in the past three years. He provided me valuable ideas for my research work and led me to finish the ITF micro power generator (MPG) project.

I would like to thank Professor Li Wen Jung who is the PI of ITF micro power generator project which provided me the RA position for the past two years. A number of discussions with him led me towards new and successful applications for MPG project.

I would like to thank Professor Lee Kin Hong, Professor Young Fung Yu Evangeline and Prof David Levy for suggestions and comments for improving this work.

I would like to thank Mr Lee Ming Ho for providing the micro power transducers and their experimental results.

I would like to thank Mr Lam Hiu Fung for sharing idea on the prototpye of the 2D input ring.

I would like to thank Gerry for providing idea on RF measurement.

I would like to thank Mr Wong Ming Yee and Mr Ma Chung King for technical support.

I would like to thank my colleages, Mr Sham Chi Wing, Mr Cheung Yu Hoi, Mr Tsoi Kuen Hung, Mr Lam Yuet Ming, Mr Ho Chun Hok, Mr Wu Fei, Mr Yu Chiu Man, Mr Tong Ka Yau, Miss Lam Ka Man, Miss Li Xiao

Qi and Miss Jiang Ming Fei for their support to my research and bring me a comfortable working atmosphere.

Last but no means least, I thank my parents and Sammi for their love and care.

Contents

List of Figures

List of Tables

Chapter 1

Introduction

1.1 Motivation

Energy can be scavenged from vibrations.

Most modern portable electronic devices are powered by electrochemical batteries which require replacement or charging once consumed. Obviously, alternative non-exhaustive power sources would be more convenient. Vibrational energy is an option which is readily available. However, mechanical energy (from vibrations) has not been often used since the power which can be generated from a miniature vibration-based generator is very small. Improvements in integrated circuit technology has been steadily reducing the power consumption required by portable systems and miniaturized vibrational powered systems are now a reality.

Self-powered wireless sensors are poised to have a very important role in the future. Engineers can attach them to the building to test their structural behavior (such as bridge) under vibrations caused by strong wind or earthquake [4]. Scientists can monitor plants, trees and animals to better understand their physiology. The sensor can report real-time information, even in dangerous environments.

Sensor networks can improve living standards and life style.

With the system-on-chip technology and MEMS processes, an integrated circuit which is self-powered by vibrations for controlling smart appliances wirelessly can be fit into a very small volume, such as a ring. Wearing the device, people can record their habits and interact with other computerized devices more conveniently. If a large group of sensors are used to form an ad hoc network at home, they can be embedded in the furniture and under the floor to observe their activities, which can be used to monitor the elderly [28]. It is very likely that sensor networks will become as common as the Internet today.

1.2 Aims

The objective of this research was to develop low power sensor applications which can be powered by batteries or non-exhaustive sources, since information from the environment and transmit the data via a wireless communications link. Therefore, the sensor applications developed under our scheme have small geometries, wireless communication ability and long operating time with single or no battery. The detailed research aims were:

- Develop a generic platform (GP) which combines sensors and wireless transmission and can be used for both battery sources and vibration powered sources. For long-term monitoring, the scientists, based on GP, can design its own applications without the knowledge of low power integrated circuit design.

- Optimize the electronics for a miniature, vibration-to-electrical power transducer. Although it does not need to be recharged, the power output of the transducer is extremely low and unable to directly drive off-the-shelf circuits.

- Develop an application which uses both the vibration-based generator (VBG) and GP to implement a wireless temperature monitoring system. This illustrates how to integrate an application circuit with a power generator and provides a functional test for the VBG.

- Develop a wireless ring input device which can be used as a general computer interface. In this system, a battery power is used. It illustrates GP can be applied to other power sources. Also, the wireless ring input device can be applied to stroke or gesture recognition which introduces a novel communication interface between human and the electronics.

1.3 Contributions

The main contributions of this dissertation are as follows:

- The issue of developing the power conversion circuitry for an AA-sized micro power generator was considered. As the size of a micro power generator (MPG) is reduced, it is a challenge to develop power management circuit with trade-offs between size, static power consumption and efficiency. An optimized power management circuit was designed and implemented. This involved step-up conversion of the AC micro power transducer (MPT) [1] circuit to a DC value, a startup circuit and a thorough analysis of the efficiency of the design. To the best of author's knowledge, this is the first practical AA-sized MPG with DC output.

- A generic low power wireless sensor platform (GLPWSP) which can be used for a wide range of applications was developed. Applications derived from GLPWSP inherits all its nice features: low power, wireless

[1] The MPT was developed by Johnny Ming Ho Lee, Neil N. H. Ching and Dr. Wen J. Li from the ACAE department of the Chinese University of Hong Kong.

connectivity, ease integration with sensors, high signal processing power and long period self timing.

- A completely self powered wireless thermometer system was developed and it is the first such work (self powered and start-up system) reported.
- A battery powered 2D input ring, based on GLPWSP, was implemented. This ring was designed to control personal computer and appliances. It has an IrDA transceiver which can communicate with most of portable consumer electronics, such as portable digital assistant (PDA), Hi-Fi, etc. The 2D input ring can emulate the computer mouse via an RF link as well as control a camera. This application demonstrates an example of a new application which is made possible by low power wireless sensor systems and to the best of the author's knowledge, is the first example of a ring based generic input device with no moving parts.

1.4 Thesis Organization

In chapter 2, a review of related work on vibration-to-electrical conversion and sensor circuits is given. Chapter 3 introduces the power management circuit for the micro power generator (MPG) and chapter 4 presents the architecture of the generic low power wireless sensor platform and the operational details of the startup module. In chapter 5 a practical micro power generator application, namely an RF temperature sensor is presented. In chapter 6, a battery powered 2D input ring is presented to demonstrate a novel input method which uses finger motion. Finally, the conclusion and suggestions for future work are presented in chapter 7.

Chapter 2

Background and Literature Review

2.1 Introduction

Energy enables bodies to do work and energy conversions occur around us every day. Humans intake food to gain power to move and work. This is a living example of how chemical energy (in food) can be converted to mechanical energy (movement).

Energy can be classified into renewable and non-renewable sources. Non-renewable energy sources include crude oil, coal, natural gas and nuclear. Once consumed, the resulting work products are discarded. Portable electronics, such as mobile phone, PDAs, etc., are powered by electrochemical batteries. An electrochemical battery is a non-renewable power source, requiring recharging or replacement when exhausted. Renewable energy sources include solar energy, tidal energy, wind energy, etc. This chapter aims to give readers some background information on power sources which are commonly used for sensor systems or portable electronics. A review of previous wireless sensor systems will also be given.

2.2 Vibration-to-Electrical Transducer

Thanks to advances in silicon fabrication process and System-on-Chip (SoC) technology, modern electronic appliances are getting smaller, requires less power, yet achieve greater functionality. Most of them are directly powered by electrochemical cells. Electrochemical cells have the advantages of high energy capacity, are able to provide large instantaneous output current, yet have a compact size. However, batteries are not the ideal power source for long term monitoring applications because they require replacement. Turning ambient vibrational energy into electrical energy is an alternative renewable power source. Vibration-to-electrical converting methods can be classified into three categories [40]: electromagnetic (inductive), electrostatic (capacitive), and piezoelectric. Challenges for designing vibration-to-electrical transducer are to:

1. model the methodology mathematically and optimize the model by simulation; fortunately, Mitechson et al. [27] discuss the architectures for vibration-driven micropower generators, including detailed mathematical modelling.

2. improve the efficiency of the energy conversion.

3. convert AC power to DC power as electronic components normally operate on DC.

Those converting methodologies will be reviewed in this section. AC to DC and DC to DC power conversion techniques will be explained in section 4.2.1.

2.2.1 Electromagnetic (Inductive) Power Conversion

Electromagnetic power conversion is the most well-known method which generates power using a spring, coil and a magnet. Its principle comes from Faraday's law: when the coils cut the magnet's field, an AC current is induced.

A mathematical model was constructed to model electromagnetic conversion system by Williams et al [55]. A simplified version is presented in chapter 3.

Several research groups [55, 2] have developed electromagnetic converters. Williams [55] developed a general second order linear model. He also developed an electromagnetic generator which was 1 mm thick, and thus the power density of the system was $10 - 15\ \mu W/cm^3$. However, Roundy [40] criticized that the output voltage and current for that device were too low to be rectified because its output voltage was much lower than a diode's forward bias voltage.

Amirtharajah and Chandrakasan [2] designed an electromagnetic converter. The electromagnetic converter was designed for vibrations generated by a person walking, using a vibration magnitude of about 2 cm at about 2 Hz. The maximum system output power was reported to be 400 μW with measured voltage output of 180 mV. Its size was 4 $cm \times 4\ cm \times 10\ cm$ and the power density was 2.5 $\mu W/cm^3$.

Li et al [31] developed methods to improve the efficiency of springs for vibrational-to-electrical transducers. The main idea is to control the spiral, thickness and nature of materials for the spring, so that the quality factor Q of spring is optimized (becomes sharp) at particular frequencies. Therefore, at the desired frequency, the spring is resonant and it converts most of energy from vibration to electrical form. In 2000, Li et al [24] had demonstrated a magnet-based generator with total volume of 4.7 cm^3 which was able to drive an off-the-shelf circuit from vibrations with amplitude $\sim 150\ \mu m$ and frequency 105 Hz. Its power output was measured as 830 μW and its power density was calculated as 176.59 $\mu W/cm^3$.

2.2.2 Electrostatic(Capacitive) Power Conversion

Others have proposed to generate power from two precharged metal plates under vibration. The simple circuit in figure 2.1 illustrates the idea of electrostatic power conversion. When two precharged metal plates are separated by distance d, they form a capacitor. The voltage, capacitance and energy stored at the capacitor are given by equations 2.1.

$$\begin{aligned} V &= \frac{Qd}{\varepsilon_0 lw} \\ C &= \frac{Q}{V} \\ E &= \frac{Q^2}{2C} \end{aligned} \tag{2.1}$$

where Q is the charge on the plates, V is the voltage across the capacitor, E is the stored energy at capacitor, l is the length of the plate, w is the width of the plate, and ε_0 is the dielectric constant of free space. Imagine that two metal plates are vibrated by external force (separation d varies), the voltage across two metal plates varies if the plates' charges are kept constant. If the voltage across output capacitor and vibrated capacitor are the same initially, the voltage across the output capacitor will be charged to the maximum voltage output of the vibrated capacitor (assuming an ideal diode). Therefore, the vibrational energy is converted to energy stored on the output capacitor.

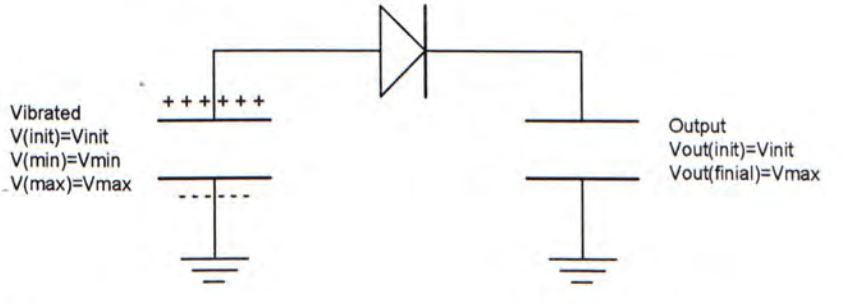

Figure 2.1: A simple circuit illustrates the idea of electrostatic power conversion [40].

Meninger et al [25] proposed to fabricate two comb-like metal plates inside

a chip. For first time usage, metal plates are precharged. AC current is induced during vibration. The predicted power output was 8.6 μW for volume of 1.5 $cm \times 0.5\ cm \times 1\ mm$ from a vibration source at 2.52 kHz, giving a predicted power density of 114.6 $\mu W/cm^3$.

Roundy [40] reported a macro-scale electrostatic converter was as shown in figure 2.2. At an operation frequency of 100 Hz, the output power was measured to be 1 nW for a 9 V DC source which was used to maintain the charges on the plates.

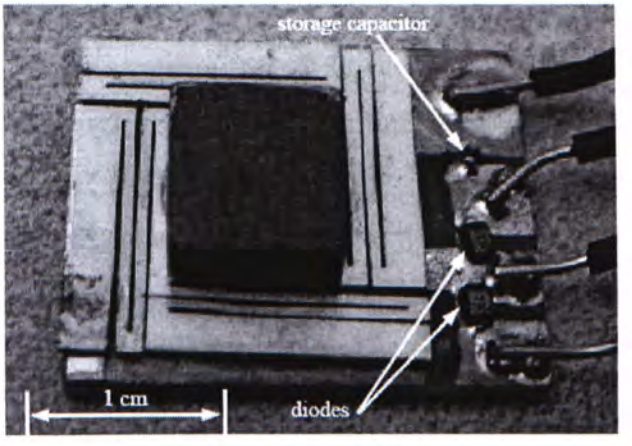

Figure 2.2: Photograph of Roundy's macro-scale electrostatic converter [40]. Photo courtesy of Shad Roundy

2.2.3 Piezoelectric Power Conversion

Piezoelectric material, ie. polycrystalline ceramic can produce electrical charges when mechanically deformed. The material is processed in a large electrical field which orients its crystalline structure in the direction of the external field. The processed polycrystalline ceramic can vary its voltage if it is elongated or compressed by an external force. The equations for a piezoelectric materials are given in equations 2.2.

$$\begin{aligned} \delta &= \frac{\sigma}{Y} + dE \\ D &= \varepsilon E + d\sigma \end{aligned} \tag{2.2}$$

where δ is mechanical strain, σ is mechanical stress, Y is the modulus of elasticity (Young's Modulus), d is the piezoelectric strain coefficient, E is the electric field, D is the electrical displacement (charge density), ε is the dielectric constant of the piezoelectric material.

Roundy [40] implemented three piezoelectric generators. Two are shown in figures 2.3 (Roundy's design 1) and 2.4 (Roundy's design 3). For input vibration at $85Hz$ and 2.25 m/s^2, the maximum power output was reported as 207 μW and 90 μW for a resistive load and capacitive load respectively. Roundy's design 1 was regulated by a piezoelectric circuit (shown in figure 2.5) to power a wireless transmitter at 1% duty cycle. The piezoelectric circuit contains a full-wave rectifier and a inductor-based step-down regulator. The full-wave rectifier changes the AC input to DC ($2 - 12$ V). Then the rectified input is down converted to 1.5 V or 3 V DC by a switch mode regulator. Roundy's design 3 was a large version of design 1. Its maximum power output was measured to be 1700 μW. It was tested to drive the MICA node shown in figure 2.6. The maximum demonstrated power densities of Roundy's piezoelectric generators were 207 $\mu W/cm^3$ and 335 $\mu W/cm^3$ for design 1 and design 3 respectively.

Figure 2.3: Photograph of Roundy's piezoelectric generator (Design 1) [40]. Photo courtesy of Shad Roundy

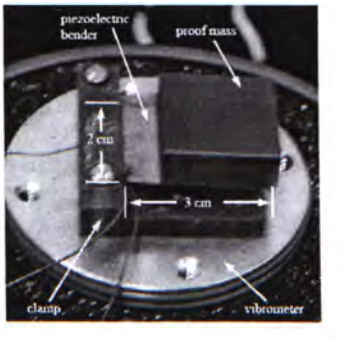

Figure 2.4: Photograph of Roundy's piezoelectric generator (Design 3) [40]. Photo courtesy of Shad Roundy

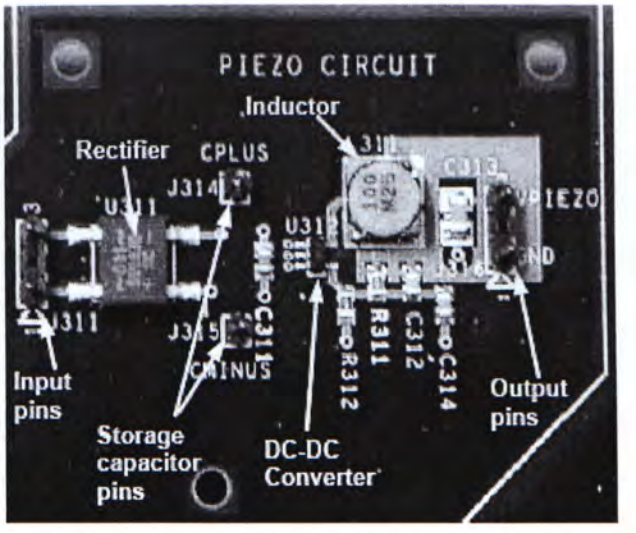

Figure 2.5: Photograph of power circuit of piezoelectric generator [40]. Photo courtesy of Shad Roundy

2.3 Wireless Sensor Platform Examples

2.3.1 MICA[13] from UC Berkeley[49]

Hill and Culler reported a wireless platform for deeply embedded networks called MICA. MICA is a small and low-cost wireless sensor. It consists of a TR1000 radio transceiver, ATEMGA 103 microcontroller, FPGA hardware accelerators, DS2401 unique ID tag, 4-Mbit flash and a power regulator MAX1678. The photograph and block diagram of MICA node are shown in figures 2.6 and 2.7 respectively. The MICA node is controlled by a software operating system, TinyOS [50], designed for networked sensor applications. The operation of a MICA is as follows: For power saving, MICA activates itself every five minutes (programmable). It then measures the environment via its sensor. A MICA node has an analog-to-digital converter (ADC), for interface to the sensor. MICA has a microcontroller as well as a control unit and a hardware FPGA accelerator which can be programmed to do any kind of digital signal processing to process the input data. The RF transceiver provides a wireless medium to communicate with other nodes in an ad hoc networking manner.

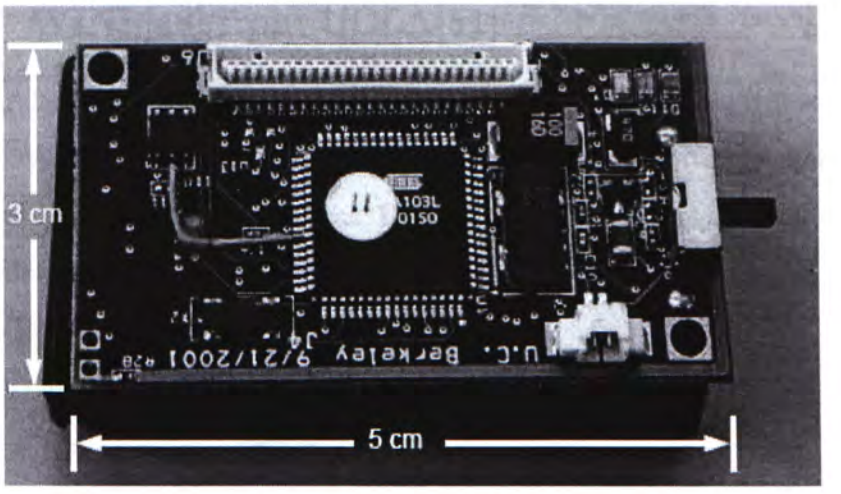

Figure 2.6: Photograph of MICA node [40]

The developers of the MICA system had put the whole system into an ASIC to further reduce the size and power.

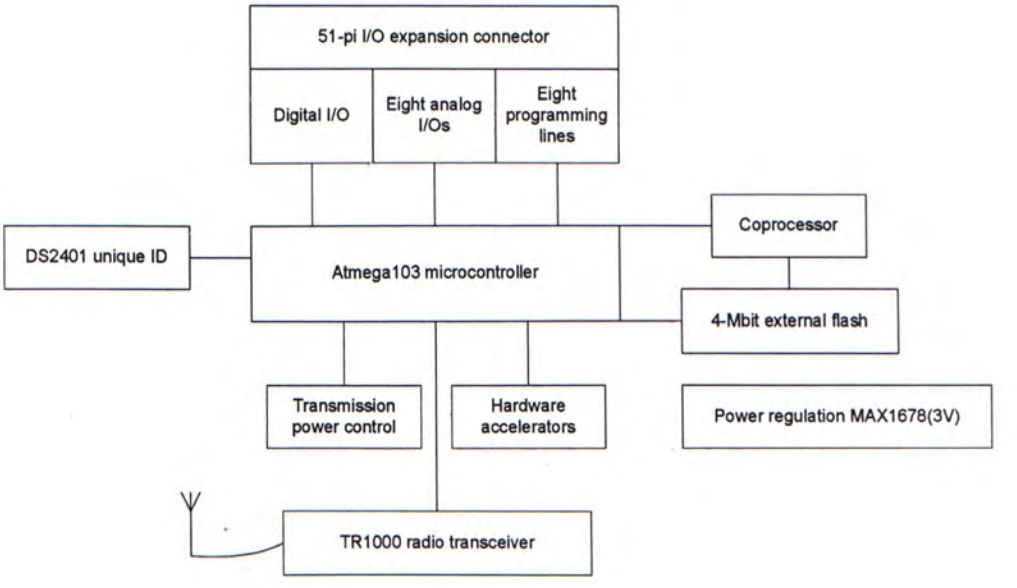

Figure 2.7: Block diagram of MICA node [13]

2.3.2 WINS[48] from UCLA[51]

The Wireless Integrated Network Sensors (WINS) project started at UCLA in 1993. WINS is an ASIC version of MICA without operating system. The measured power consumption was 110 μA with 3 V supply and multi-hop communication. Figure 2.8 shows WINS node architecture. The size of chip was 2160×2554 μm^2 in a 0.6 μm CMOS process [54].

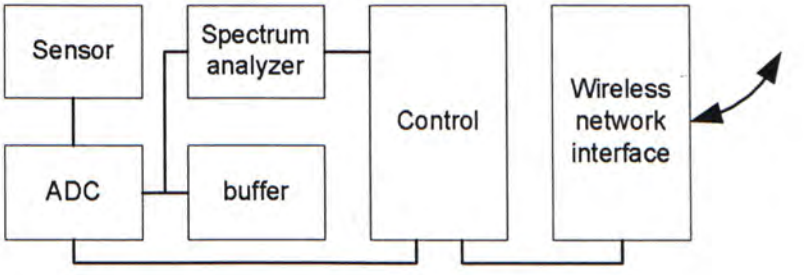

Figure 2.8: WINS node architecture [48]

2.3.3 Wong's Infrared System[5]

An external-triggered infrared system developed at the Chinese University of Hong Kong used a quadrupler circuit as the voltage step up circuit for the micro-power generator mentioned before. An infrared temperature sensor application was also implemented to evaluate the performance of the micro-power generator. The schematic diagram of infrared sensor system is shown on figure 2.9. It consists of a quadrupler, an IR transmitter SM5021 [16], a microcontroller SX28 [47] and a temperature sensor DS1620 [43]. The circuit was verified to operate correctly at 1.8 V. Since the average output of micro-power generator was about 400 μW, it could not directly power the system. The generator was first used to charge up a 1.2 mF capacitor, which in turn was used to power the IR transmitter. An IR signal could be sent to receiver every time a key was pressed. The signal was a 140.8 ms IR pulse train. For a 2.0 V power supply, the current drawn during a key press was measured to

be 1.5 mA and, in standby mode, 2.4 μA. 58 s was taken to charge up the capacitor for the first activation, and 30 s was required to recharge the system in subsequent activations.

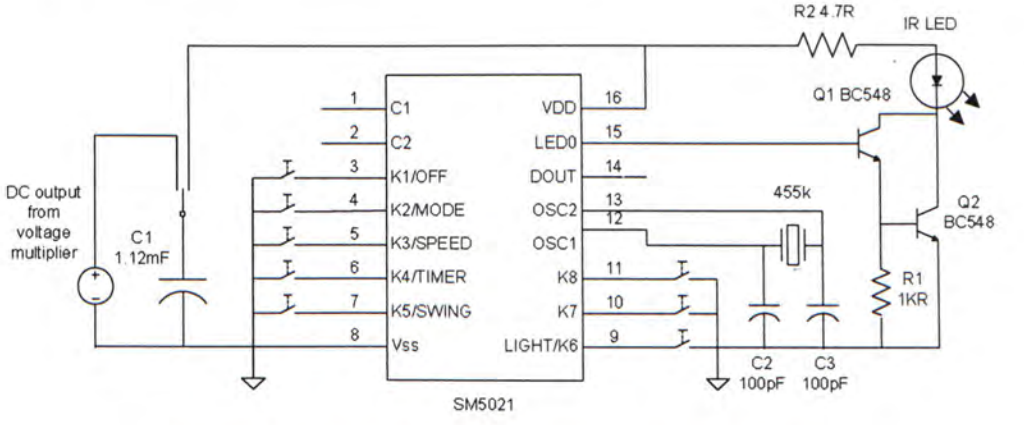

Figure 2.9: Wong's Infrared system block diagram [5]

2.4 Summary

In this chapter, vibrational-to-electrical conversion methodologies and some low power wireless sensor platforms were covered. They are divided into three categories: electromagnetic, electrostatic and piezoelectric. For electrostatic conversion, Meninger et al created a SoC solution with simulated power density of 114.6 $\mu W/cm^3$. Li et al implemented an electromagnetic generator which was able to drive a thermometer circuit with infrared transmission link. Its measured power density was 176.59 $\mu W/cm^3$. Roundy [40] demonstrated a piezoelectric generator with power density of 207 $\mu W/cm^3$ which was able to power a 1.5 V wireless transmitter, and thus, this generator has the highest rating on power density.

For low power wireless sensors, MICA [13] and WINS [48] both are well-known. MICA designed by UC Berkeley, is a commercial sensor node which can form a multi-hop network to monitor a region. It was estimated to have

a 10 years battery life using with 2 AA-size alkaline batteries. MICA has an component-based operating system which reduces the code size and software development time. WINS designed by UCLA, is like an ASIC version of MICA without operating system. It was measured to consume 110 μA at 3 V supply.

Chapter 3

Micro Power Generator

3.1 Introduction

In this chapter, AA-size Micro Power Generator (MPG) is presented. The information provided is a summary of two papers co-published by the ACAE [29] and CSE [30] departments of the Chinese University of Hong Kong (CUHK). Interested parties should refer to the original references [23, 5].

The AA-size MPG consists of a tripler and two Micro Power Transducers (MPT). Both MPTs can be connected in series or in parallel. To provide large drive current, MPTs should be connected in parallel, otherwise, serial connection would give higher output voltage. The MPT is the key component to convert ambient mechanical energy (from vibration) into electrical energy. It consists of an inner housing, a MEMS spring with designable spring constant k, a $N45$ grading rare earth permanent magnet which has mass m and magnetic field strength B, copper coil of length l. The inner housing is to secure the spring with magnet attached on. In figure 3.1, the illustrative drawing shows the orientation of outer and inner housing, magnet and the resonating spring of MPT.

MPT generates AC power when the whole system is vibrated. When the generator housing is vibrated with an amplitude Y_t, the magnet will then vibrate with an amplitude Z_t. This relative movement causes magnetic flux to

cut through the coil. According to Faraday's law of electromagnetic induction, voltage is induced in the loop of coil. The average power output P of the vibration-induced power generating system can be derived as 3.1:

$$P = \frac{m\xi_e y_0^2 (\frac{\omega}{\omega_n})^3 \omega^3}{[1-(\frac{\omega}{\omega_n})^2]^2 + (2\xi\frac{\omega}{\omega_n})^2} \tag{3.1}$$

where ξ_e is the electrical damping factor, Y_0 is the input vibration amplitude, ω is the input vibration angular frequency, ω_n is the resonance frequency of the spring-mass system and ξ is the sum of the electrical and mechanical damping factors of the system. From the equation 3.1, at resonance, the average power and voltage output is maximized:

$$P = \frac{m\xi_e y_0^2 \omega^3}{4\xi^2} \tag{3.2}$$

$$V = \frac{BlY_0\omega_n}{2\xi} \tag{3.3}$$

According to equations 3.2 and 3.3, both power and voltage output are at maximum when the system is at resonance with maximum amplitude and electrical damping factor.

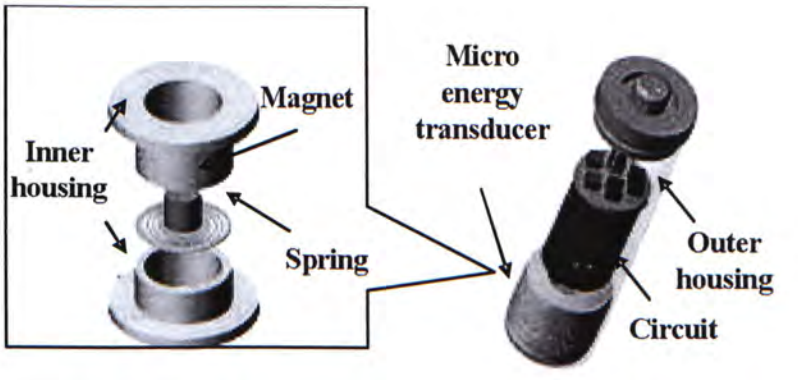

Figure 3.1: Illustrations of: (a) Inner structure of the micro power generator; (b) the AA-size micro power generator which is integrated with a power-management circuit. Photo courtesy of Johnny M. H. Lee

3.2 MEMS Resonator

The key design issue for the MPT is to fabricate a spring with controllable resonance frequency. A variety of materials were studied, and copper found to be the best material for the spring, since it has relatively low Young's modulus and high yield stress compared to silicon. Brass, titanium and 55-Ni-45-Ti may be alternatives for special operating environment. For example, 55-Ni-45-Ti can be used in situations where low resonance frequency is required.

Currently, two MEMS techniques were explored to obtain the spiral resonating spring: *laser-micromachinery* and *lithographic electroplating.*

3.2.1 Laser-machinery

A Q-switch (Nd:YAG 1.06 μm wavelength) laser was used to micromachine the spiral resonating spring. The SEM photo of the resulting spring is shown in figure 3.2. A copper spring with diameter of 8 mm and 0.1 mm thickness was used for first generation of AA-size MPG. Using a laser to cut the spring out from a copper disc provides accurate control of the spiral of the spring. However, the thickness of spring cannot be controlled and the cutting edge is not very smooth as shown in figure 3.2.

3.2.2 Electroplating Fabrication

Instead of shaping the spring with a laser, lithographic techniques can be used to fabricate the spring with controllable spiral dimensions and thickness. A 1 μm thickness can be achieved using this process. The fabrication process is illustrated in figure 3.3. First, a gold layer is put on the substrate. The gold layer acts as a *conducting seed* for the copper ions. Second, lithographic techniques are used to secure a SU-8 negative PR mask on the gold layer. Third, copper is electroplated. Fourth, the spring is separated from the substrate. The springs produced by lithographic electroplating can be thinner with smoother

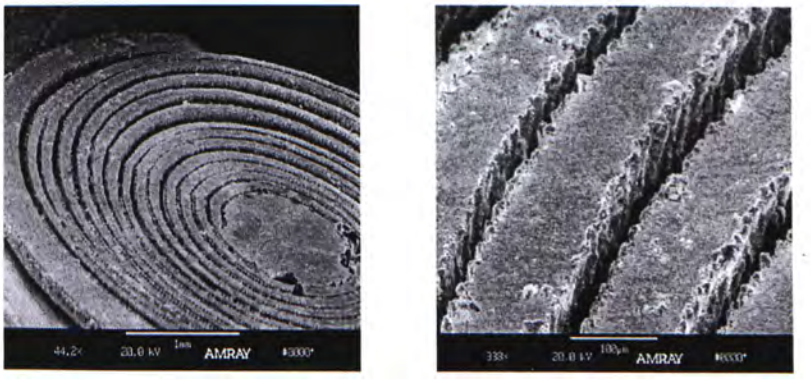

(a) (b)

Figure 3.2: SEM pictures of: (a) a laser-micromachined copper spring with diameter of 5 mm, (b)close-up of the copper spring; width of spring is $\sim$ 100 μm. Photo courtesy of Johnny M. H. Lee.

edges than those produced via laser cutting, resulting in a lower resonance frequency. This process is also more suitable for mass production since many springs can be made in a single batch.

3.3 Voltage Multiplier

The AC output voltage (V_{rms} = 450 mV) supplied by the MPT is not suitable for driving a conventional digital circuit. A Voltage Multiplier (VM) was introduced to step up and rectify the AC output of two MPTs to produce a DC voltage. The circuits shown in figure 3.4 are a voltage doubler, tripler and quadrupler. The output characteristics of a quadrupler compared with a tripler and doubler are shown in figure 3.5. As can be seen, voltage quadrupler is made by cascading two voltage doublers. The principle of the voltage doubler is first explained. The doubler contains two diodes and two capacitors. The number describes a node label eg. $V_{(2,1)}$ means the voltage of capacitor C_1. V_{AC} represents the amplitude of input sine-wave and are two half-wave rectifier circuits in series. Observe its behavior for sine wave input on first stage rectifier. The positive half cycles bring the voltage of node 1

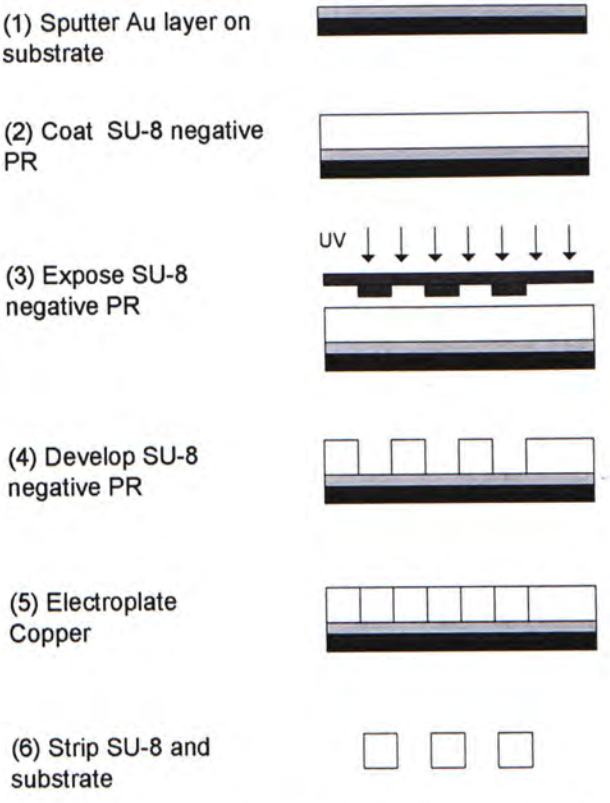

Figure 3.3: Copper spring fabrication process. Photo courtesy of Johnny M. H. Lee

from ground to V_{AC}. The negative half cycles charge up C_1 by introducing current from ground terminal of diode D_1. By superposition, V_2, with respect to ground, is a sine-wave offset to V_{AC}. The second stage rectifies this offset sine-wave. Thus, a doubled output voltage is produced. A voltage quadrupler can be thought as two voltage doublers DB_1 and DB_2. DB_1 doubles the V_{ref} of DB_2 with respect to V_{AC}. Based on V_{ref}, DB_2 quadruples and rectifies the input. The PSpice simulation in figure 3.6 shows that time is required for the voltage multiplier to achieve the final output, mainly due to the charging up time of capacitor C_1 and output capacitor C_3. The prototype circuit was built using KEMET type T491 10 μF, 10 V capacitors and Toshiba 1SS374 silicon epitaxial schottky barrier Type diodes. The 1SS374 diode was chosen as it has relatively low forward voltage (0.23 V) which allows an increase in efficiency of the quadrupler. KEMET T491 tantalum capacitors are used because these

make the rectifying circuit compact and have lower leakage. A capacitor of 1.0 mF is connected with the quadrupler and acts as a reservoir to store the electrical energy generated by the MPG. The reservoir capacitor also acts as a decoupling capacitor to smooth the output of voltage multiplier.

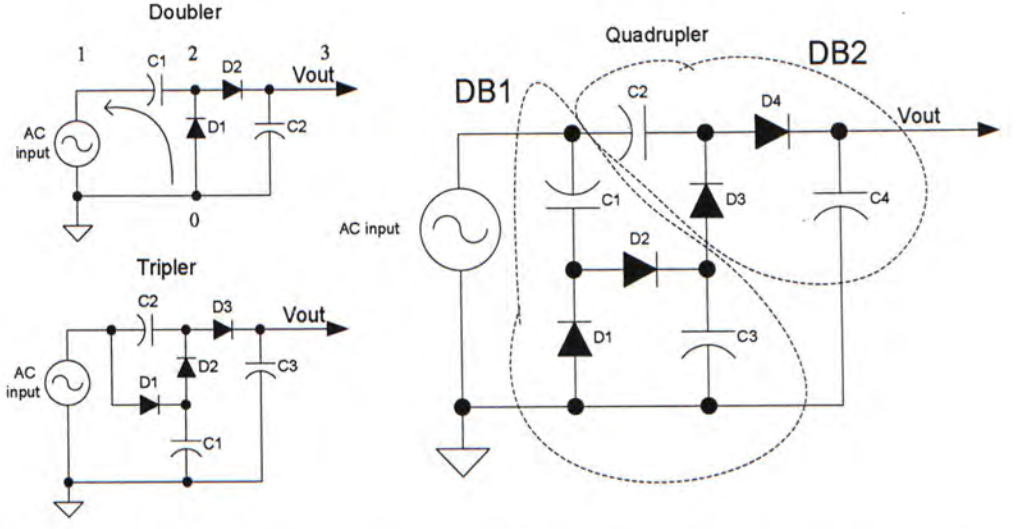

Figure 3.4: The schematics of voltage doubler, tripler and quadrupler [14]

3.4 Modeling, Simulations and Measurements

The micro power generator was integrated as shown in figure 3.9 and tested using a vibration drum (shown in figure 3.8) and signal generator. The input acceleration was measured as 4.63 m/s^2 with an accelerometer attached on vibration drum. Figure 3.10 shows the photo of the MPG. Our MPG weighs 10.5 $gram$ about half the weight of a typical alkaline cell. Two transducers were observed using a stroboscope and oscilloscope. They were vibrated in 3 different modes X, Y and Z. The experiment showed that the spring delivers more energy when the mass experiences translational and rotational vibration, rather than horizontal vibration. It is because the former vibration mode provides higher rate of change in magnetic flux than the latter.

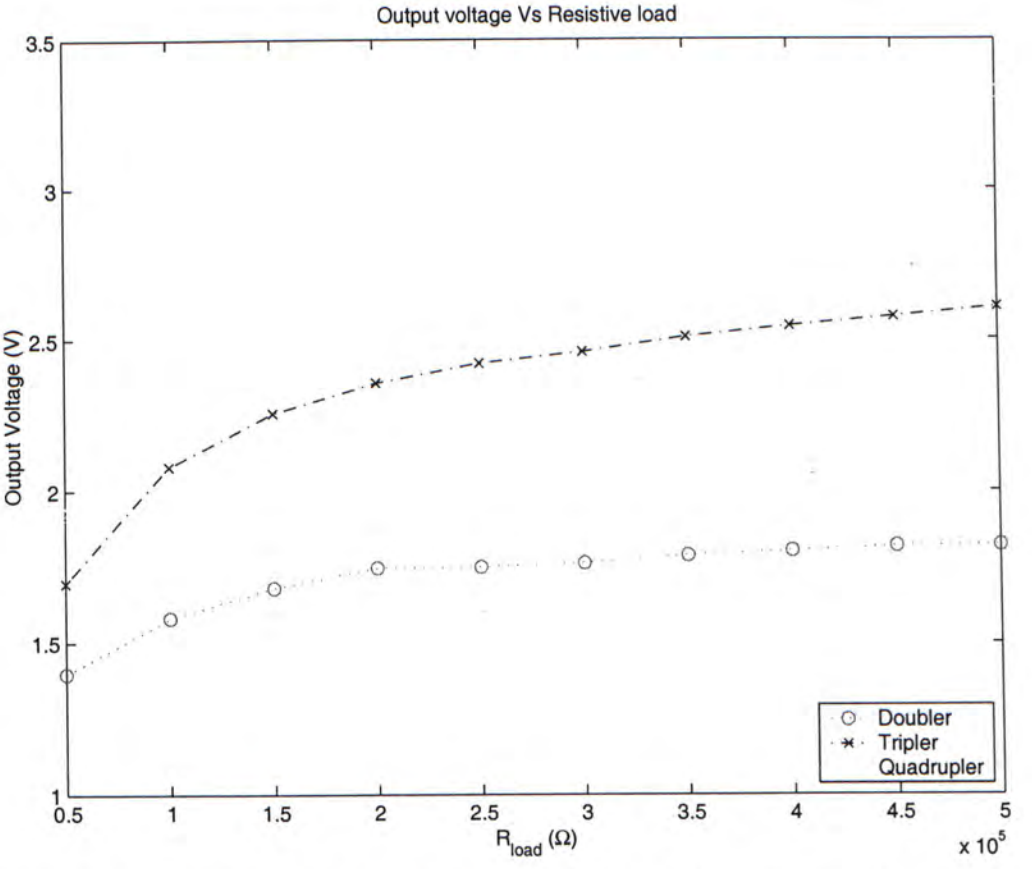

Figure 3.5: The output characteristics for voltage doubler, tripler and quadrupler with different loading (simulated by PSpice, OrCAD)

Two experiments were further set up, in order to determine the characteristics of MPT with voltage multiplier. The experiment apparatus setup is shown in figure 3.7 and the results are shown in figure 3.11 to 3.14. The first experiment collected information which can be modeled the MPTs, so that the PSpice simulation can be applied to judge which voltage multiplier is the best option for MPTs. From figure 3.11, the output power of two coils in series was estimated to be 20 to 120 μW for 1 $k\Omega$ to 30 $k\Omega$ loads. And the power density of two MPTs was estimated as 53.1 $\mu W/cm^3$ (see table 3.1 for comparisons on different V-to-E technologies). For simplicity, two coils were modeled as an AC source with an internal resistance R_{int}, whose value was measured as 1030 Ω (from the curve slope in figure 3.12). Based on this AC model, a number of

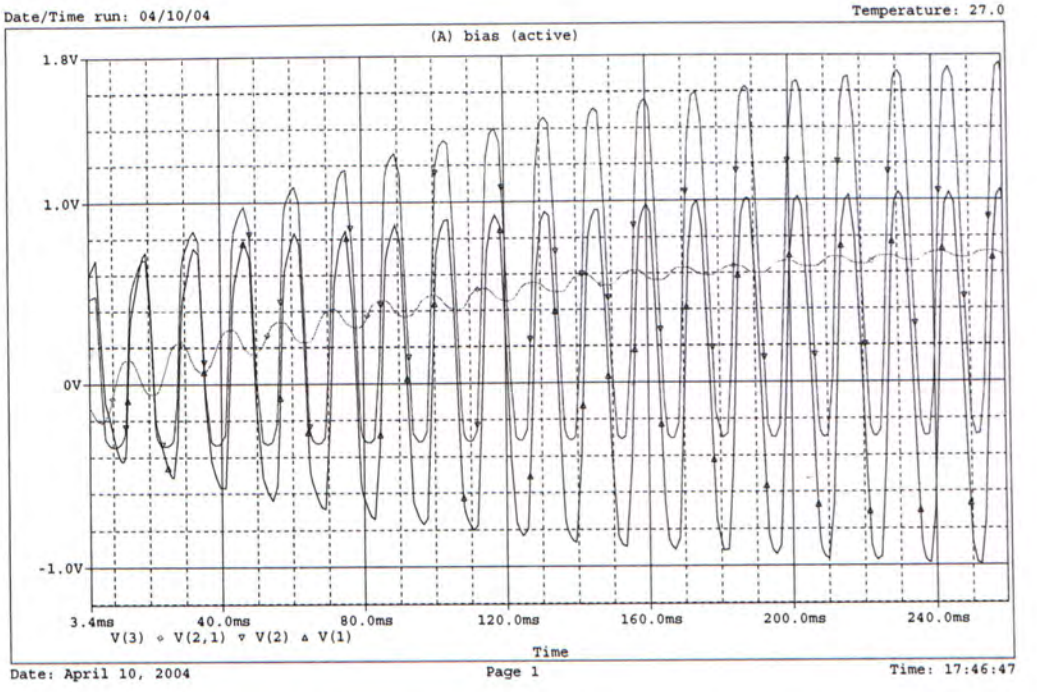

Figure 3.6: PSpice simulation for voltage doubler with $C = 10\ \mu F$ and $R_{load} = 350\ k\Omega$

PSpice simulations were performed on voltage multipliers (doubler, tripler and quadrupler). Tripler was selected from other VMs to test with MPTs since it outperformed others in PSpice simulations. From figure 3.13 and 3.14 show the relationship between power input/output and the input voltage of the tripler.

	Input acceleration (*Ampl.* or *accel.*, f)	Power Output (*Power*, V_{out})	Size (H, (L, W) or D)	Power density ($\mu W/cm^3$)
Williams [55]	-	-	-	$10-15$
Amirtharajah and Chandrakasan [2]	$2\ cm$, $2\ Hz$	$400\ \mu W$, $180\ mV_{rms}$	$4\ cm \times 4\ cm$ $\times 10\ cm$	2.5
Li [24]	$150\ \mu m$, $105\ Hz$	$830\ \mu W$, $1.414\ V_{rms}$	$1.5\ cm$ $\times(1)^2\pi\ cm^2$	176.59
Meninger [25]	- $2.52\ kHz$	$8.6\ \mu W$ -	$1\ mm\times$ $1.5\ cm \times 0.5\ cm$	114.6
Roundy [40] design 1	$2.25\ m/s^2$, $85\ Hz$	$207\ \mu W$ $12\ V_{dc}$	$1\ cm^3$	207
Roundy [40] design 3	$2.25\ m/s^2$, $85\ Hz$	$1700\ \mu W$ $12\ V_{dc}$	$5.1\ cm^3$	335
Two MPTs in series	$4.63\ m/s^2$, $80\ Hz$	$120\ \mu W$ $2.4\ V_{rms}$	$2\ cm\times$ $(0.6)^2\pi\ cm^2$	53

Table 3.1: Comparisons between different vibration-to-electrical transducers

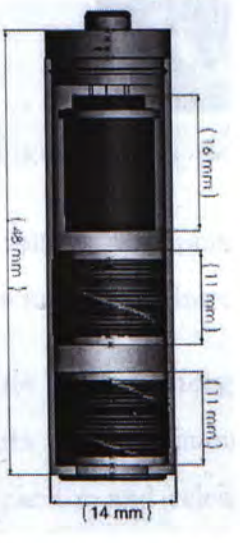

Figure 3.9: Illustrative drawing for micro power generator. Photo courtesy of Johnny M. H. Lee

Figure 3.10: MPG (left) weighs less than the normal AA-size battery (right). Photo courtesy of Johnny M. H. Lee

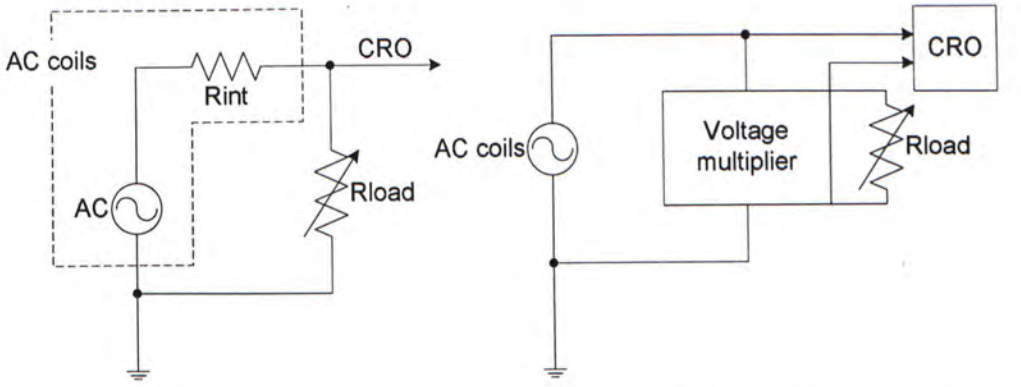

Figure 3.7: The experiment apparatus for measuring MPG coils characteristics.

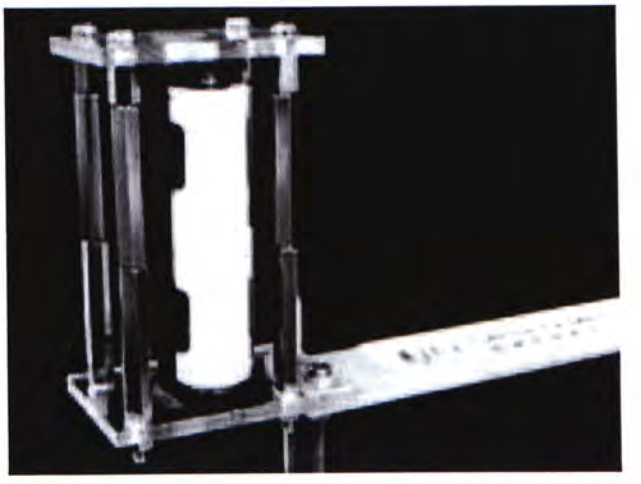

Figure 3.8: Vibration drum. Photo courtesy of Johnny M. H. Lee

The voltage multiplier is a device to convert AC to DC power. Some performance metrics are introduced to quantify the performance of the converters.

Available stored energy The MPG is too weak to power off-the-shelf circuits in a continuous manner. Input energy will be stored in a storage capacitor and released in bursts as required. This method is the so-called Duty Cycle Approach (DCA). The MPG can be applied to any off-the-shelf circuit with startup module (its details are covered in chapter 4). Startup module controls the amount of energy stored in storage capacitor $C_{storage}$ with voltages across $C_{storage}$, $V_{th}(H)$ and $V_{th}(L)$. Available Stored Energy (ASE) is defined as stored energy in capacitor

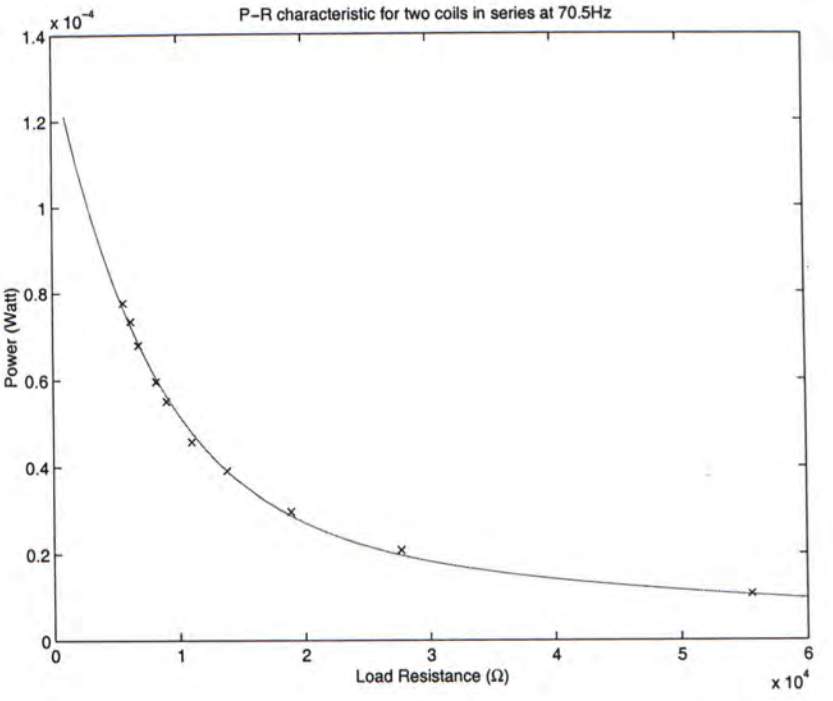

Figure 3.11: Output power versus load resistance for two MPG coils in series stimulated at 70.5Hz

which can be released at once after each charging finished, in the other words, the energy flows into $C_{storage}$ from $V_{storage\ cap} = V_{th}(L)$ rising to $V_{storage\ cap} = V_{th}(H)$. Mathematically, $ASE = \frac{1}{2} \times (V_{th}(H)^2 - V_{th}(L)^2)$.

Startup time (ST) is defined as the elapsed time required to charge the potential of storage capacitor from zero to $V_{th}(H)$ via the MPG.

Recharge time (RT) is defined as the elapsed time required to charge the storage capacitor from $V_{th}(L)$ to $V_{th}(H)$ via the MPG.

Average input power Input Energy (IE) is required to charge $C_{storage}$ from a low threshold voltage $V_{th}(L)$ to a high threshold voltage $V_{th}(H)$. Average Input Power (AIP) is defined as input energy per unit charge time. Mathematically, $AIP = \frac{IE}{RT}$. Higher rating on AIP means poor performance.

Energy efficiency This term is to measure the efficiency of a device from

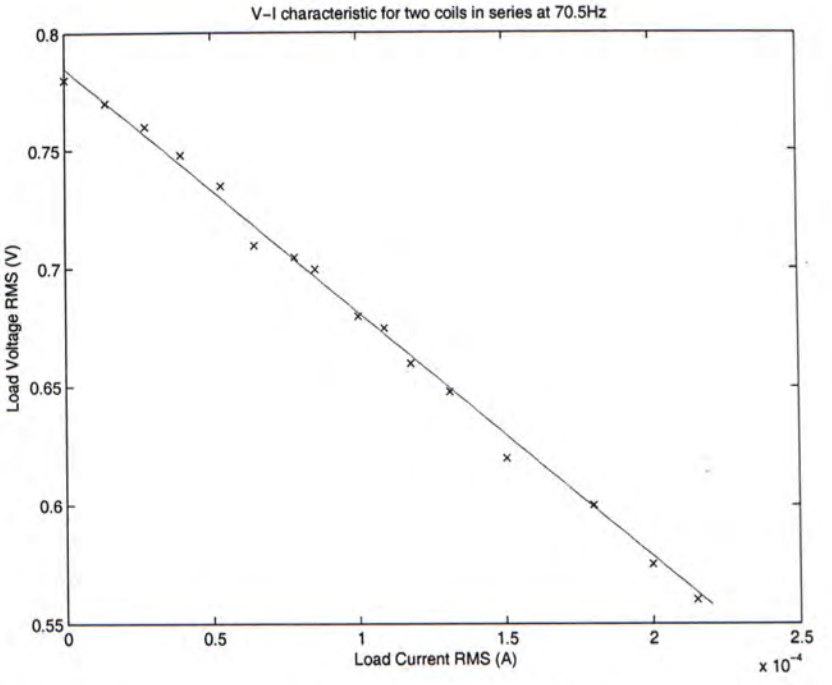

Figure 3.12: Load voltage versus load current for two MPG coils in series stimulated at 70.5Hz

the view of energy. Energy Efficiency (EE) is defined as available stored energy per unit input energy. In mathematically, $EE = \frac{ASE}{IE} \times 100\%$. Higher rating on EE means better performance.

Output load (Capacitive and Resistive) The output of VM will be connected to a storage capacitor and a resistive load. Because the duty cycle approach requires a large storage capacitor, typically 1 mF, so the output capacitance will dominate the resistive load. The resistive load represents the loading from startup module and application circuit in shutdown/sleep mode. Therefore, the resistive loads in the simulations are typically small, in the range of 50 $k\Omega$ to 500 $k\Omega$ (equivalent loading of startup module). Energy dissipated in the resistive load is not considered *useful energy*, so it will not be included to the calculation of output power. The *useful energy* refers to energy stored in capacitor, ASE.

A proposed simulation circuit contained a test VM, a resistor (R_{int}) and

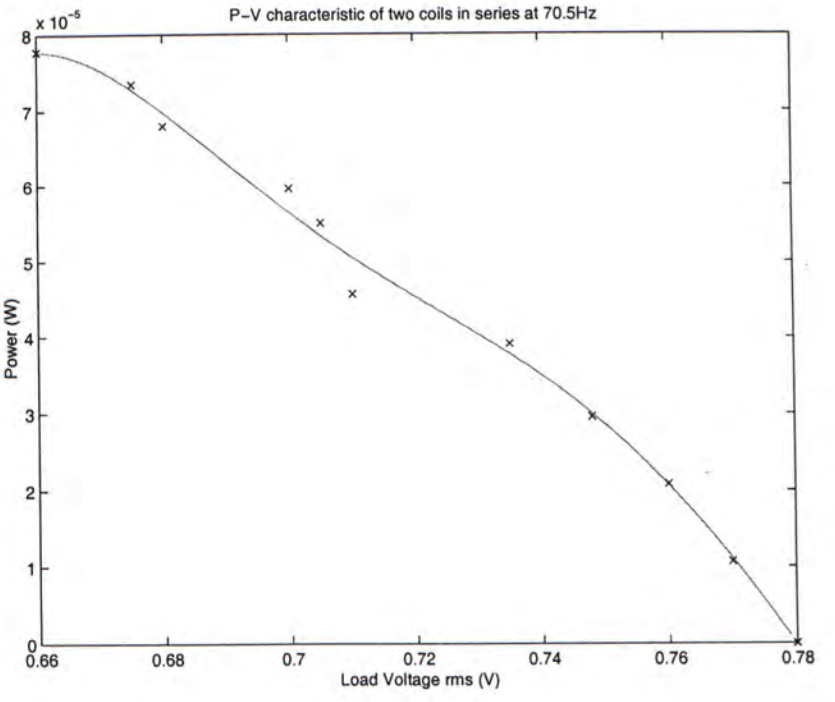

Figure 3.13: Output power versus load voltage of two MPG coils in series stimulated at 70.5Hz

a AC source ($V_{p-p} = 2.4$, $f = 70.6\ Hz$). The storage capacitor of VM is 1 mF. They were connected in series. Three predefined groups of threshold voltages ($V_{th}(L)$, $V_{th}(H)$) and corresponding ASE were used. Table 3.2 shows the relationship between threshold voltages and ASE. The criteria for choosing threshold voltages were based on the minimum input voltage requirement of DC-DC converters and startup module used in proposed low power wireless sensor system in chapter 4. VMs were evaluated with average input power, energy efficiency, startup time and recharge time on different resistive load. The simulation results are shown in figures 3.15 to 3.26. From figures 3.15 to 3.17, low order VM works better than higher order VM in view of the average input power required. A doubler takes less power to store a particular amount of energy than tripler does, and a tripler takes less than a quadrupler. However, a doubler is not able to store energy when the groups' $V_{th}(H) \geq 1.8\ V$ because the output of a loaded ($load > 450\ k\Omega$, the equivalent loading

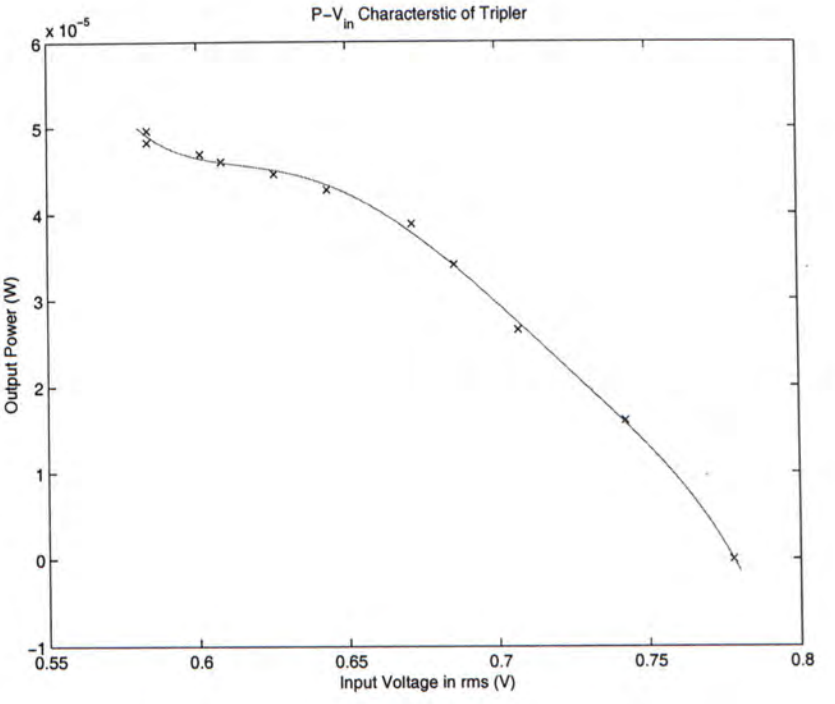

Figure 3.14: Output power versus input voltage of tripler

of our application circuit in standby mode) doubler can't achieve $\geq 1.8\ V$. From figures 3.18 to 3.20, tripler is more efficient than the quadrupler for converting power. From figures 3.21 to 3.26, a tripler takes more time to startup or recharge than a quadrupler generally. Thus a tripler was chosen to be incorporated into the MPG because its overall performance meets the requirements at ($V_{th}(H) = 1.8\ V, V_{th}(L) = 1.4\ V$). Its AIG is around $100\mu Js^{-1}$ which is close to the maximum power output of two MPGs. Also, it got the modest rating at full range of tested load (50 $k\Omega$ to 500 $k\Omega$) for charging voltage level from $V_{th}(L) = 1.4\ V$ to $V_{th}(H) = 1.8\ V$. The comparison of VMs is mainly concentrated on energy efficiency and average input power at charging voltage level ($V_{th}(L) = 1.4, V_{th}(H) = 1.8$) because the minimum switch threshold low for startup circuit is 1.35 V. Energy stored at the capacitor below this voltage can not be used by application circuit directly. The startup time of tripler was estimated to 32 seconds. The recharge time was estimated at 18 seconds, and the energy efficiency was estimated to be 53%, with average input power

$(V_{th}(L), V_{th}(H))$	ASE
$(1.0\ V, 1.4\ V)$	$0.48\ mJ$
$(1.4\ V, 1.8\ V)$	$0.64\ mJ$
$(1.8\ V, 2.2\ V)$	$0.8\ mJ$

Table 3.2: The relationship between threshold voltages and ASE

below $100\mu W$.

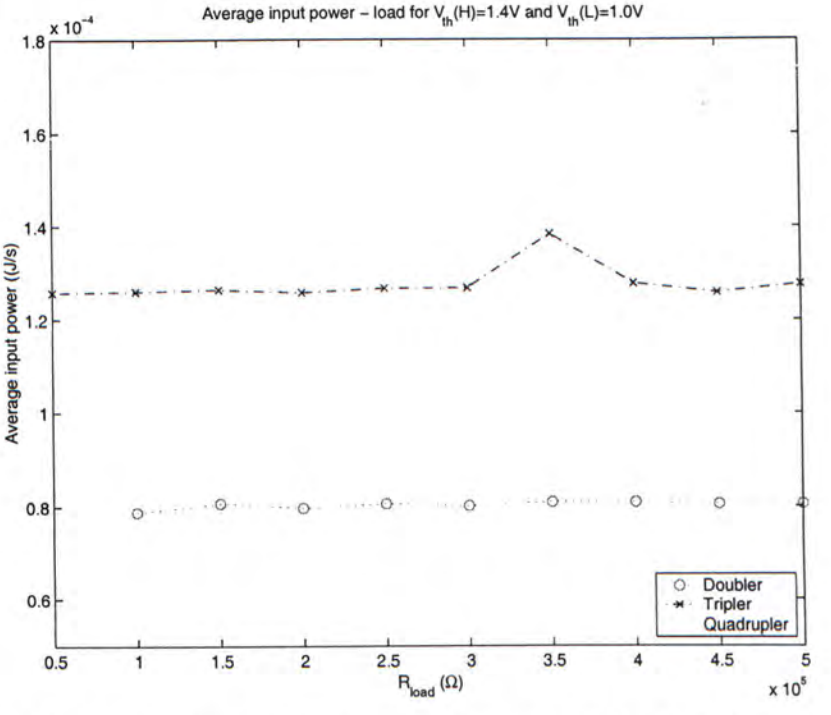

Figure 3.15: Average input power versus resistive load for $V_{th}(H) = 1.4\ V$ and $V_{th}(L) = 1.0\ V$ (simulated by PSpice)

3.5 Summary

Vibration-to-electrical transducers were not a new research topic in 2004. Many researchers used classical techniques to convert vibration into electrical power. The MPG outperforms other techniques in energy-to-density because MPT contains a high Q spring, which was made by lithographic electroplating on accurate mathematical model. The other useful feature of our MPG is that

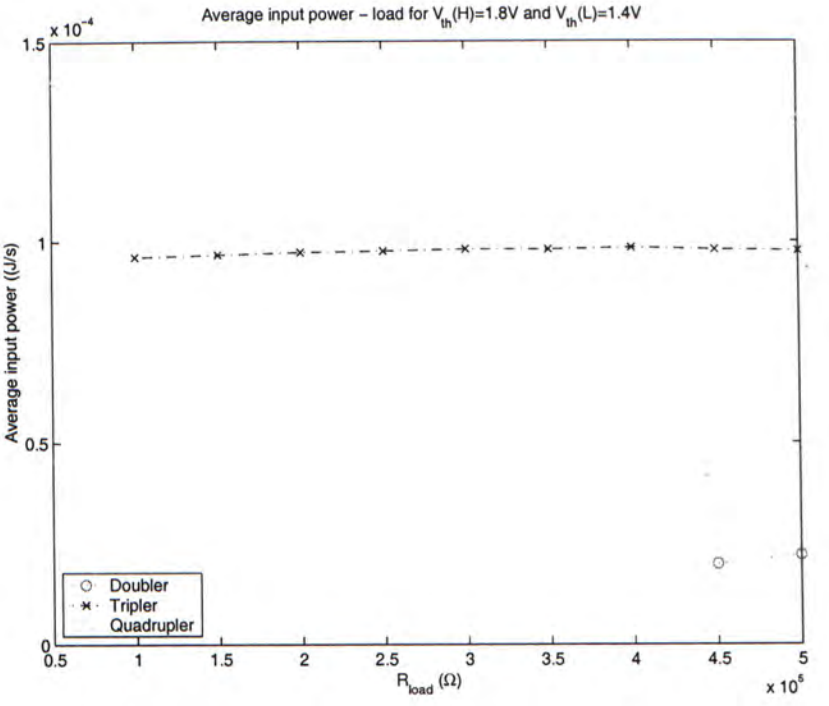

Figure 3.16: Average input power versus resistive load for $V_{th}(H) = 1.8\ V$ and $V_{th}(L) = 1.4\ V$ (simulated by PSpice)

it can power any off-the-shelf circuits. In section 4.2.1, the startup module and its duty-cycle operating mechanism will be discussed.

Finally, two evaluation metrics were introduced to quantify the performance of different VMs. A tripler was chosen for the MPG because of its overall performance. The metrics can be applied to evaluate any duty cycled AC-DC power converters.

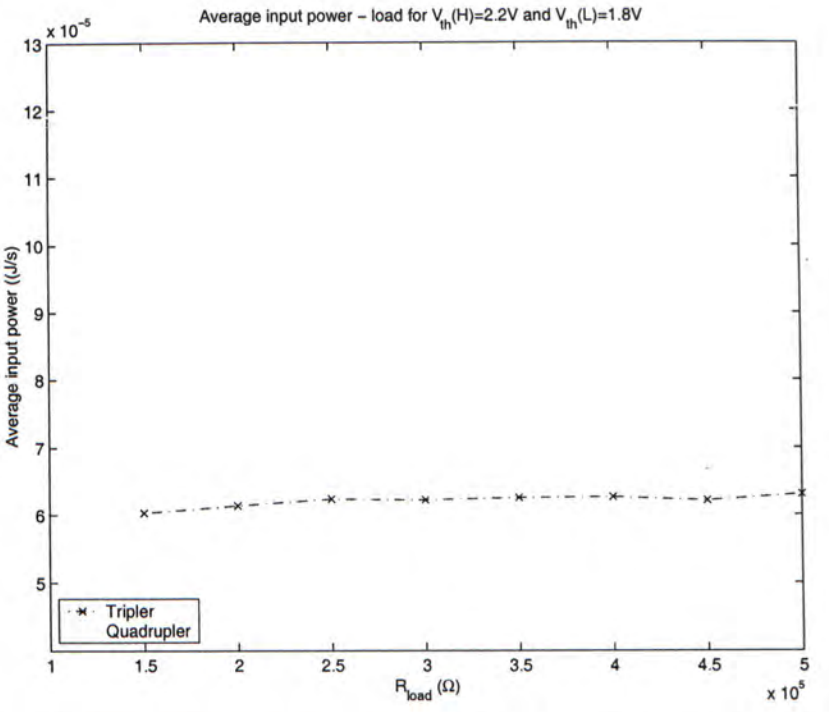

Figure 3.17: Average input power versus resistive load for $V_{th}(H) = 2.2\ V$ and $V_{th}(L) = 1.8\ V$ (simulated by PSpice)

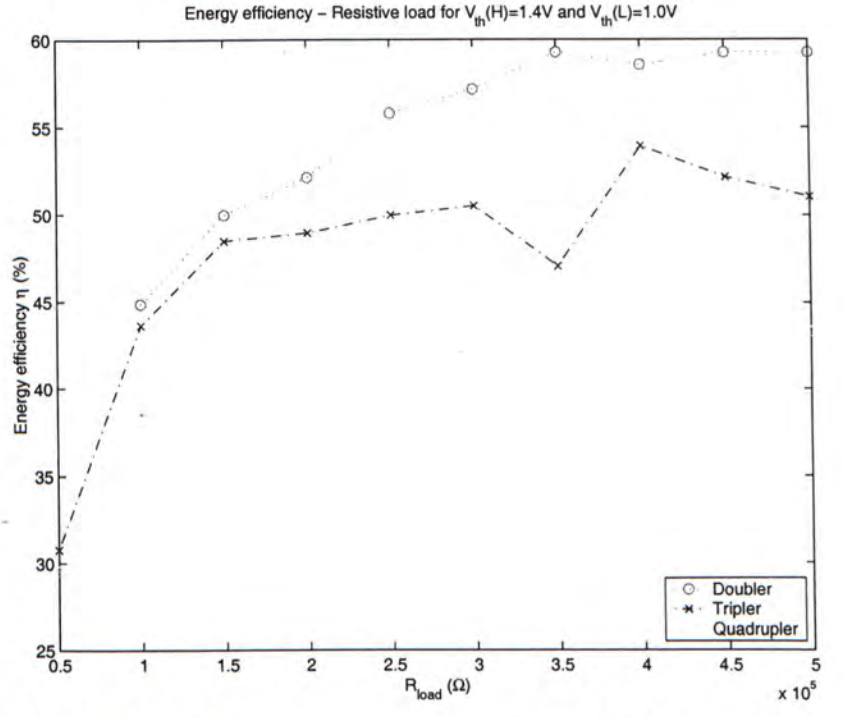

Figure 3.18: Energy efficiency versus resistive load for $V_{th}(H) = 1.4\ V$ and $V_{th}(L) = 1.0\ V$ (simulated by PSpice)

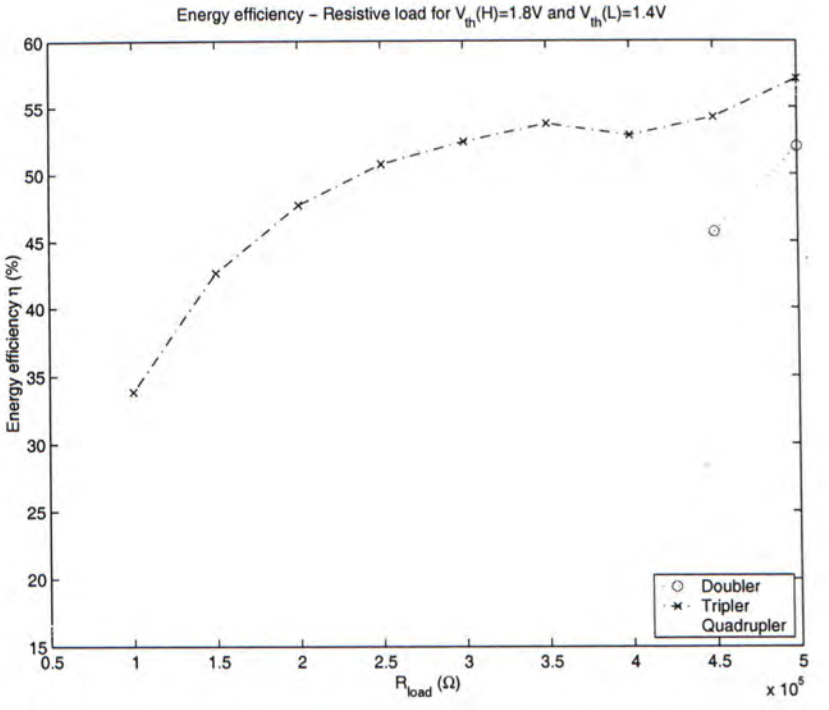

Figure 3.19: Energy efficiency versus resistive load for $V_{th}(H) = 1.8\ V$ and $V_{th}(L) = 1.4\ V$ (simulated by PSpice)

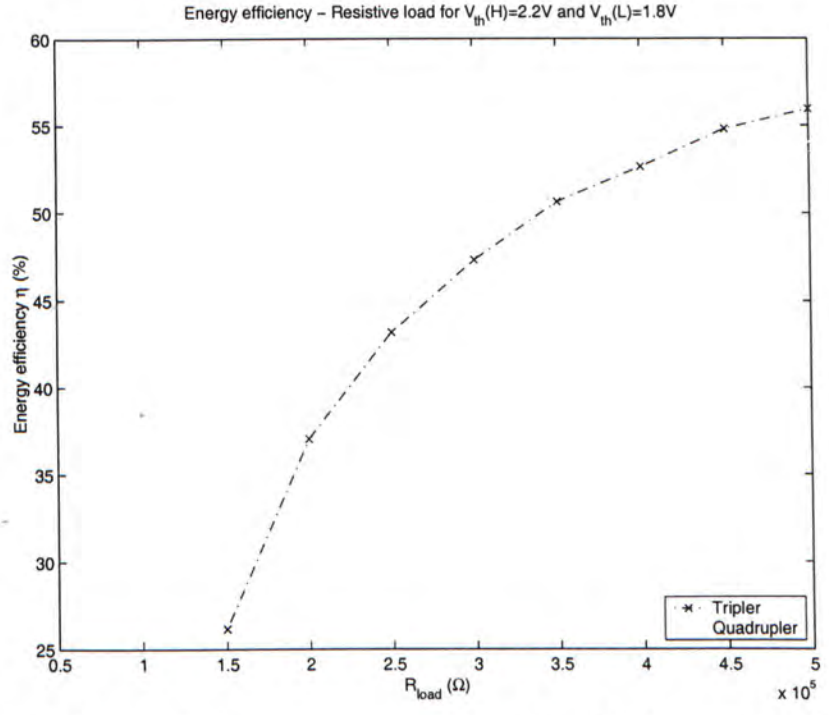

Figure 3.20: Energy efficiency versus resistive load for $V_{th}(H) = 2.2\ V$ and $V_{th}(L) = 1.8\ V$ (simulated by PSpice)

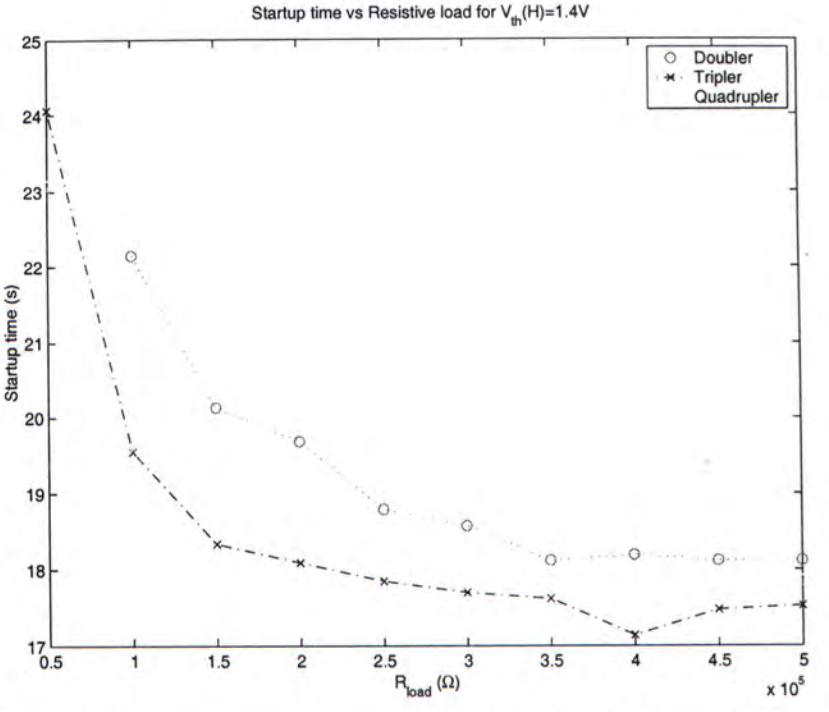

Figure 3.21: Startup time versus resistive load for $V_{th}(H) = 1.4\ V$ (simulated by PSpice)

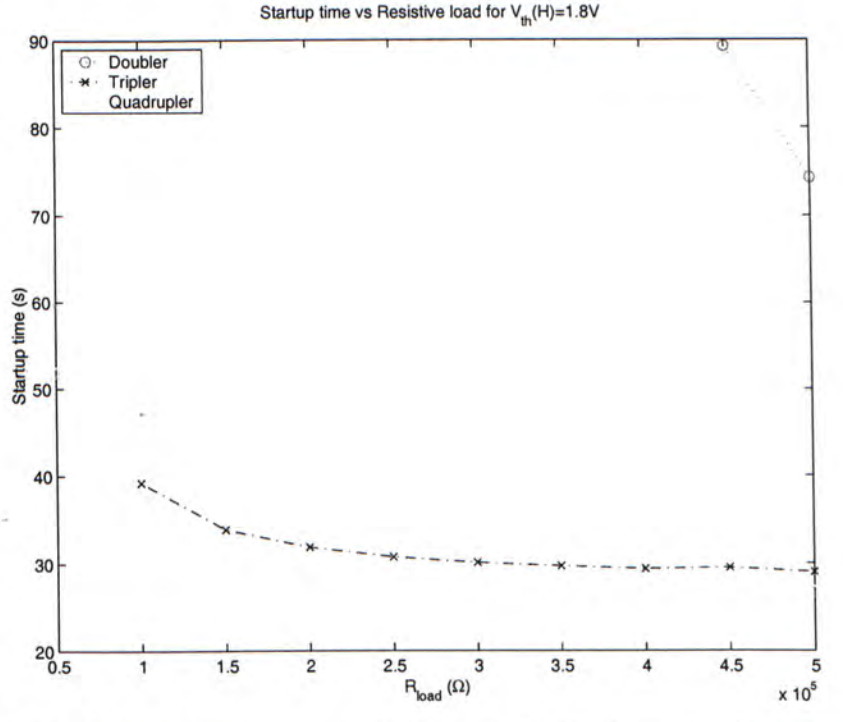

Figure 3.22: Startup time versus resistive load for $V_{th}(H) = 1.8\ V$ (simulated by PSpice)

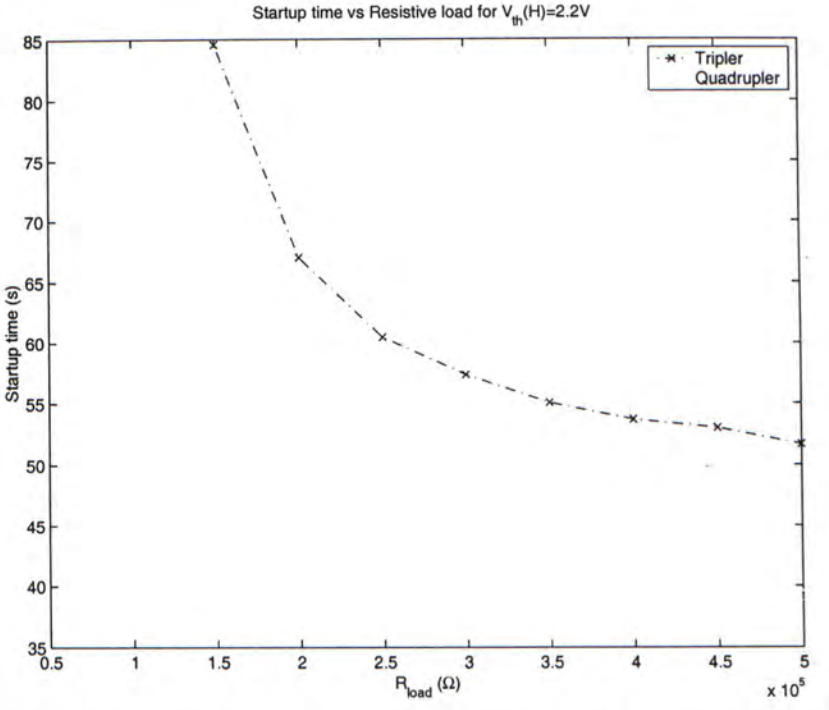

Figure 3.23: Startup time versus resistive load for $V_{th}(H) = 2.2\ V$ (simulated by PSpice)

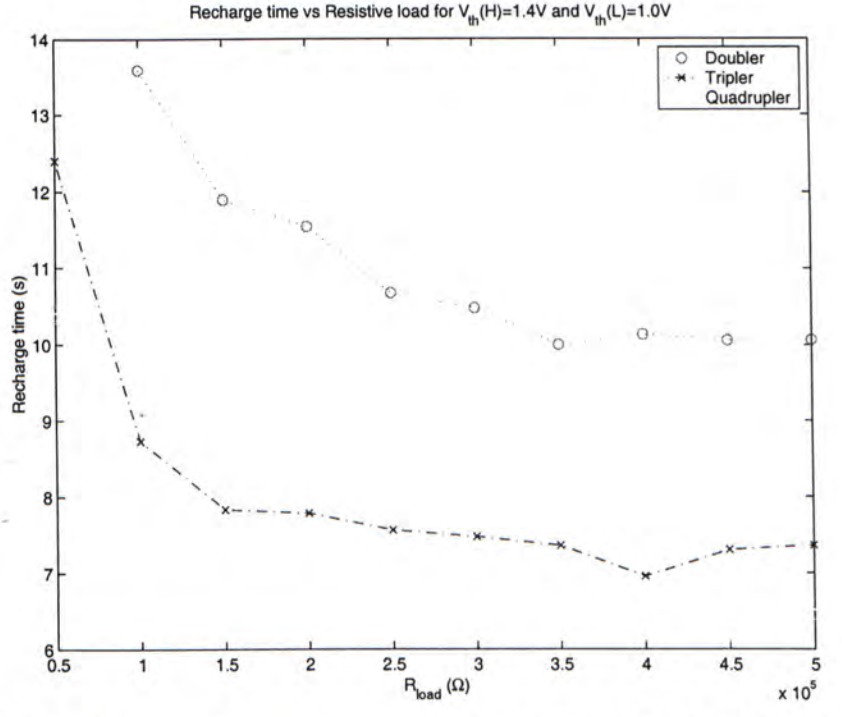

Figure 3.24: Recharge time versus resistive load for $V_{th}(H) = 1.4\ V$ and $V_{th}(L) = 1.0\ V$ (simulated by PSpice)

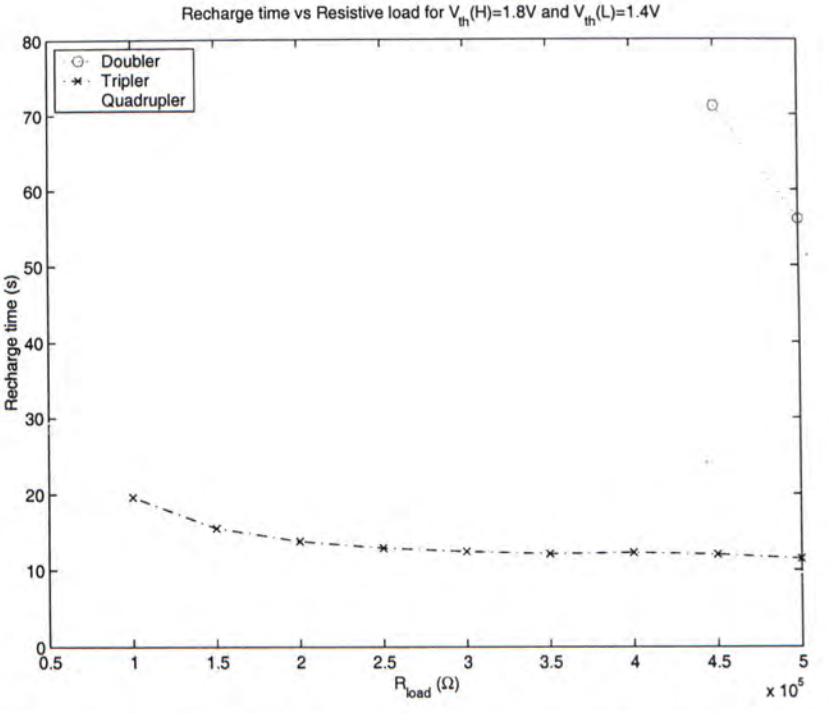

Figure 3.25: Recharge time versus resistive load for $V_{th}(H) = 1.8\ V$ and $V_{th}(L) = 1.4\ V$ (simulated by PSpice)

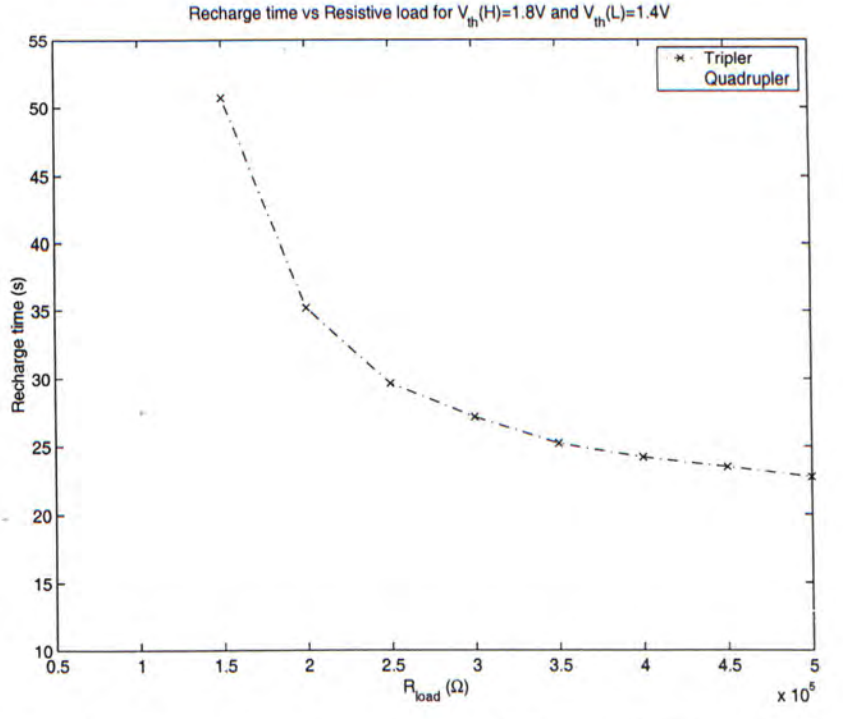

Figure 3.26: Recharge time versus resistive load for $V_{th}(H) = 2.2\ V$ and $V_{th}(L) = 1.8\ V$ (simulated by PSpice)

Chapter 4

Low Power Wireless Sensor Platform

4.1 Introduction

For long-term monitoring applications, vibrational-to-electrical power transducers are a good power source option because they provide a non-exhaustible supply. In many applications, however, the transducer must be small, typically of same order of magnitude to sensor circuit and this limits the power generated to a range of few hundred micro-watts if the volume is constrained to 1 cm^3 to 3 cm^3. Besides power considerations, designing wireless sensors involves many tradeoffs. In this chapter, the architecture of a low power wireless sensor will be covered.

4.2 Generic Platform

A Generic Platform (GP) is proposed to fulfill the requirements of general monitoring applications. The block diagram of the GP is shown in figure 4.1. The GP will be powered by a battery or a micropower generator as described in chapter 3. The power source is connected to a power management circuit which consists of a startup module and power regulator. The startup module

acts as an active switch between the application circuit and power source. It will monitor the voltage level of power source and activate the application circuit only when the stored energy is sufficient. Because the output voltage level of power source will vary within a defined range, a power regulator is introduced to step up/down the voltage so that a stable supply voltage can be presented to the application circuit.

The application circuit consists of a microprocessor, an Analog-to-Digital Converter (ADC), secondary storage, long period timer and some sensor peripherals. The microprocessor controls the system's peripherals and the data communication between them. The microprocessor must have **G**eneral **P**urpose **I**nput **O**utput pins which connect and exchange data with the digital sensors. For sensor with analog output, an ADC acts as a voltage interface which digitizes the analog output of the sensors. The secondary storage is a non-volatile device which stores system information and post-processed data from the microprocessor. The long period timer should be driven by a crystal operated at low frequency. It can trigger the microprocessor with a pre-programmed period to wake the system from sleep mode or to make a time record. The sensor peripherals monitor or measure the behaviors or changes of the environment. The GP can communicate with other GPs or computing hosts via its wireless RF transmitter (one-way) or Infrared transceiver (two-ways).

4.2.1 Startup Module and Power Management

Startup Module

The startup circuit is not a part of the MPG. However, it is essential for the MPG because it guarantees that the application circuit (loading of MPG) activates at the right time. The startup module only applies power to the application circuit when the voltage at the output of the tripler exceeds a fixed threshold, $V_{th}(H)$. Without the startup module, the application circuit

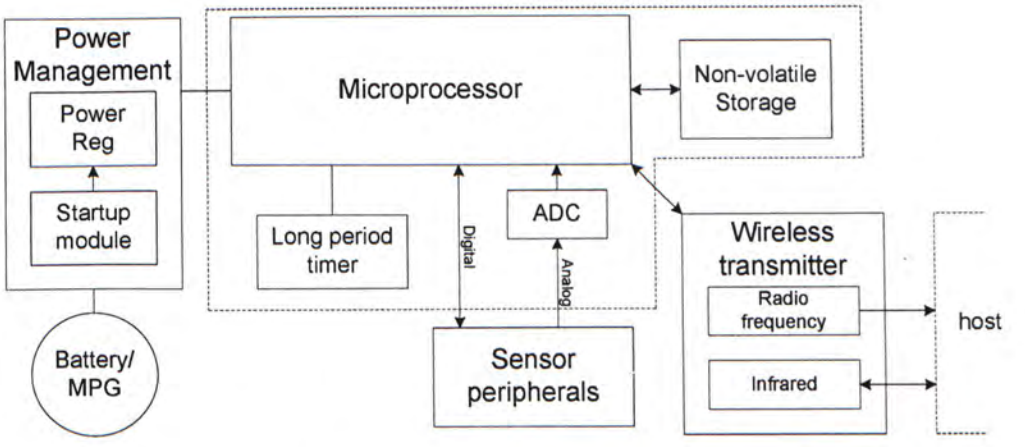

Figure 4.1: Generic platform block diagram

will begin to operate well before the minimum voltage required for correct operation is reached, a large current consumption. This results in a situation in which the voltage at the output of the tripler cannot continue to rise as shown in figure 4.2. The schematic of the startup module is shown in figure 4.4. Three resistors connected to positive input of comparator set the hysteresis of the startup module, i.e. the value of $V_{th}(H)$ and $V_{th}(L)$. Equation 4.1 shows the calculation [32] to determine the resistor values shown in figure 4.4. The output of startup circuit is active-high. It will switch on the NMOS transistor T_1 when the supply voltage is higher than $V_{th}(H)$ and will switch off T_1 when the supply voltage drops lower than $V_{th}(L)$. Thus, T_1 acts as a power switch for the application circuit. When T_1 turns on, a return path between system ground of application circuit and power ground is provided. Figure 4.3 shows the output characteristics of startup module and system supply. The input capacitor of the startup module must be large enough to provide sufficient energy for one time activation of the application circuit. For example, the wireless RF thermometer, described in chapter 5 consumes 212.62 μJ per activation. Therefore a 1 mF capacitor is sufficient. Equation 4.2 shows the amount of energy available in a charged 1 mF capacitor with $V_{th}(L) = 1.4\ V$ and $V_{th}(H) = 1.9\ V$.

$$
\begin{aligned}
\text{Select } R_3 &= 1.2\ M\Omega \\
\text{Choose the hysteresis band, } V_{HB} &= 1.9 - 1.35 \\
&= 550\ mV \\
\text{Calculate } R_1 &= 1.2\ M \times (\frac{550\ mV}{1.9\ V}) \\
&= 347\ k\Omega \\
V_{th}(H) &> 1.25 \times \frac{347\ k\Omega + 1.2\ M\Omega}{1.2\ M\Omega} \\
1.9\ V &> 1.61145\ V\ ....\surd \\
R_2 &= 1/[\frac{V_{th}(H)}{V_{ref} \times R1} - \frac{1}{R1} - \frac{1}{R3}] \\
&= 1/[\frac{1.9}{1.25 \times 347\ k\Omega} - \frac{1}{347\ k\Omega} - \frac{1}{1.2\ M\Omega}] \\
&= 1.5032\ M\Omega \\
R_1 &= 349\ k\Omega,\ R_2 = 1.5\ M\Omega,\ R_3 = 1.2\ M\Omega \\
&\quad \text{were selected for stock available.} \\
\text{Verify the trip voltage, } V_{th}(H) &= V_{ref} \times R_1 \times (\frac{1}{R_1} + \frac{1}{R_2} + \frac{1}{R_3}) \\
&= 1.904375\ V\ ....\surd \\
V_{th}(L) &= V_{th}(H) - \frac{R_1 \times 1.9}{R_3} \\
&= 1.35179\ V\ ....\surd \\
\text{Hysteresis} &= V_{th}(H) - V_{th}(L) \\
&= 552.585\ mV\ ....\surd \qquad (4.1) \\
\text{Available Energy, } E \text{ for } 1.0\ mF &= C \times \Delta V \times V \\
&= C \times (V_{th}(H) - V_{th}(L)) \times \frac{V_{th}(H) + V_{th}(L)}{2} \\
&= 1\ m \times (1.9 - 1.4) \times \frac{1.9 - 1.4}{2} \\
&= 825\ \mu J \qquad (4.2)
\end{aligned}
$$

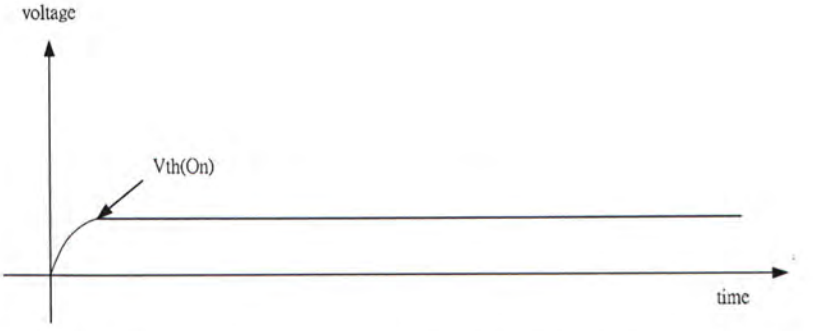

Figure 4.2: System supply stuck at Vth(On) without startup module

Conversion Technique

Conventional vibration-to-electrical transducers produce AC power. Neither voltage nor current is easy to store in AC form. The most common way is to convert the AC output to DC and store the energy in a capacitor or battery. The former is preferred since capacitors suffer less from self-discharge (in the μA range).

AC-DC For AC-DC conversion, a voltage multiplier [14] provides the simplest solution. It is constructed entirely from diodes and capacitors, and hence does not need a DC voltage supply to operate. Three types of voltage multipliers, described earlier in section 3.3, are shown in figure 4.5.

DC-DC(Inductor-based Switching Regulator) A simple boost regulator [33] is shown in figure 4.6. Imagine that the switch has been open for a long time. Assuming no load, the voltage at the output capacitor is $V_{in} - V_{diode\ drop}$. Once the switch is closed, one end of the inductor is connected to ground. The diode prevents a backward current and thus voltage at the output is unchanged. The inductor current increases before being saturated and develops a field on the inductor. When the switch is open, the end of inductor (originally connected to ground) will virtually connect to the output because the output diode will be forward-biased. The stored energy in the magnetic field of the inductor

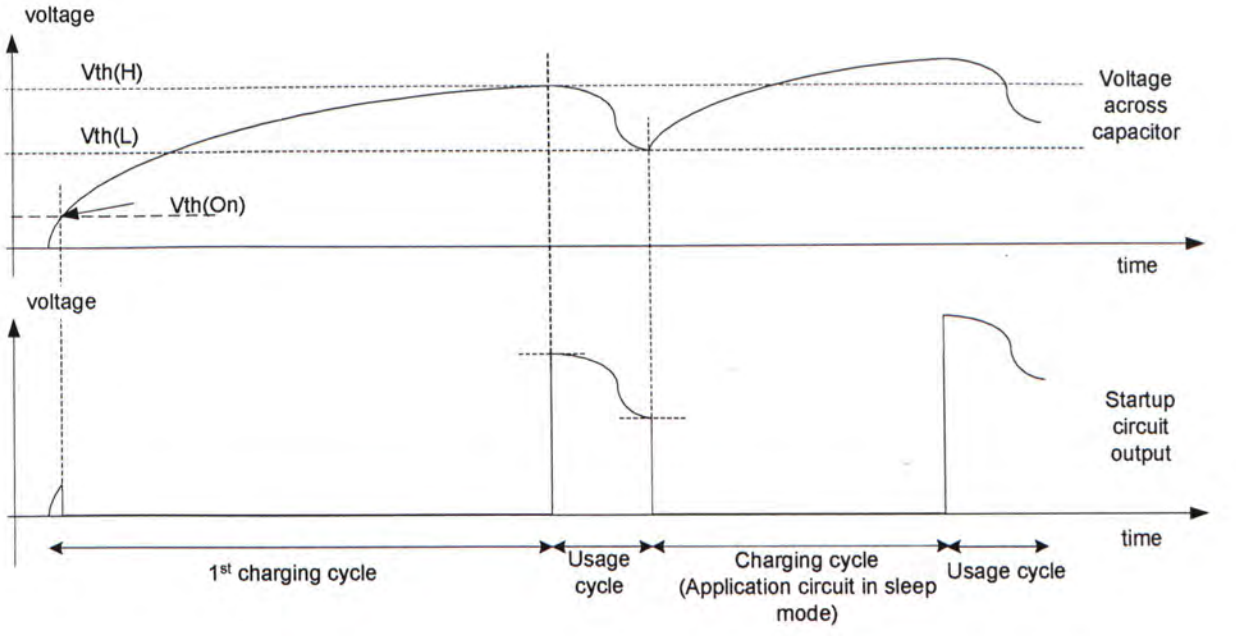

Figure 4.3: Output characteristics of startup module and system supply

will be released to maintain the current which flows out to the output before the stored energy vanishes. The voltage across the inductor will be greater than the output voltage ($V_L > V_{out}$), and charge will be transferred to the capacitor. To maintain a desired output voltage level, the switching process must not be interrupted. To achieve high efficiency, the switching on/off time must be tuned so that the inductor is almost saturated. Microprocessors with built-in inductor-based switching regulators are available [26]. In figure 4.7, a simplified schematic diagram of the internal switching regulator of the PSoC chip from Cypress [42] is shown.

DC-DC(Capacitor-based Voltage Converter) Capacitor-based voltage converters use capacitors to store and transfer energy. Since the capacitor can't change voltage levels abruptly, multiple capacitors and switches may be used to step up/down input voltage. Also, the maximum drive

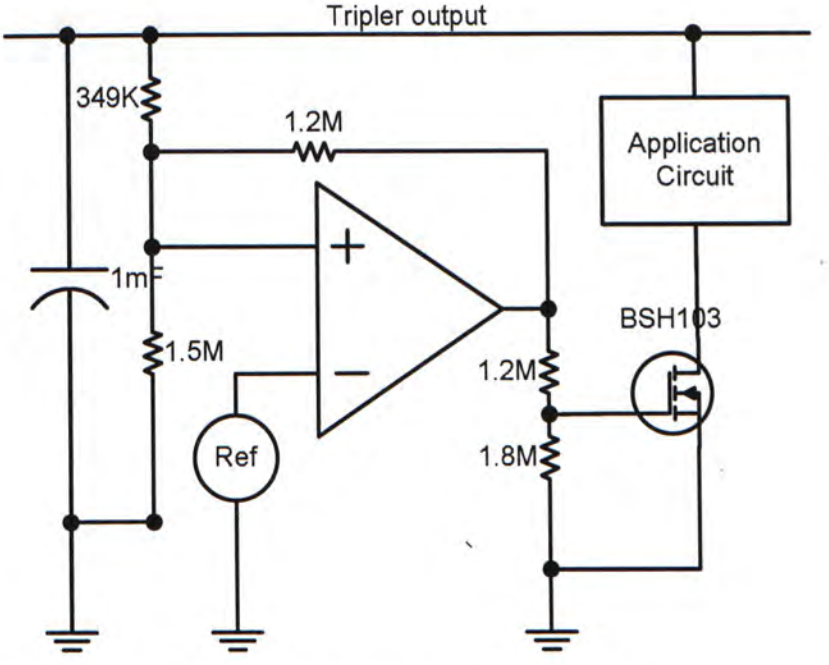

Figure 4.4: Schematic of startup module

current for capacitor-based voltage converters is low, but clean (less ripple). A good introduction to capacitor-pump voltage converters can be found in [34]. Capacitive voltage conversion is achieved by switching a capacitor periodically. In figure 4.8, a circuit demonstrates the generation of $-V_+$ from a supply voltage V_+. Two pairs of switches (S1,S3) and (S2,S4) are turned on/off alternatively. For the positive input cycle, (S1,S3) are closed and C1 is charged to V_+. For the zero input cycle, (S1,S3) are opened and (S2,S4) are closed and charges sharing occurs between C1 and C2. Thus, a voltage $-V_+$ is developed at V_{out}. A voltage of 2 V_+ can be achieved by connecting the load between V_+ and V_{out}.

4.2.2 Control Unit

Three different kinds of microprocessors were analyzed to judge which is the best to be placed in our generic platform. They are listed below:

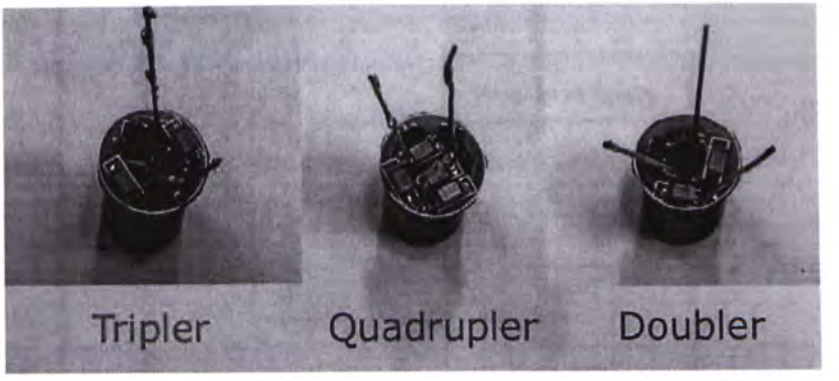

Figure 4.5: Voltage multipliers: tripler, quadrupler and doubler

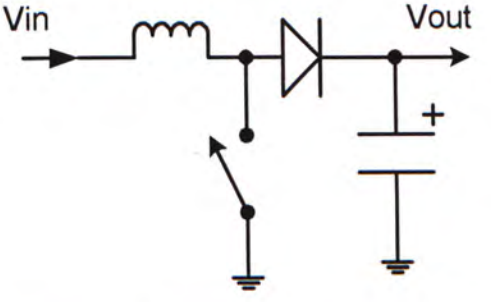

Figure 4.6: Simple boost converter [33]

Programmable System on Chip [26] from Cypress [42] A reconfigurable microprocessor, Programmable System-on-Chip (PSoC). PSoC is a microprocessor embedded with analog and digital reconfigurable cells. The analog and digital reconfigurable cells can be configured to implement functional blocks, ie. analog filters, timers, temperature sensors, UARTs, ADCs, etc. via a module library. There are two types of analog reconfigurable blocks. Both are based on switch capacitor circuits to minimize mismatch effects. Besides the reconfigurable ability, the PSoC has many nice features. It has a sleep timer with 1 s period, a built-in switch mode pump designed for stepping up a battery input ($\geq$ 1.2 V) to pre-programmed supply voltage (say 3.3 V) with 50 % efficiency. Figure 4.7 shows the schematic diagram of the switch mode pump in the PSoC.

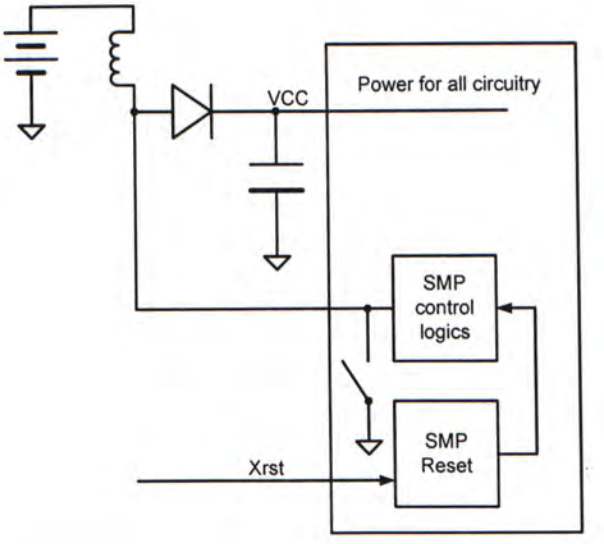

Figure 4.7: Programmable System on Chip has built-in switching regulator [26]

Microcontroller with integrated PLL - Atmel Smart RF [7] This wireless data microtransmitter was designed for Remote Keyless Entry systems (RKE). It has a built-in Phase Lock Loop (PLL) and Power amplifier (PA), so that only an external inductor and a crystal are required for the wireless transmission. The Intermediate Frequency (IF) can be selected from $264 - 456\ MHz$. The IF is controlled by the natural frequency of the crystal (for *Atmel Smart RF*, $f_{IF} = 24 \times f_{crystal}$). *Atmel Smart RF* implements On-Off Keying (OOK) modulation or Frequency Shift Keying (FSK) modulation by changing the configuration of internal capacitor arrays. To improve transmission rate, an internal timer (bit timer) is used to control, pulse/space encoding. *Atmel Smart RF* has 128 *Bytes* of non-volatile storage and six I/O pins. Finally, it is worthwhile to mention that it can be programmed with a couple of pins in I^2C format.

Ultra-low power microcontroller - TI MSP430 [20] This 16-bit Micro Control Unit (MCU) was designed for ultralow power applications. It

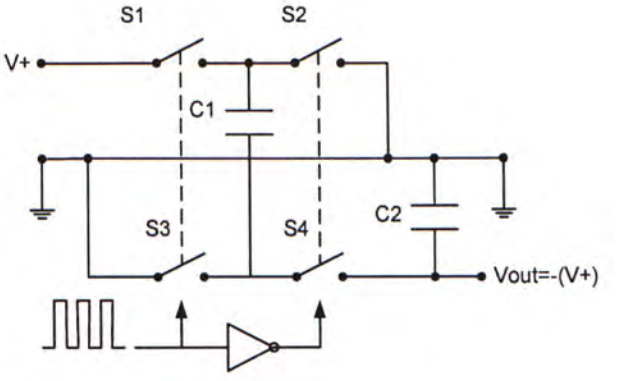

Figure 4.8: These essential components illustrate the mechanics of charge-pump operation. [34]

has five power modes and interval timers. In power mode 3, the power consumption of the MCU is as small as 2 μA with 3 V supply. The interval timer sourced by a 32 kHz crystal can wake up the system from power mode 3 6 s intervals. This MCU has GPIO pins which can cause individual of interrupts. Some versions of the MSP430 have built-in modules such as ADCs and DACs for analog peripherals. This MCU also has flash memory for storage.

These MCUs have tradeoffs, and are evaluated in chapter 5.

4.2.3 Input Units (Sensor Peripherals)

In this section, three kinds of sensors are introduced which enable the generic platform to measure temperature, sense motion and measure the sound level.

Temperature sensor TMP100 [19]

There are many ways to measure temperature. The simplest way is to measure the voltage across a thermistor which connects with resistor and voltage source in series. However, this may require an ADC to translate the analog voltage level into digital form for the MCU. Texas Instructment's (TI) TMP100 is a digital temperature sensor which provides a digital output, simplifying its

interface. The TMP100 takes at most 75 ms to make a 9-bit temperature conversion with current consumption of 70 μA at 3 V. It can be shut down with a very low quiescent current consumption, typically $0.1 - 1$ μA and comes in a 3 $mm \times 3$ $mm \times 1.45$ mm package.

iMEMS accelerometer [15]

The iMEMS accelerometer is a 5 $mm \times 5$ $mm \times 2$ mm monolithic IC from Analog Device, Inc. It measures both dynamic and static acceleration for single or double axis. The outputs are analog voltage or digital signals whose duty cycles (ratio of pulsewidth to period) are proportional to acceleration. An ADC or a counter can be used to decode the output of the accelerometer, the period being set by an external resistor. The accelerometer can achieve $2mg$ (g stands for gravitational force, typically 9.8 ms^{-2}) resolution at 60 Hz bandwidth. It operates at supply voltage $3 - 5.25$ V with supply current < 0.6 mA.

Digital microphone from BSE [9] and National [44]

A microphone is a pressure-to-electrical transducer. It converts sound to a small analog signal. A conventional Electret Condenser Microphone (ECM) contains a JFET preamplifier. Conventional ECMs have low noise immunity due to its analog output. Aire van Rhijn [52] reported that a digital ECM to improve Signal-to-Noise Ratio (SNR) compared to an analog ECM. The idea is to replace the JFET by a preamplifier and a sigma-delta modulator. Therefore the output becomes digital. The digital ECM has four pins: Vcc (power), Clock-in, Data-out and Vss (ground) and is easily interfaced. The sound level can be acquired by averaging the accumulated output of the sigma delta modulator.

4.2.4 Output Units (Wireless Transmitters)

Infrared and radio frequencies are two common *mediums for wireless transmission.* Their details are covered below:

Infrared

Infrared transmission requires line-of-sight, although reflection is allowed at a smooth surface, ie. metal plate, mirror, etc. It is commonly adopted in remote controls, RKE system where short range and low transmission rates are acceptable. An infrared Light Emitting Diode (LED) is sufficient to form an infrared transmitter. Modern portable electronics use infrared transceivers to form short range communication links.

Radio Frequency

Radio Frequency (RF) transmitters do not require line-of-sight. RF transmitter can be constructed by LC circuits (LC), PLLs or Surface Accoustic Wave (SAW) components.

LC A single-transistor FM transmitter was built to test its performance [11]. The schematic of FM transmitter is shown in figure 4.9. The FM transmitter was designed to work in the commercial FM radio band 88 – 108 MHz with a 2 V supply. Data in digital form can be input to the circuit. C_1 and C_2 forms a potential divider to reduce the AC signal to 1/10 of its original value. Q_1 acts as a common base oscillator, with feedback provided by C_4. R_1 provides the bias for the transistor, and R_2 provides emitter bias. A $2N2222A$ VHF transistor was chosen for the oscillator. Any NPN transistor operating at 500 MHz or above should work with different modulation characteristics. The tank circuit L_1 and C_3, along with stray circuit and transistor collector-to-base capacitances, determine the frequency of oscillation. The collector-to-base capacitance

is a function of collector-base voltage, and this voltage is modulated by the input voltage from C_1, causing direct frequency modulation of the oscillator frequency. Because the oscillator power output also varies with collector voltage, some AM components will also be present. The FM broadcast is approximately at a 3-meter wavelength (100 MHz) approximately. C_3 is approximately 8 pf and the transistor and stray capacitances are approximately $2 - 5$ pf. L_1 is 0.25 μH. C_5 is used as a DC-blocking capacitor and is generally around the same value as the tank-tuning capacitor for optimal performance. As for antenna, it is usually made about one-forth of a wavelength and for 100 MHz, is about 70 cm. However, for short ranges, up to 7.5 meters, radiation from the circuit or coupling on supply rails is adequate for transmission. An experimental transmitter was implemented and it consumed $\approx$ 300 μA with 2.3 V supply in continuous transmission mode. Its transmission range was about 1.5 meters. The calculation of power consumption and transmission range is presented in equations 4.3 and 4.4.

Assume that the supply voltage is 2 V, current consumption is 300 μA, transistor Q_1 is a $2N2222A$ which has gain $\beta = 40$ and forward voltage $V_f = 0.6$ V, commercial radio's sensitivity is 0.01 mW. No antenna is required which reduces the transmission power to 30 %. The steps for calculation are listed below [11]:

1. Define the input swing, here it is 0 V to 3 V at the input of C_1. The input is coupled to node between C_1 and Q_2 and reduces the maximum input voltage to 0.3 V.
2. Calculate voltage V_E across resistor on emitter of Q_1.
3. Use current gain equation to calculate I_B.
4. Calculate base resistor of Q_1, R_B.
5. Calculate emitter resistor of Q_1, R_E.

6. Calculate output power of transistor Q_1.
7. Calculate ideal transmission range.
8. Calculate effective transmission range when there is no antenna and obstacle between transmitter and emitter.

$$\begin{aligned}
V_{bias} &= \frac{2-0.6}{2} + 0.6 \\
&= 1.3\ V \\
V_E &= \frac{2-0.6}{2} \\
&= 0.7\ V \\
I_B &= \frac{I_B}{\beta+1} \\
&= \frac{300\ \mu}{40+1} \\
&= 7.317\ \mu A \\
R_B &= \frac{2-1.3}{7.317\ \mu} \\
&= 95.67\ k\Omega \\
R_E &= (\frac{2-0.6}{2})/300\ \mu \\
&= 2.3\ k\Omega \\
P_{transistor} &= (2 - \frac{2-0.6}{2}) \times 300\ \mu \\
&= 0.39\ mW \qquad (4.3) \\
\text{Tx Distance}_{ideal} &= \sqrt{\frac{0.39\ m}{0.01\ m}} \\
&= \sqrt{39} \\
&= 6.24 \text{ meters} \\
\text{Tx Distance}_{effective} &= 6.24 \times 30\% \\
&= 1.873 \text{ meters} \qquad (4.4)
\end{aligned}$$

PLL with crystal To provide a wide frequency-tunability and high frequency-stability, a crystal-based frequency synthesizer using a Phase-Locked

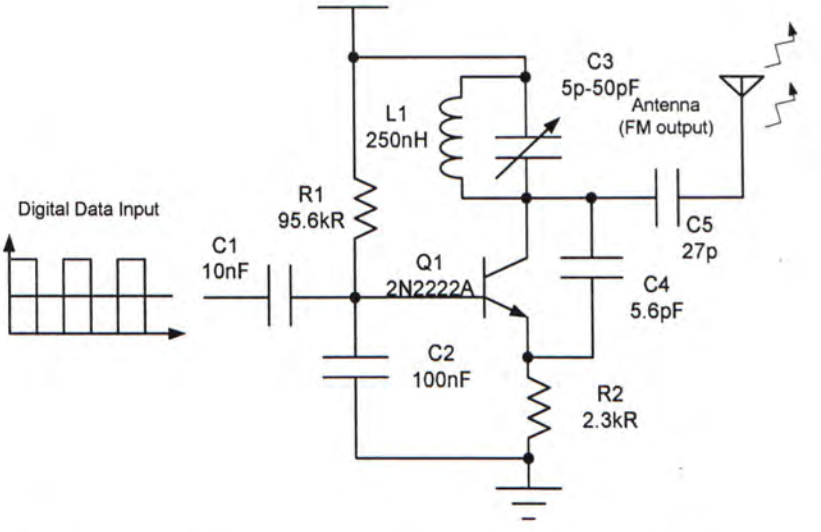

Figure 4.9: Schematic of LC-based radio frequency transmitter

Loop (PLL) [53] can be used. Figure 4.10 is a simplified diagram of a common single-loop PLL synthesizer. It takes a low-frequency crystal oscillator as a reference clock. The clock signal is fed into the R divider, which decreases the reference frequency via an adjustable frequency divider. The frequency output of the R divider is further inserted into the phase comparator, which compares the phase of the R divider to that of the adjustable N frequency divider. The phase comparator determines the phase difference between the outputs of divider R and divider N. For a charge pump type PLL, its output is in duty-cycle format which is further rectified into a DC correction voltage for the VCO by the loop filter. The negative feedback loop makes the desire frequency lock with reference clock frequency from crystal oscillator, $f_{vco} = f_{ref} \times \frac{N}{R}$. A crystal-based PLL transmitter combines a crystal-based PLL oscillator with a Power Amplifier.

Both On-Off Keying (OOK) and Frequency Modulation (FM) can be implemented using a PLL. For OOK, an Intermediate Frequency (IF) is generated by feeding crystal signal into the PLL. By-passing the IF

to the output denotes *one* and shortening the output to ground denotes *zero*. For FM, two different frequencies can be generated by changing the $\frac{R}{N}$ ratio slightly. The drawbacks of the PLL are:

1. complex, since the design of loop filter is very critical.
2. large power consumption. The PLL involves many components and they are ON for transmission of both *zero*'s or *one*'s.

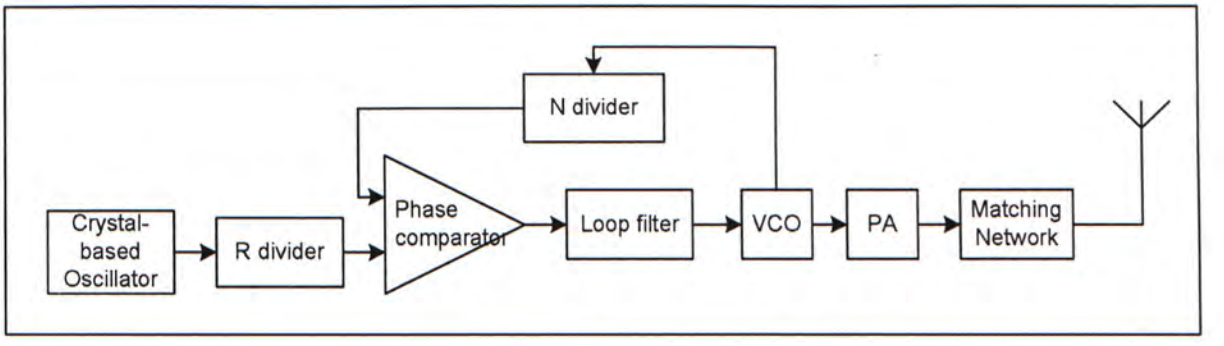

Figure 4.10: System block diagram of PLL with crystal

SAW-stabilized Figure 4.11 shows a schematic diagram of SAW-stabilized ASK transmitter [37] which is similar to the LINX LC series transmitter [46]. The Surface Acoustic Wave (SAW) resonator combines with a wideband RF transistor to form a SAW oscillator and PA. When data is applied on the input switch, the oscillator is tuned on and off according to the input data stream. This input sequence will be amplified and send to matching network at output stage, then the signal will radiate out via antenna. The SAW-stabilized ASK transmitter is an OOK transmitter which is also known as Carrier Present Carrier Absent modulation (CPCA) [41]. The SAW-stabilized ASK transmitter outperforms either LC or PLL for low power wireless sensor applications because it has good immunity to noise and low power consumption, since it consumes little power when sending *0*.

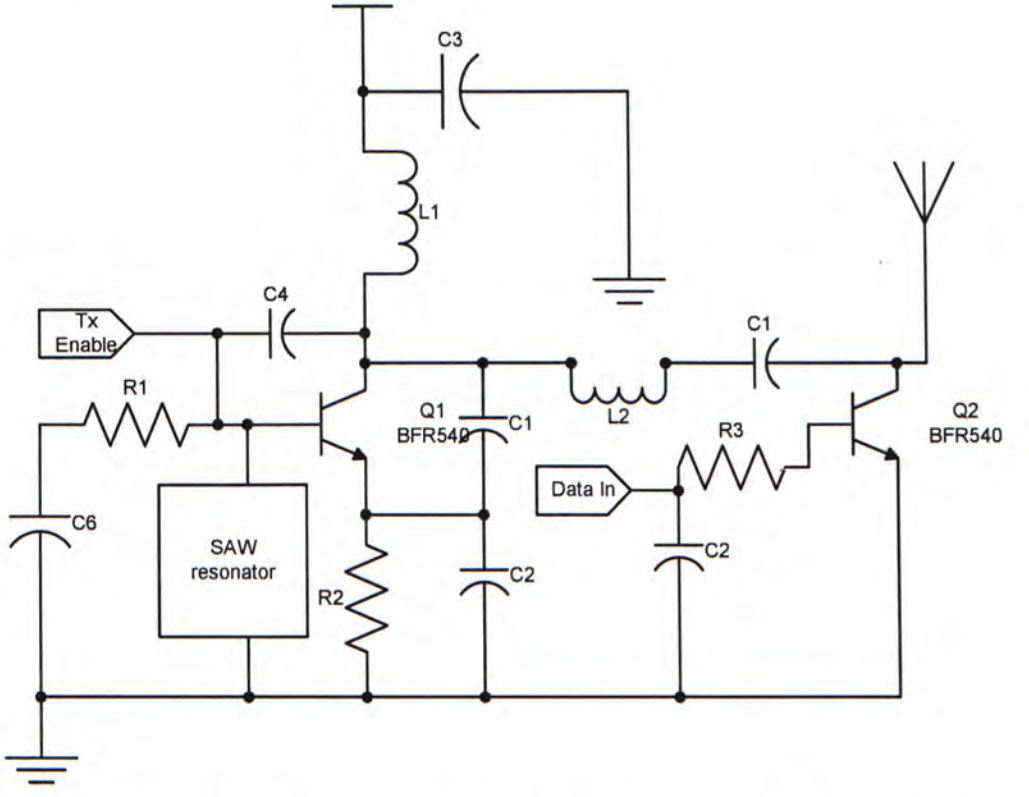

Figure 4.11: Schematic of SAW-based On-Off Keying RF transmitter [36]

Modulation and Coding Schemes

This section gives a brief introduction to modulation and coding schemes. For more details, please refer to Sayre [41].

The earliest radio station broadcasted using Amplitude Modulation (AM). Modulation is a scheme to insert baseband information (ie. voice digital data, analog audio/video, etc.) into RF carrier wave. AM is a modulation scheme which embeds the information into the envelope of the carrier wave. Frequency Modulation (FM) is now more widely used because of its higher fidelity compared to AM. An FM signal can be generated by altering the frequency of the carrier according to the amplitude variation of the baseband input. The transmitter shown in figure 4.9 is an example of the former. Both AM and FM are classified as being analog modulation.

Modern wireless communication adopts Digital Modulation (DM) because it provides higher data rates and noise immunity within constrained bandwidths and noisy channels. DM involves mathematics which beyond the scope of this section, therefore, only the idea will be presented.

The most common DM schemes for low-power short range data transmission are On-Off Keying (OOK) and Frequency Shifting Keying (FSK). OOK is a type of amplitude shift keying modulation. It represents *ones* and *zeros* by turning on and off the RF carrier frequency. FSK is another DM scheme which represents *ones* and *zeros* by two different non-harmonic frequencies, called *mark* and *space.*

For infrared remote control [38], the information bitstream is modulated with a $\sim 40\ kHz$ frequency. The types listed below are the common codings for an infrared remote control:

Pulse code varies the length of the pulses. A *One* is coded with longer pulse and a *zero* is coded with short pulse.

Space code varies the space between the pulses. The length of space represents the coding.

Shift code alters the order of pulse space. A *space+pulse* represents *one* and a *pulse+space* represents *zero.*

Transmitting data via RF is different from the media of wire. The RF bitstream is bit serial and must be encoded with a clock. Due to the on-off time of the oscillator, the duty cycle width of OOK for sending *zero* and *one* may not be 50/50. Therefore, Manchester codes are used. Referring to Federal Standard 1037C [1], the definition of Manchester code is:

> "A code in which (a) data and clock signals are combined to form a single self-synchronizing data stream (b) each encoded bit contains a transition at the midpoint of a bit period, (c) the direction of

transition determines whether the bit is a *zero* or a *one*, and (d) the first half is the true bit value and the second half is the complement of the true bit value."

The implementation of a Manchester code is covered in chapter 6.

Antenna

An antenna is a device designed for radiating energy efficiently from one media to another. Different shapes and geometries of antenna have different radiation characteristics. To evaluate an antenna, terms such as antenna diversity, antenna pattern, return loss, VSWR, beamwidth, etc. are used. Standard procedures to design and evaluate an antenna are as follows:

1. According to the nature and geometry of application, the antenna type is chosen.

2. The design is drawn and simulated with high frequency synthesis tools, such as Ansoft HFSS [6], aiming to optimize the quality factor and minimize the return loss of the antenna at the carrier frequency.

3. The design is fabricated and sometimes balun, which acts as a transmission line transformer for converting unbalance input and output, is placed. The impedance and S-parameter of the antenna output are matched using a network analyzer and Smith charts.

4. An output matching network is built. The matched antenna is connected to the transmitter. Further testing is required for transmission power and output spectrum in order to fulfill the regulations of the FCC.

Interest parties should refer to Setian's book [45].

Application note [18] provides a good introduction for compact antenna design. The common antenna types are listed below:

Frequency in MHz	315	418	434	868	916
1/4 Wave in *inches*	8.91	6.72	6.48	3.24	3.07

Table 4.1: Antenna wire length from [17]

1/4 wavelength A tin-plated copper wire between 22 to 32 gauge with a length of one quarter wavelength of the carrier frequency is the simplest antenna. Table 4.1 shows the length of antenna corresponding to carrier frequencies in the range 315 MHz – 916 MHz. For 433 MHz, the length of a 1/4 wavelength monopole is 6.5 inches which is too long for a portable device. The length of the monopole may be reduced by winding its lower end, which is called a *Short Whip*.

Spiral To further cut the size of a whip, the wire can be coiled up to form a flattened coil of wire or directly fabricated on PCB as a spiral trace. A planar antenna will fit into a 19 $mm \times 19$ mm square. A groundplate, however, must be placed to enhance the performance of the planar spiral antenna. The size and the location of the groundplate must be carefully designed, otherwise the performance of the antenna is reduced. It is worthwhile to mention that the quality factor of a spiral antenna is very high. Therefore, it can only be optimized for a particular carrier frequency. In the other words, it cannot function as a wideband antenna.

Helix The helical antenna is similar to a spiral, but it is not flattened. The wire size, coil diameter, turn spacing and number of turns are the factors to judge the characteristics of a helical antenna. The problem with this type of antenna are its bulk size and that it is easily detuned by nearby objects.

Adequate matching of the antenna can be achieved by the following procedure:

Diameter	Transmission range
1.5 mm	8 meters
1 mm	3 meters
wire wrap wire	1.5 meters

Table 4.2: Antenna diameter and transmission range

1. Calculate the transmission range from the power of the transmitter (shown in equations 4.3 and 4.4.).

2. Cut a tin-plated copper wire or plastic-coated copper wire with $> 1/4$ wavelength and connect to the transmitter.

3. Move the transmitter away from the receiver as far as possible until receiver ceases receiving correct data.

4. Shorten the antenna slightly and repeat step 3 to see whether a longer transmission distance can be achieved. Halt the process if a shorter transmission distance resulted.

5. Record the wire length which has the longest transmission range.

These procedures were used to evaluate different wire diameters for a 433 MHz SAW-based transmitter and receiver. The antenna was wound in a helix form (with 4 turns and turn diameter = 1.3 cm). The results are shown in table 4.2.

4.3 Summary

In this chapter, a generic platform for low power wireless sensor application is introduced. A low power startup module was designed to interface between a GP and micropower generator. Beside a power management circuit, the GP consists of an MCU, long-period self-wakeup timer, non-volatile storage, GPIO and ADC, wireless transmitters (RF and infrared) and sensor peripherals. The

usage and operating details of each these modules were explained. Up-to-date commercial products for each GP modules are also presented.

Chapter 5

Application I - Wireless RF Thermometer

5.1 Overview

A wireless thermometer is presented which provides a practical application for the MPG described in chapter 3. The wireless thermometer is based on the low power wireless sensor platform stated in chapter 4. The system block diagram is shown in figure 5.1. Implementation details are described in this chapter.

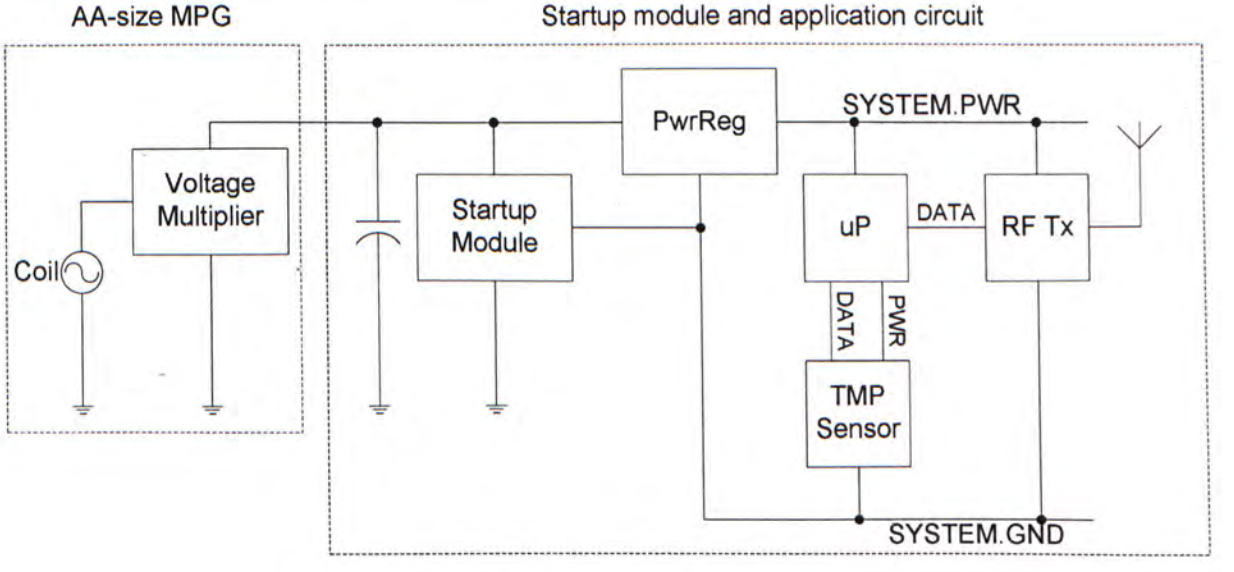

Figure 5.1: System block diagram

5.2 Implementation

Four prototypes of wireless RF thermometers were built. Different kinds of MCUs, temperature sensors, RF transmitter and power regulators were tested and their tradeoffs were evaluated.

5.2.1 Prototype 1

Prototype 1 has the similar setup to Wong's system described in section 2.3.3 with the main difference being that it uses an analog LC transmitter instead of an infrared LED. This eliminates the line-of-sight transmission problem. The photograph of prototype 1 is shown in figure 5.2. The transmitted data is received by a commercial radio and displayed on a CRO. The disadvantages of prototype 1 are:

1. The system must be powered by 3 V directly since there is no voltage regulator.

2. The system requires external intervention. The system has no self-timer, therefore it can't wake up itself.

3. The LC transmitter is easily influenced by proximity to conducting objects and temperature-drift.

5.2.2 Prototype 2

Due to low accuracy, temperature-drift and slow startup time of prototype 1, a commercial LINX chip whose carrier frequency is 433 MHz was used in the second prototype to replace the analog transmitter. The transmitter was tested with a data rate 5 *kbit* (with proper coding) and 91.4 *meters* transmission range. Besides a SAW transmitter, prototype 2 used the PSoC micro control unit (MCU). The PSoC MCU has a built-in voltage regulator which steps-up

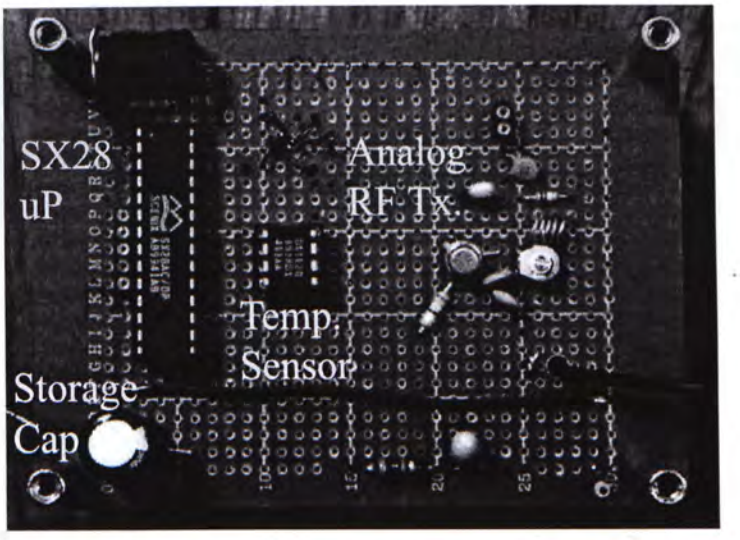

Figure 5.2: Photograph of prototype 1

a 1.2 V input supply to 3.3 V which is used by the whole system. PSoC has reconfigurable blocks which can be programmed as a temperature sensor. The photograph of prototype 2 is shown in figure 5.3. The drawbacks of prototype 2 are:

1. The built-in inductor-based switch regulator has only 50 % efficiency. It also requires a RLC filter to smooth output ripples.

2. The temperature sensor built with the reconfigurable block measures a junction temperature inside the chip which is isolated from the environment. Although a thermistor can be used to measure temperature outside the chip, this occupies extra space.

3. Although PSoC has a watchdog timer which can wake the system up from sleep mode, the watchdog timer has a significant power consumption penalty (typically 10 μA). The power consumed in the watchdog timer is more than the MPG can generate.

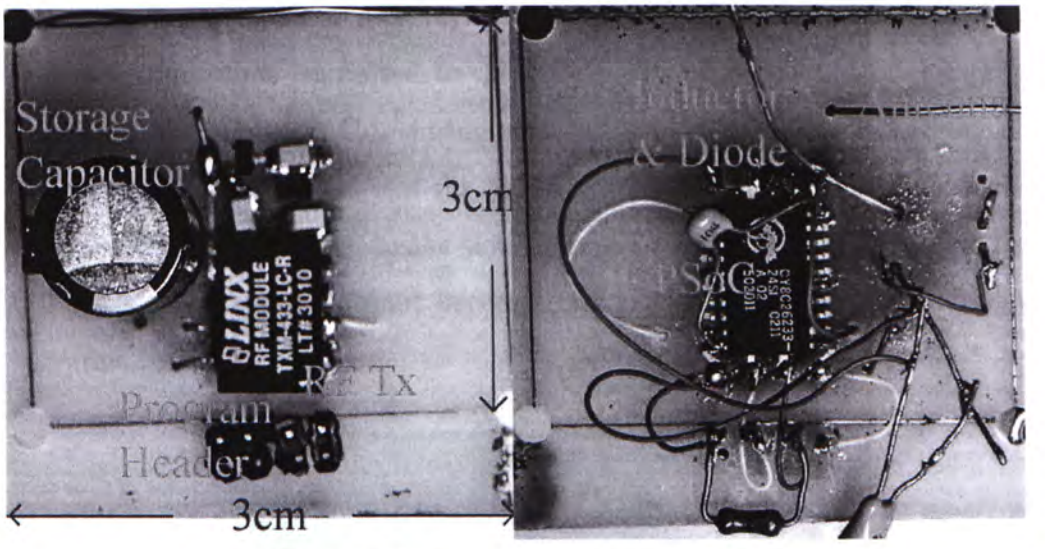

Figure 5.3: Photograph of prototype 2

5.2.3 Prototype 3

Sacrificing a little in power consumption, a special focus on component count and size was made for prototype 3. Prototype 3 uses an Atmel Smart RF MCU as the central processing unit because it has an integrated RF transmitter. In figure 5.4, a photograph of prototype 3 is shown. The MCU is a 8-bit processor and runs at $3 - 5\ MHz$. Prototype 3 contains an inductor-based switch regulator (MAX1724 [35]), temperature sensor and accelerometer. MAX1724 can step up an input voltage from $> 0.9\ V$ to $3.0\ V$ with 90 % efficiency and $1.5\ \mu A$ quiescent current consumption. A TMP100 temperature sensor is used because of its accuracy and small size. The drawbacks of this system are:

1. It has no timing module to wake the system up after the system entered sleep mode.

2. The antenna output of Smart RF requires $3\ V$ bias. However, the output of the switching regulator is very noisy and the noise will couple to the antenna.

3. To solve problem 2, a large capacitor C_{out} and inductor can smooth

the output ripple of the switching regulator. This causes two serious problems when connected to the MPG: (i) a large amount of charge is required to charge C_{out} during startup, also (ii) a rapid discharging of C_{out} is required to prevent the MCU running at a supply voltage outside the design range, due to the slow falling of supply voltage supported by C_{out}. The startup circuit becomes less efficient and difficult to design due to these two issues.

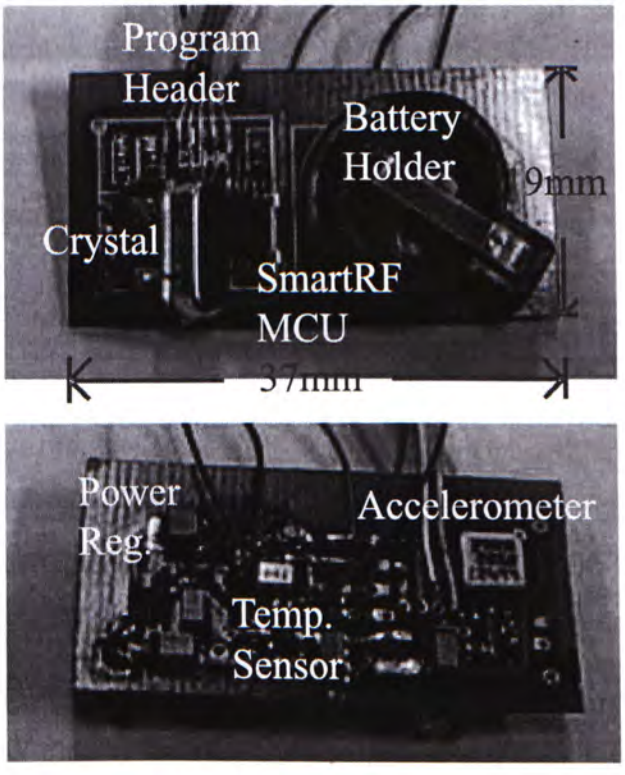

Figure 5.4: Photograph of prototype 3

5.2.4 Prototype 4

Prototype 4 was implemented with an aim to achieve the best power consumption, size and component count. A similar configuration targeted on battery supply can be found in the application note [21] which was published by Texas

Instructments. The system consists of TI MSP430 MCU, TMP100 temperature sensor, custom-made SAW transmitter and switch-cap regulator. MSP430 is a 16-bit MCU designed for ultra-low power applications. It has a long period (3.67 s) timer clocked with a low frequency crystal (76.8 kHz). Its GPIO pin is connected to the TMP100 to collect temperature readings. A custom-made SAW transmitter gives a high degree of flexibility for controlling the transmission power and matching antenna impedance. A Switch-cap power regulator has up to 90 % efficiency with 2 μA quiescent current consumption. It also has less output ripple than an inductor-based design, typically 30 mV. Prototype 4 was built with a startup module, so that the MPG can connect directly with it. The flow chart in figure 5.6 shows the operating sequence of both the startup module and the application circuit. The operating sequence is listed below:

1. When the system is vibrated, the MPG charges up the output storage capacitor C_{out}. The charge in C_{out} is assumed to be initially zero.

2. The startup module switches off the application circuit until the voltage across C_{out} rises higher than $V_{th}(H)$ at which point the application circuit is allowed to operate.

3. The application circuit performs MCU initialization, temperature conversion and data transmission.

4. After the application is done, the circuit sleeps for a preprogrammed period and waits for next activation if energy is sufficient. Otherwise, it will wait for next charge-up of C_{out} above $V_{th}(H)$ and then will startup.

The photograph of prototype 4 is shown in figure 5.5.

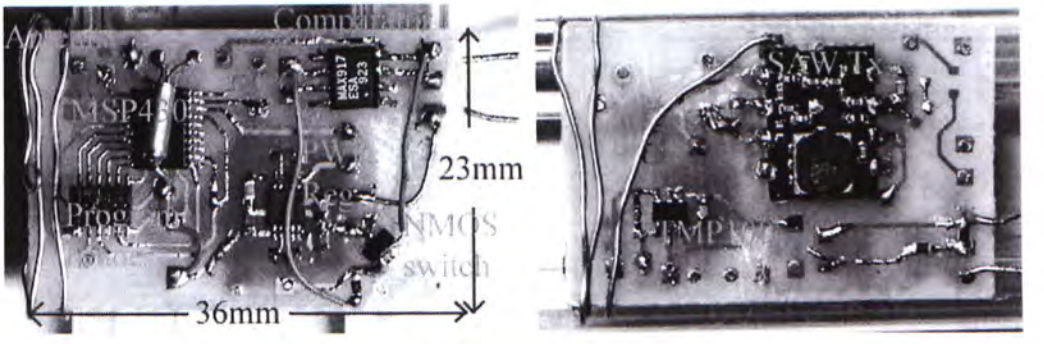

Figure 5.5: Photograph of prototype 4

5.3 Results

The main features of prototypes 1, 2 and 4 are summarized in table 5.1. Unfortunately, prototype 3 could not transmit since the noise from the power regulator coupled to the antenna via the supply biasing.

Prototype 4 is the only one (out of 4 prototypes) which can be powered by the MPG. The startup module was verified to provide stable operation for fifty transmission cycles by applying vibration to the system randomly. One of these experiments was recorded and a CRO screen capture is shown in figure 5.7. In the figure, the middle trace shows the voltage of comparator output, the comparator is used to switch on/off the application circuit. The bottom trace shows the voltage level of the system supply. The top trace shows the signal pin of the MCU (it is asserted when the MCU turns on). The startup time of power regulator was measured as 600 μs. The startup time of MCU was measured as 545.4 μs.

The power consumption of prototype 4 was measured and analyzed with the experiment setup shown in figure 5.8. A 2.0 V voltage supply is in series with a 22 $k\Omega$ resistor to emulate the MPG by limiting current entering the 1 mF storage capacitor to 27 μA (at 1.4 V to 2.0 V). The instantaneous current consumption can be acquired by measuring the voltage across 3 Ω resistor, thus, the instantaneous power consumption is calculated by multiplying the current across the resistor and the voltage across the storage capacitor. Table

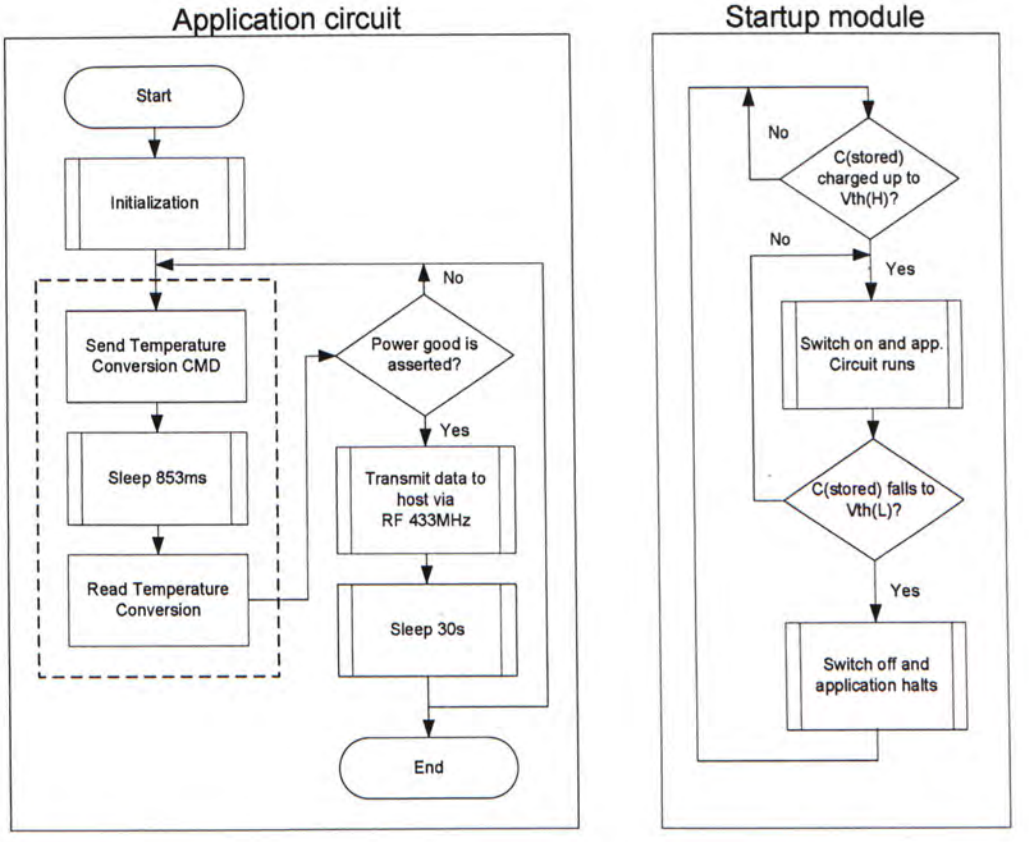

Figure 5.6: Operating flow chart of prototype 4

5.2 shows the measurement and the graphical representation is shown in figure 5.9. The total energy consumed for a single activation was measured as 212.62 μJ. 30 % of the total energy is consumed in the regulator startup and MCU initialization. This consumption can be avoided for consecutive temperature measurements if the MPG generates more power than the application circuit consumes in sleep mode (22.38 μW). 17 % of the total energy is consumed in temperature conversion. Wireless transmission consumed most of energy, 53 %. It takes 1.42 s for single measurement. During charging up by the MPG, the system has a 4.5 μA current consumption which is considered as the minimum overhead of the startup module. Therefore, the MPG must provide more than 4.5 μA supply current in order to keep the circuit continuously ready to accept activaation.

Prototype	1	2	4
MCU	SX28	PSoC	MSP430
TMP Sensor	DS1620	TMP100	TMP100
Power regulator	no	MCU built-in	switch cap
Input voltage (min.)	3 V	1.2 V	0.9 V
Shutdown mode	yes	yes	yes
Wakeup timer	no	yes	yes
RF transmitter	RC analog	LINX SAW-based	custom SAW-based
RF receiver	commercial radio	LINX ASK	LINX ASK
RF carrier frequency (in MHz)	FM band $(80-200)$	315, 418, 434	315, 418, 434 868 or 916
Tx range (in meters)	2	10	10
Dimensions ($L \times W \times H$ in cm^3)	$9 \times 7 \times 2$	$3 \times 3 \times 3$	$3.6 \times 2.3 \times 1$
Driven by MPG	no	no	yes

Table 5.1: The summary of prototype 1, 2 and 4

5.4 Summary

Four versions of wireless thermometers were designed, prototyped and evaluated. Prototype 4 was tested with the MPG. Its power consumption was carefully analyzed. The system takes 1.42 s for each temperature measurement and consumes 212.62 μJ of energy. To initiate the application, the MPG must generate more than a 4.5 μA supply current to charge up the storage capacitor and support the operation of the startup module. To maintain continuous system operation, the MPG must provide more than 22.38 μW power.

	Time taken	Energy Consumption		Power consumption
		Estimated	Measured (+Corrected)	Calculated
Reg. startup	600 μs	n/a	49.01 μJ + 0.006 μJ = 49.02 μJ	81.70 mW
uP startup	545.4 μs	n/a	14.944 μJ + 0.0928 μJ = 15.0368 μJ	27.57 mW
Temp conv.	1.4109 s	33.1875 μJ	18.855 μJ + 17.195 μJ = 36.05 μJ	25.55 μW
Wireless tx	4.167 ms	109.431 μJ	112.447 μJ + 0.06107 μJ = 112.509 μJ	27.00 mW
Sleep	t	20t μJ	22.38t μJ	22.38 μW
Total	(212.62 + 22.38t) μJ			

Table 5.2: Energy consumption statistics for startup and application circuit at each stage

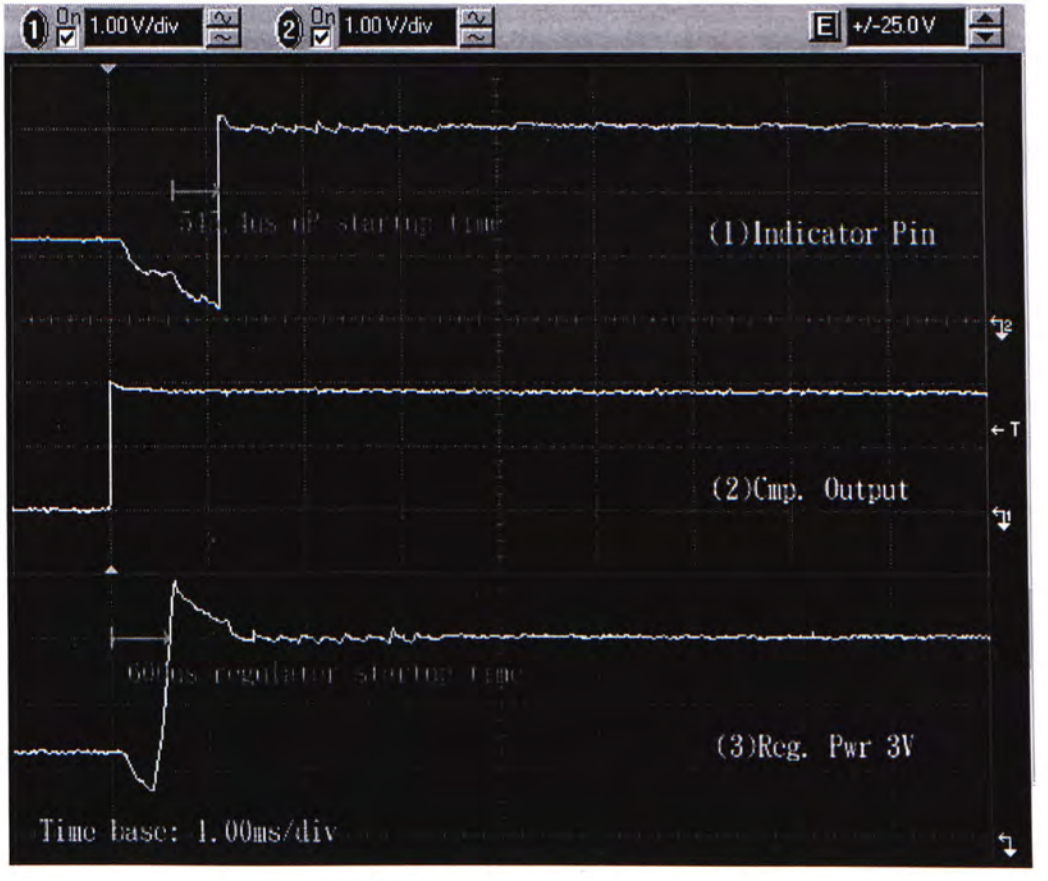

Figure 5.7: CRO screen capture for system startup

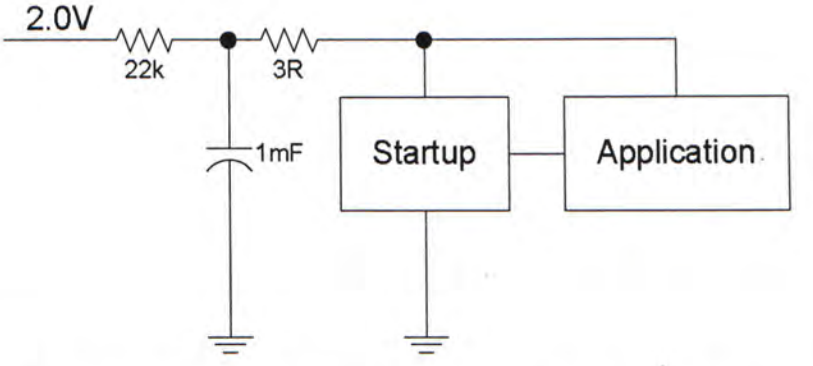

Figure 5.8: Setup for measuring power consumption of the startup and application circuit

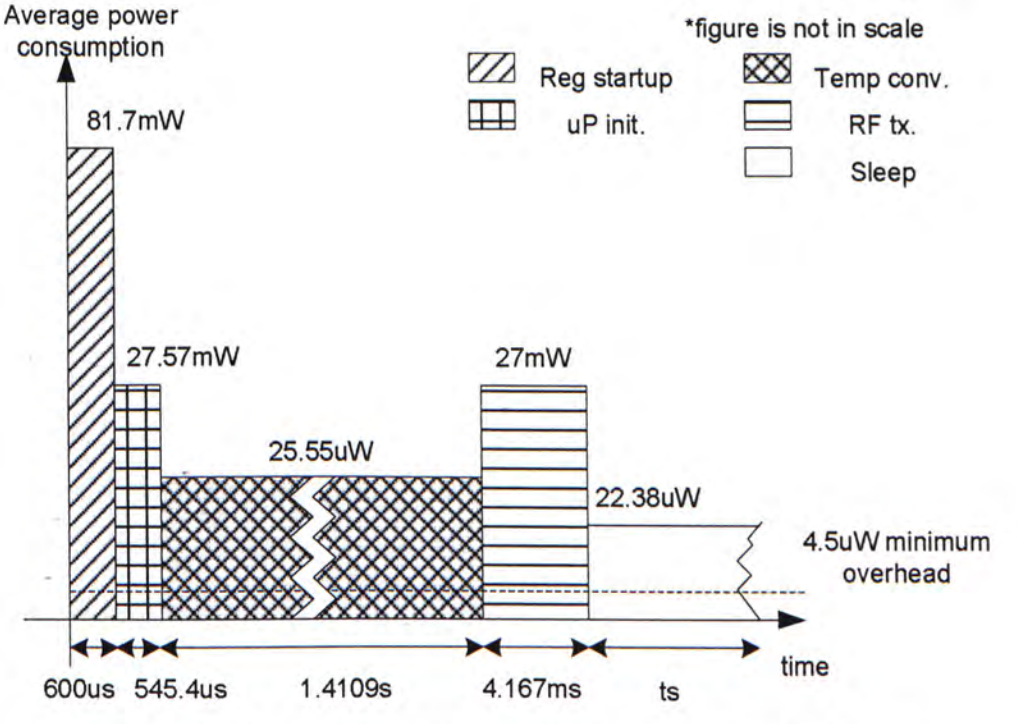

Figure 5.9: Average power consumption of the system in each stage

Chapter 6

Application II - 2D Input Ring

6.1 Overview

A 2D input ring was implemented to demonstrate the utility of the generic platform (GP) described in chapter 4. The ring is a device for ubiquitous computing, such as controlling a Personal Computer (PC). The current prototype is able to emulate a computer mouse via RF RS232 port. It is also able to control home appliances and portable electronics equipped with an infrared or IrDA transceiver.

6.2 Architecture

The hardware architecture of the 2D input ring is based on a low power wireless sensor platform (excluding the startup module). A battery is used to support continuous operation. In order to detect finger motion, an accelerometer (iMEMS ADXL202E) is installed. The illustrative drawing of the 2D/3D ring is shown in figure 6.1. The 2D ring consists of two 2 $cm \times 2$ cm PCB boards which communicate via a connector. Photographs of both boards are shown in figures 6.2 and 6.3. Besides the two axis accelerometer, the 2D ring consists of a MSP430 microcontroller, power management circuit, RF transmitter, a program socket, 2 buttons (B1, B2) and a LED indicator. The program socket

has two functions: to connect to host a computer for MCU programming and to connect interface add-on modules, such as an IrDA [3] transceiver, Liquid Crystal Display (LCD), external flash storage, etc. Figure 6.4 shows the prototype PCB which was made using a PCB rapid prototype machine. The prototype PCB was used to verify the spacing and width of the tracks and pads before fabrication.

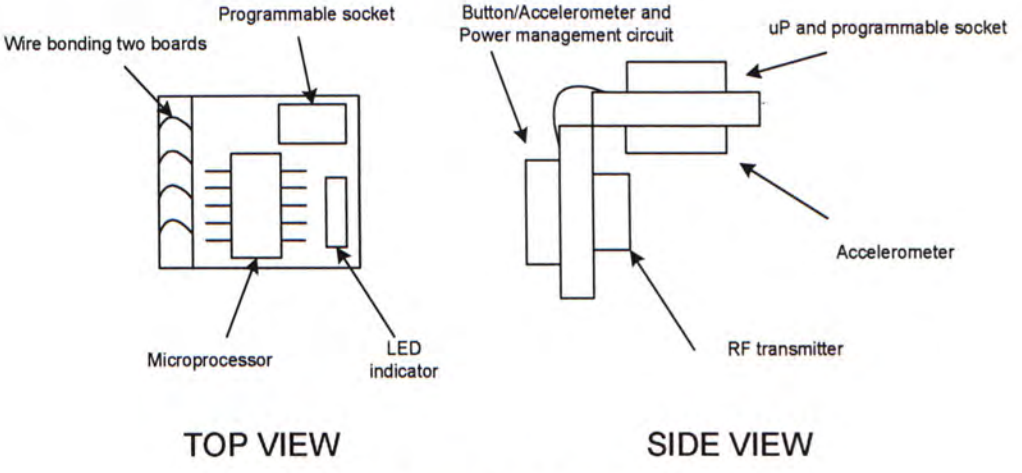

Figure 6.1: Illustrative drawing of 2D ring

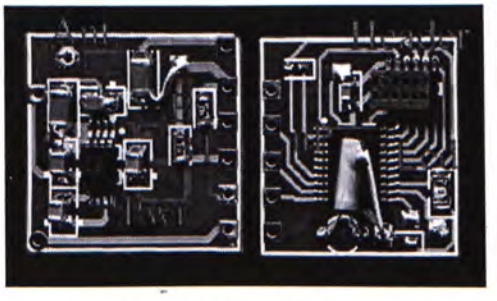

Figure 6.2: Photograph of ring board (top view)

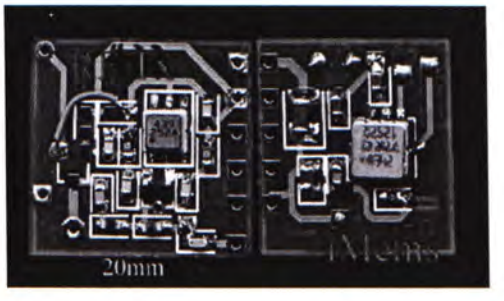

Figure 6.3: Photograph of ring board (bottom view)

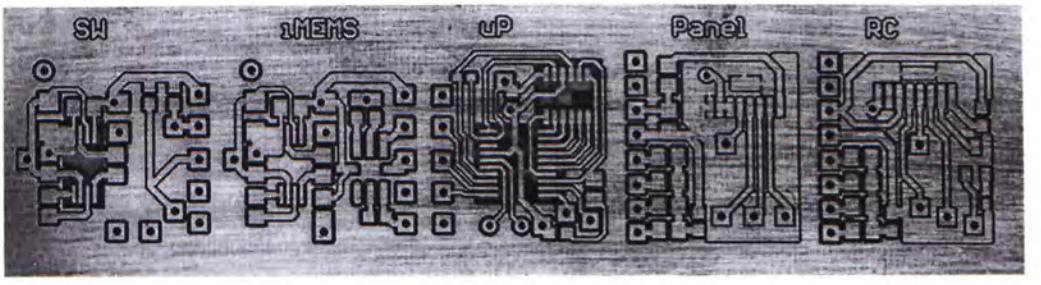

Figure 6.4: Rapid prototype of 2D Ring boards

6.3 Software Implementation

6.3.1 Methodology

The wireless ring detects the motion of an accelerometer which measures 2 perpendicular axes. The accelerometer is placed horizontally (and perpendicular to gravity). Since gravity is a constant accelerating force to all objects on the earth, therefore, the accelerometer reports different readings, depending on its orientation. The cursor is driven up, down, left or right by rotating left/right or pointing up/down. The idea is illustrated in figure 6.5.

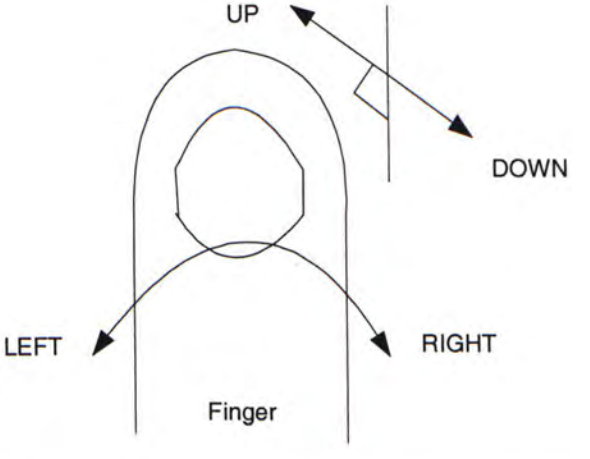

Figure 6.5: The operation details of 2D ring

6.3.2 Error Control Code

An error control code is used to maintain data integrity from one system to another via the noisy wireless channel. There are many kinds of error control coding schemes; some of them detect errors and some of them detect and correct errors, e.g. hamming codes, turbo codes, etc. Sometimes, errors may not relate to the transmission channel but to the architecture itself. For example, to save power, the SAW RF transmitter turns off its oscillator when transmitting *0*. However, the SAW oscillator's startup time and turn-off time is not the same. This non-symmetrical property limits the data rate. To overcome this problem, a Manchester code is introduced. The Manchester code represents binary data with edge transitions, the so-called biphase code. It improves the data rate of a SAW RF transmitter from 2.4 $kbit/s$ to 4.8 $kbit/s$. The ring system is not only protected by an outer code (Manchester code), but also by an inner code (XOR check sum). Both techniques are used to detect errors, and detected faulty packets are discarded. Compared to error correction codes, an error detection code is more suitable for a ring system because:

1. the error detection code used is simple and consumes less computation time, therefore faster response time is achieved;

2. for the computer mouse application, a numerous data is generated to describe the trajectory of the cursor. Loss of packets is not terribly important (assuming no burst error), since the errors caused by missing packets can be corrected almost subconsciously by the user.

The diagram in figure 6.6 explains Manchester encoding on the transmitter side. Data words to be transmitted are buffered in a 16-bit register and they are clocked out sequentially by an interrupt timer. When data is ready, 8 bits of data is stored into the low byte of a data buffer, and the high byte of the

data buffer is used to store the 8 bit data's complement. For 4800 bit/s, a 9600 Hz timing interrupt is required. When the MCU is interrupted by the timer, the least significant bit (LSB) of the data buffer is transmitted. Then the complement and data byte are swapped. The complement bit (now in the data byte) is clocked out on the next interrupt arrived. The 16-bit data register is then shifted after both bits are sent. The *send and shift* process repeats until 8 bits of the data are processed. The transmitted byte ends up in the low byte of the data buffer as a by-product. For the receiver side, a GPIO pin, a timer and a register are used to decode the data. A GPIO pin detects edge transitions and a timer records the elapsed time between two consecutive transitions. A register is used to store the received data. Figure 6.7 gives the nature of the Manchester coded bits. The figure shows two consecutive received bits: the previous bit and the current bit. *R-R/F-F* denotes a rising/falling edge is followed by a rising/falling edge. *R-F/F-R* denotes a rising/falling edge is followed by a falling/rising edge. If the previous bit is known, the current bit value can be extracted by observing the elapsed time between previous and current edges. Rather than measure the precise rise and fall time, *Nbound*, *Sbound* and *Bbound* are used to check whether the time measured is in the accepted range. It is worthwhile to mention that Manchester coding requires tight alignment of the data. Figure 6.8 shows the packet format which enables independent alignment of each packet. Each packet contains a *PREAMBLE*, *CMD*, three data bytes (*D1, D2, D3*) and *CHKSUM*. PREAMBLE is used to align each packet. The CMD byte is reserved for control signals. The CHKSUM verifies the correctness of the three data bytes (D1, D2, D3).

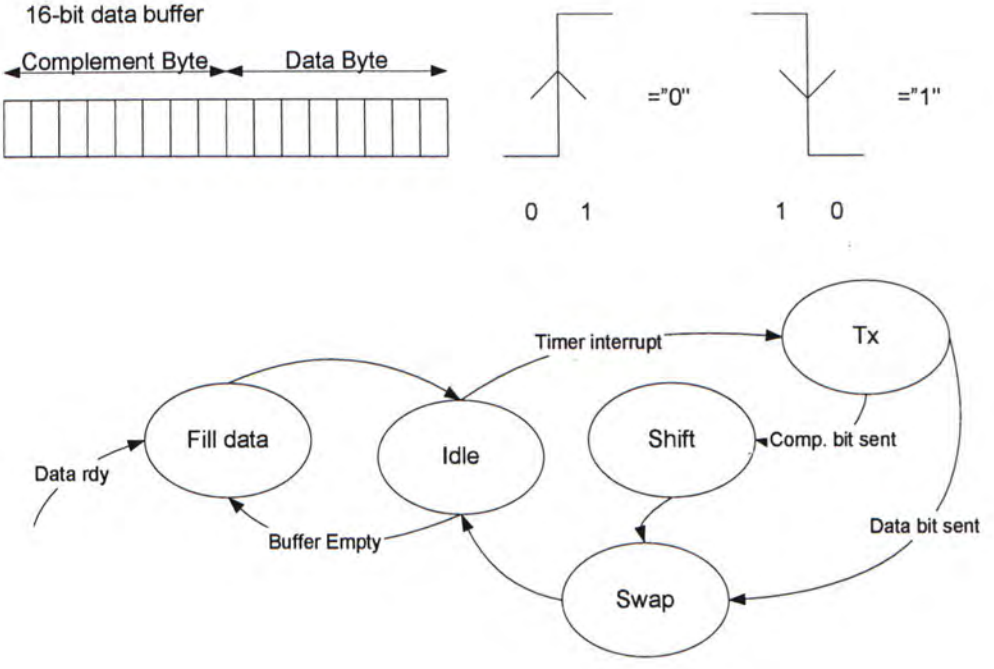

Figure 6.6: State diagram explains Manchester encoding

6.3.3 Peripheral Control Protocol

MS Serial Computer Mouse

The Microsoft [8] (MS) serial computer mouse protocol was implemented, based on [10, 12], so that the 2D ring can be used directly on any PC OS with generic mouse support. The data packet format for the MS mouse protocol is shown in figure 6.9. Three bytes are used to describe the displacement of the cursor. The first byte describes the status of the mouse's *left* and *right* buttons. It also stores the two most significant bits of the X and Y displacement. The second and third bytes store the remaining data bits of the X and Y displacement. For the receiver side, minimal handshaking was implemented to acknowledge the host via the *RS*232 port, so that the computer mouse client is recognized by the host computer.

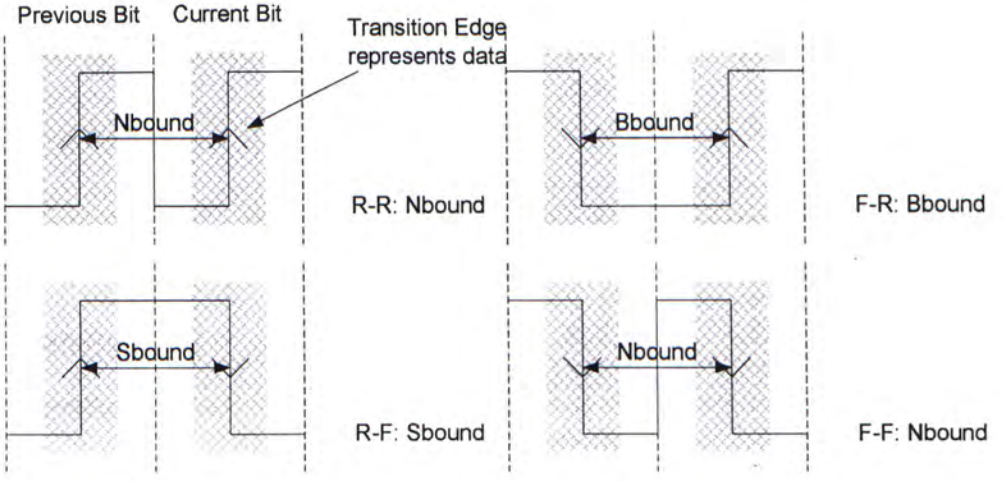

Figure 6.7: Timing diagram 1 explains Manchester decoding

Figure 6.8: Data packet format for wireless transmission

Protocol for Smart Appliances and PDAs

For controlling the portable electronics remotely, infrared was the first carrier widely used. Many electronic devices, including MP3 players, TV, HiFi, etc., come with an infrared remote control. Infrared has advantages over other wireless carriers in that it is low cost and simple to implement. For short range and low data rate transmission, many data coding methods exist (different manufacturers use different coding schemes) and their operating details were explained in section 4.2.4.

To illustrate its remote control ability, a 2D input ring was programmed to be a 2-button remote control pad for a film camera. The coding scheme of the film camera was recovered by observation of the infrared signals using an IrDA transceiver and digital oscilloscope. The data word format was recognized as a space code and is shown in figure 6.10. Each data packet is formed by a preamble and 7 bits of data. In each packet, *high* is represented by a 38.46 kHz signal train (38/62 duty cycle) and *low* is represented by a ground

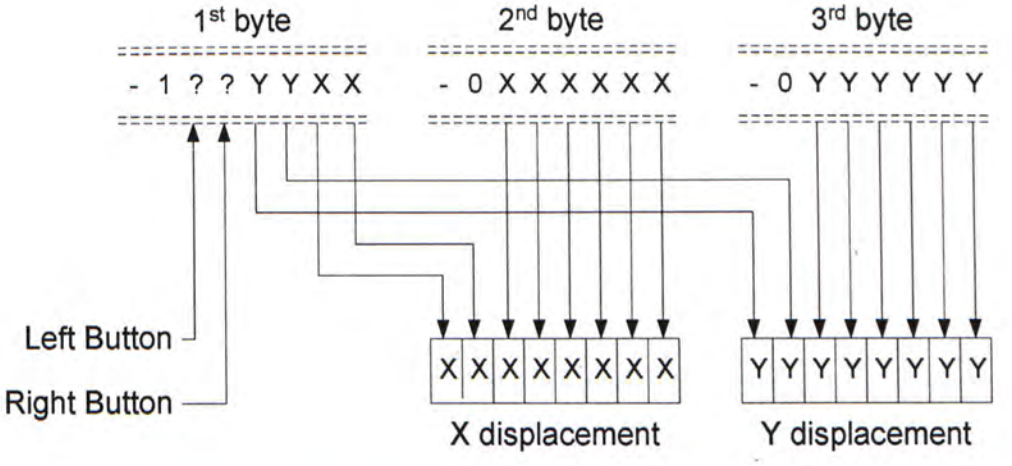

Figure 6.9: Data packet format for MS mouse protocol [10, 12]

level. A preamble is constructed by sending high for 12.945 ms and then low for 3.032 ms. 7 bits of data are then sent, with each bit coded by the space between two consecutive signal highs, where a 1 ms space represents *0* and 3 ms space represents *1*. Figure 6.11 shows the CRO screen capture of two data words from the Pentax film camera's remote control. The top trace shows the data word of key 1 in inverted manner (from the view of receiver). The middle trace shows the data word of key 2 in complement. The bottom trace shows the data word of key 2 emulated by the ring (transmitter output). The remote control protocol was implemented on the 2D ring and it was verified using the camera. Figure 6.12 shows the photograph of the 2D remote control ring.

6.4 Results

The 2D ring was successfully tested as a computer mouse. The basic functions such as move, button click, and button drag and drop were implemented and verified. A fully charged NiMH battery (rated at 2.4 V and 15 $mAhr$) can

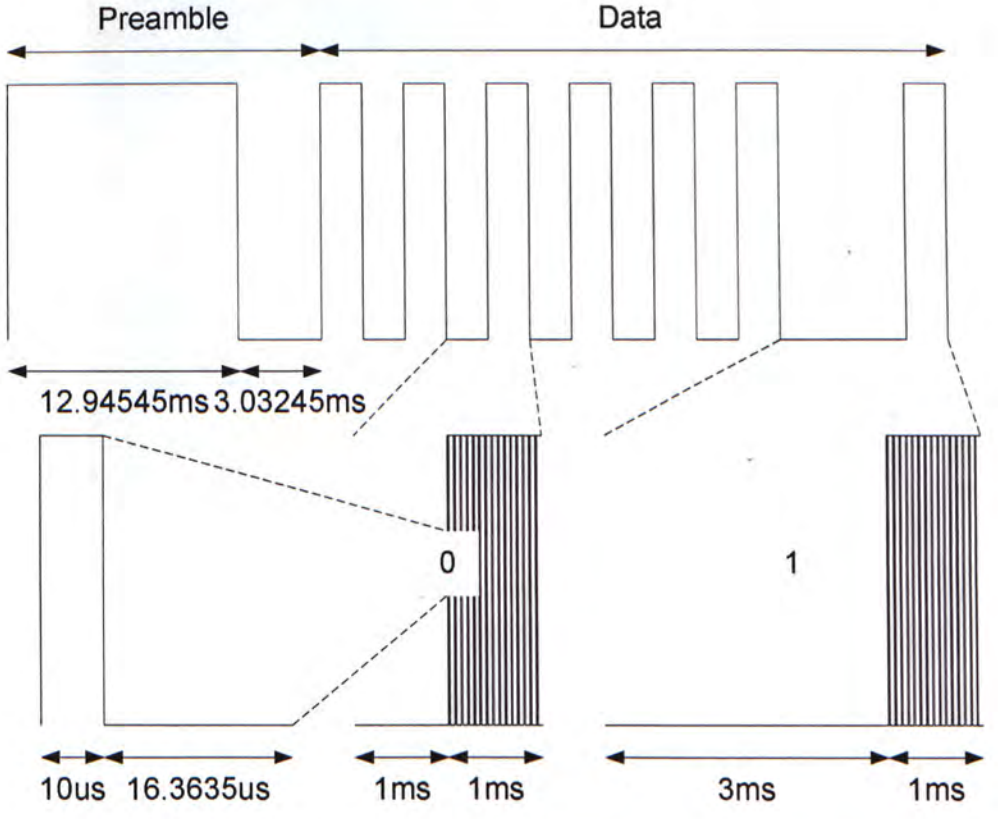

Figure 6.10: Space code example for Pentax camera remote control

support the 2D ring for 1.5 hour continuous operation (an average power consumption of 24 mW). The transmission range was tested for 3 meters with transmission power of -58.33 dBm. Figures 6.13 and 6.14 show the measurements of transmission power with a spectrum analyzer and a 1/4 wavelength monopole antenna. Table 6.3 gives a summary of the 2D ring. The output voltage ripple on the system supply rail was measured to be 12.4 mV. The output precision of the accelerometer was measured to be 7 bits. Table 6.4 shows the comparison between Lam's MIDS ring [22] and the 2D ring. The 2D ring outperforms the MIDS ring in terms of power consumption and output accuracy of the accelerometer (the accelerometer's output noise was measured as low as 0.29% (-50.75 dB) $<$ 7-bit (-42.14 dB)) because special attention was paid in choosing the voltage regulator (to reduce output ripple and achieve

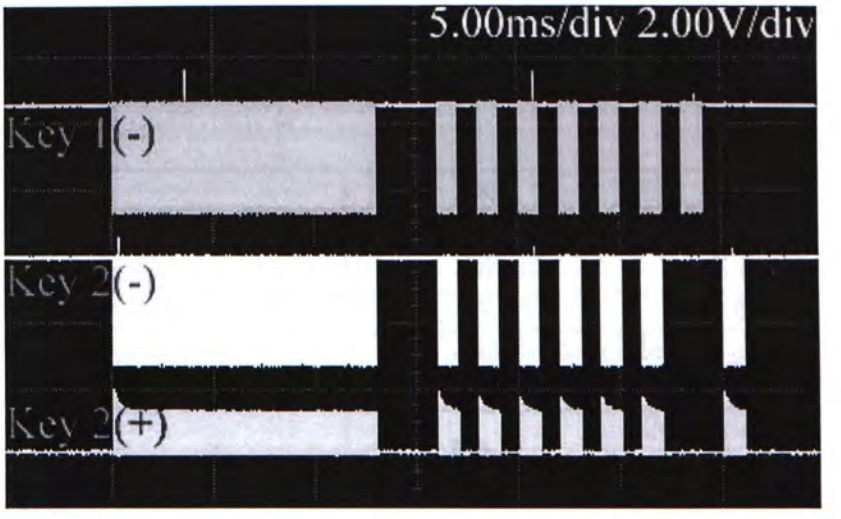

Figure 6.11: CRO screen capture of Pentax remote control data word

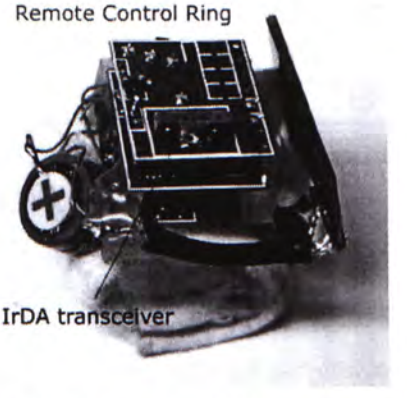

Figure 6.12: Photograph of 2D remote control ring

higher efficiency) and inserting decoupling capacitors (to minimize noise generated by the RF transmitter being coupled to the accelerometer). Figures 6.15 to 6.18 show photographs of the 2D ring (TX/RX) modules and the 2D ring demo kit.

	Rx	Tx
Dimension (W, L, H)	$4.5 \times 4.5 \times 4\ cm^3$	$1.8 \times 2 \times 2\ cm^3$
Power consumption	$25\ mA$@$3.3V$	$7.5\ mA$@$3.3V$
Input supply voltage	$1.8 - 5.0\ V$	$1.8 - 3.6\ V$
RF error control code	Manchester code and check sum	
RF carrier frequency	$433\ Mhz$	
RF TX power	n.a.	$-24.39\ dBm$ (at $0.01\ m$) $-58.33\ dBm$ (at $3\ m$)
RF Tx range	$3\ m$	
RF data rate	$4800\ bps$	
RS232 data rate	1200 baud rate	
Supply rail ripples	$100\ mV$	
Accelerometer output accuracy	n.a.	7-bit (0.29% noise)
MCU model	MSP430F1132	
MCU utilization	17.36 %	10.67 %

Table 6.1: Design summary of 2D input ring

	Lam's MIDS	2D input ring
Dimension(W, L, H)	$2\ cm \times 3\ cm \times 1\ cm$	$1.8\ cm \times 2\ cm \times 2\ cm$
Power consumption	$35\ mW$	$25\ mW$
Minimum input voltage	$3.5\ V$	$1.8\ V$
RF Transmission rate	$2400\ bps$	$4800\ bps$ with Manchester code
RF Transmission range	$3\ m$	$4\ m$
OS dependent	Yes	No

Table 6.2: Comparisons between Lam's MIDS and 2D input ring

	Rx	Tx
Dimension (W, L, H)	$4.5 \times 4.5 \times 4\ cm^3$	$1.8 \times 2 \times 2\ cm^3$
Power consumption	$25\ mA$@$3.3V$	$7.5\ mA$@$3.3V$
Input supply voltage	$1.8 - 5.0\ V$	$1.8 - 3.6\ V$
RF error control code	Manchester code and check sum	
RF carrier frequency	$433\ Mhz$	
RF TX power	n.a.	$-24.39\ dBm$ (at $0.01\ m$) $-58.33\ dBm$ (at $3\ m$)
RF Tx range	$3\ m$	
RF data rate	4800 *bps*	
RS232 data rate	1200 baud rate	
Supply rail ripples	$100\ mV$	
Accelerometer output accuracy	n.a.	7-bit (0.29% noise)
MCU model	MSP430F1132	
MCU utilization	17.36 %	10.67 %

Table 6.3: Design summary of 2D input ring

	Lam's MIDS	2D input ring
Dimension(W, L, H)	$2\ cm \times 3\ cm \times 1\ cm$	$1.8\ cm \times 2\ cm \times 2\ cm$
Power consumption	$35\ mW$	$25\ mW$
Minimum input voltage	$3.5\ V$	$1.8\ V$
RF Transmission rate	2400 *bps*	4800 *bps* with Manchester code
RF Transmission range	$3\ m$	$4\ m$
OS dependent	Yes	No

Table 6.4: Comparisons between Lam's MIDS and 2D input ring

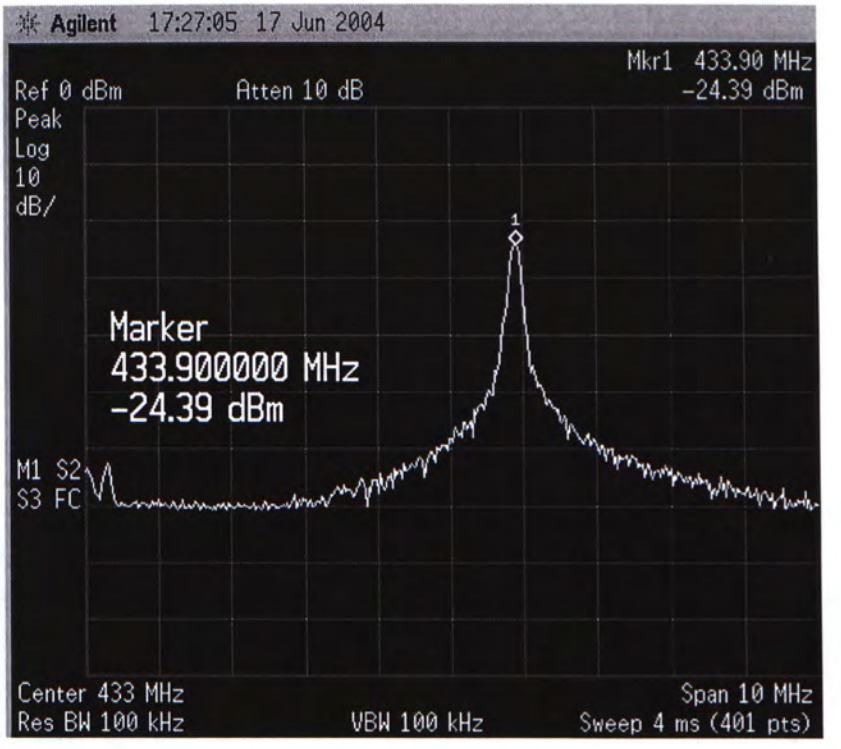

Figure 6.13: Transmission power of the 2D ring at 1 cm

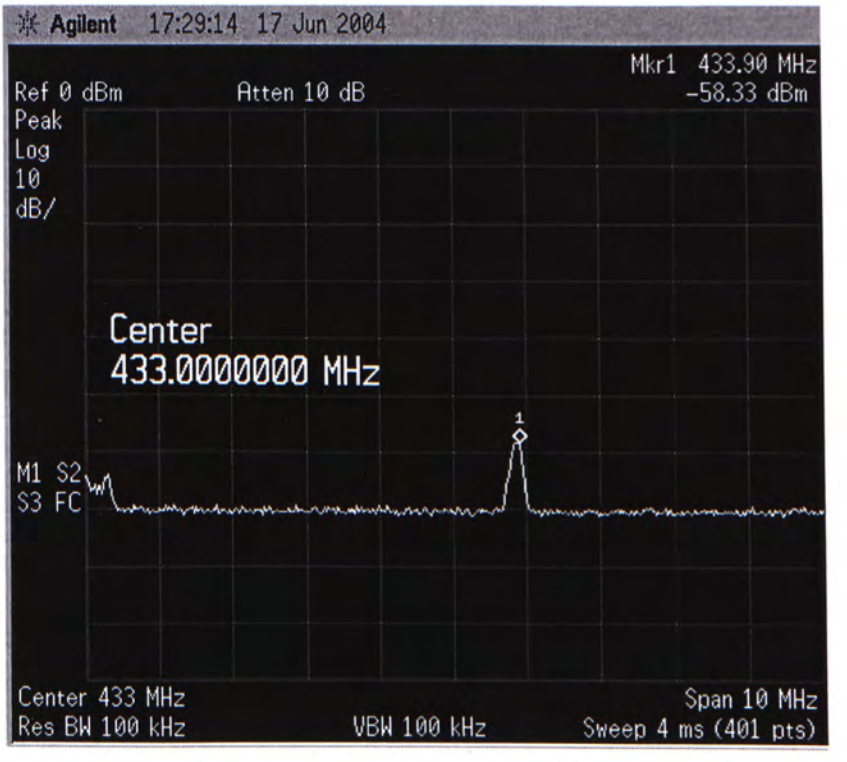

Figure 6.14: Transmission power of the 2D ring at 3 m

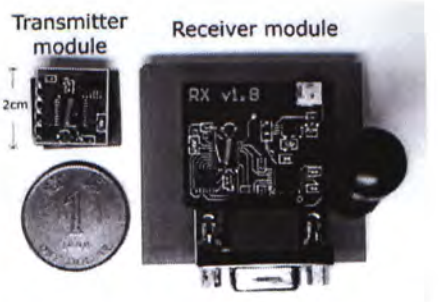

Figure 6.15: Photograph of 2D ring modules

Figure 6.16: Photograph of 2D ring receiver

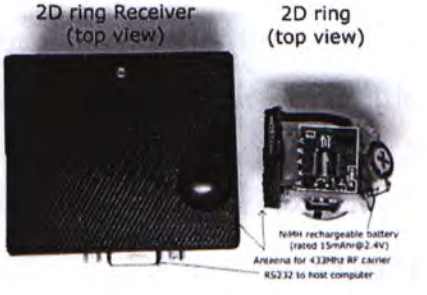

Figure 6.17: Photograph of 2D ring demo kit (top view)

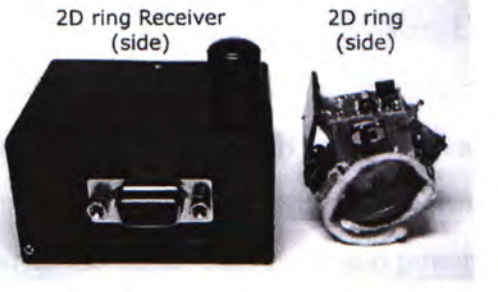

Figure 6.18: Photograph of 2D ring demo kit (side view)

6.5 Summary

In this chapter, a 2D input ring based on a generic low power wireless sensor platform (GLPWSP) was presented. This GLPWSP is useful in ubiquitous computing because it introduces an alternative user interface. The 2D input ring also outperforms Lam's MIDS (wireless version) in terms of power consumption and software portability because the ring requires no custom software driver installation, and thus is not operating system (OS) dependent.

Chapter 7

Conclusion

A generic system for low power wireless sensor applications was presented. It consists of a vibration-to-electrical transducer, power management circuit and generic sensor platform. The whole system is divided into two parts: a micro power generator (MPG) and a generic low power wireless sensor platform (GLPWSP). The MPG contains a vibration-to-electrical transducer and power management circuit. The GLPWSP contains sensor peripherals and a startup circuit.

7.1 Micro power generator

An AA-size micro power generator (MPG) was introduced. It is a battery replacement for low power wireless sensor applications. The MPG converts ambient vibration to electrical energy and is a non-exhaustible power source. It has a power management circuit which consists of a voltage multiplier (VM) and regulator which converts AC to a regulated DC voltage at a level usable by standard integrated circuits. VMs were evaluated by PSpice simulations and two evaluation metrics, average input power (AIP) and energy efficiency (EE) suggested. These metrics can also be used to evaluate other duty cycled AC-DC power converters. The voltage tripler had the best performance, achieving 53 % energy efficiency. With input acceleration of 4.63 m/s^2, the measured

power density of the MPG was 53.1 $\mu W/cm^3$. Maximum output voltage was measured to be 2.4 V. The MPG was measured to take 32 seconds to charge the reservoir capacitor (1 mF) from 0 V to 1.8 V. The recharge time was measured to be 18 seconds for charging the 1 mF capacitor from 1.4 V to 1.8 V.

7.2 Low power wireless sensor applications

A generic platform (GP) was presented for low power wireless sensor applications. It can be used to measure the properties of the environment and transmit data via a radio frequency (RF) channel. The GP is multi-functional and can measure temperature, acceleration, humidity or sound level with an appropriate sensor. Besides sending information to the host via RF, the GP can store the information in non-volatile memory (flash memory). Two applications were presented to show its utility.

7.2.1 Wireless thermometer

A wireless thermometer was designed and tested using the AA-size MPG as a power source. Equipped with a startup module, the wireless thermometer consumes only 4.5 μW in the idle state. The startup module turns on the wireless thermometer when the storage capacitor is charged to a predefined voltage (1.8 V). The wireless thermometer then takes 1.42 s to measure and transmit the temperature reading. The whole process consumes 212.62 μJ of energy, 30 % of the total energy being consumed in the regulator startup and MCU initialization. Wireless transmission consumes 53 % of the energy. The wireless thermometer with MPG is the first reported sensor system which can be both self powered and startup antonomously.

7.2.2 2D input ring

The 2D input battery powered ring is a miniature device for ubiquitous computing. It also demonstrated that the GLPWSP can be used for battery powered applications, which require similar features to the VBG based applications, ie. low power, small size, wireless and easy to integrate with different sensors. The 2D input ring can be used as a mouse and control a personal computer. Besides RF communications, the 2D input ring can control other appliances via an IrDA module. As an example, the 2D input ring was programmed to be a remote control pad which can operate with Pentax camera (zoom and shoot).

Instead of mechanical buttons, the 2D ring can recognize strokes or gestures and send commands to other devices via infrared or radio frequency channels. This introduces an alternative user interface which can be worn at all times and serve as an interface to multiple appliances.

Compared to Lam's MIDS [22], the 2D input ring has lower power consumption and higher output resolution.

7.3 Further development

The 2D input ring can be upgraded to detect 3D motion and be powered by the vibration-based micro power generator. The input ring can be completely shielded by a metal case with planar antenna on the surface. The ring requires no batteries because it is self-powered by vibrations.

Many applications can be derived for the input ring. A more robust algorithm can be developed in order to recognize finger strokes or gestures. For speech recognition, a speech algorithm, such as the Hidden Markov Model (HMM), can be applied to with slight modifications. With proper data set training and vector quantization, a compactly coded HMM system should fit on the ring.

Equipped with recognition ability, the ring acts as a communication interface between electronic appliances and humans. In the future, computer users need not to put their hands on a keyboard or a computer mouse. Instead of being confined to working on a surface, users' finger can be used to write freely in the air to command other devices via ad hoc network (similar to the idea of pico net in Bluetooth).

The 2D input ring is a good example of GLPWSP, however it is not the only one. Based on GLPWSP, scientists can design different kinds of sensor nodes to monitor different quantities. They can monitor the environmental factors (humidity, temperature, sunshine) of natural places, such as wetlands. A group of modified sensor nodes (equipped with RFID [39]) can be placed in a commercial center to track buying habits of consumers. A GP which contains MEMS sensors, microprocessor and a wireless transceiver has nice properties: low power and small size and is likely to become standard for pervasive computing. As technologies advance, miniature wireless sensor systems will become feasible and many new applications will emerge.

Bibliography

[1] Federal Standard 1037C. Manchester code.
http://www.its.bldrdoc.gov/fs-1037/dir-022/_3206.htm.

[2] R Amirtharajah and A.P. Chandrakasan. Self-powered signal processing using vibration-based power generation. In *IEEE Journal of Solid-State Circuits*, volume 33, pages 687–695, May 1998.

[3] The Infrared Data Association. Official homepage of IrDA.
http://www.irda.org.

[4] Marshall Brain. Howstuffworks "how motes work".
http://computer.howstuffworks.com/mote2.htm.

[5] Neil N.H. Ching, H.Y. Wong, Wen J.Li, and Philip H.W. Leong. A laser-micromachined vibrational to electrical power transducer for wireless sensing systems. In *the 11th International Conference on Solid-State Sensors and Actuators*, volume A: Physical, Munich, Germany, 2001.

[6] Ansoft Corporation. HFSS official product homepage.
http://www.ansoft.com/products/hf/hfss/.

[7] Atmel Corporation. Smart RF Wireless Data Microtransmitter, 2003.
http://www.atmel.com/dyn/resources/prod_documents/doc1424.pdf.

[8] Microsoft Corporation. Microsoft Official Homepage.
http://www.microsoft.com.

[9] Best Sound Electronics. Official homepage of BSE, 2003.
http://www.bsecm.com/e_index.asp.

[10] Tomi Engdahl. PC mouse information.
http://www.hut.fi/~then/mytexts/mouse.html.

[11] Rudolf F Graf and William Sheets. *Build Your Own Low-Power Transmiiter - Projects for the Electronics Experimenter.* Newnes, 225 Wildwood Avenue, Woburn MA 01801-2041, 2001.

[12] Gruime. Mouse Protocol.
http://wwww.everything2.com/?node=Mouse+protocol.

[13] Jason L. Hill and David E. Cullier. A wireless platform for deeply embedded networks. *IEEE mico magazine*, 22(6), 2002.
http://www.cs.berkeley.edu/~culler/cs294-f03/papers/micaarch.pdf.

[14] Horowitz and Hill. *The Art of Electronics.* Cambridge University Press, The Edinburgh Building, Cambridge CB2 2RU, UK, 1999.

[15] Analog Devices Inc. Low-Cost ±2 *g* Dual-Axis Accelerometer With Duty Cycle Output Data Sheet (Rev. A, 10/00), 2000.
http://www.analog.com/UploadedFiles/Data_Sheets/567227477ADXL202E_a.pdf%.

[16] Nippon Precision Circuits INC. SM5021 series crystal oscillator module ICS, 1999.
ftp://ftp.npc.co.jp/pub/pdf_e/nc9903ae.pdf.

[17] RF Monolithics Inc. Antenna Lenghts.
http://www.rfm.com/products/apnotes/antennalengths.pdf.

[18] RF Monolithics Inc. Antennas for Low Power Applications.
http://www.rfm.com/corp/appdata/antenna.pdf.

[19] Texas Instruments Incorporated. Digital Temperature Sensor with i^2c Interface, 2003.
http://www-s.ti.com/sc/ds/tmp100.pdf.

[20] Texas Instruments Incorporated. MSP430x1xx Family User's Guild (Rev.D), 2004.
http://focus.ti.com/lit/ug/slau049d/slau049d.pdf.

[21] Texas Instruments. Interfacing the MSP430 and TMP100 I2C Temperature Sensor, 2002.
http://www-s.ti.com/sc/psheets/slaa151/slaa151.pdf.

[22] Alan H. F. Lam. Micro Input Devices System MIDS: Using MEMS sensors and wireless technology for generalized computer interface functions. In *Proceedings of the 4th ACM Postgraduate Research Day 2003*, Hong Kong, 2003.

[23] Johnny M.H. Lee, Steve C.L. Yuen, Wen J. Li, and Philip H.W. Leong. Development of an AA size energy transducer with micro resonators. In *Proceedings of IEEEE/ICECS*, pages 876–879, 2002.

[24] W.J. Li, Z.Y. Wen, P.K. Wong, G.M.H. Chan, and P.H.W. Leong. A micromachined vibration-induced power generator for low power sensors of robotic systems. In *Proc. of the World Automation Congress*, Hawaii, USA, 2002.

[25] Scott Meninger, Jose Oscar Mur-Miranda, Rajeevan Amirtharajah, Anantha P. Chandrakasan, and Jeffrey H. Lang. Vibration-to-electric energy

conversion. In *IEEE transaction on Very Large Scale Integration System*, volume 9, pages 64–76, Feb 2001.

[26] Cypress MicroSystem. Datasheet of PSoC, 2003.
`http://www.cypress.com/cfuploads/img/products/CY8C26443.pdf`.

[27] Paul D. Mitcheson, Tim C. Green, Eric M. Yeatman, and Andrew S. Holmes. Architectures for vibration-driven micropower generators. In *Journal of Microelectromechanical Systems*, volume 13, pages 429–440, Jun 2004.

[28] Elizabeth D. Mynatt, Anne-Sophie Melenhorst, Arthur D. Fisk, and Wendy A. Rogers. Aware Technologies for Aging in Place: Understanding User Needs and Attitudes. In *IEEE Pervasive Computing*, volume 3, pages 36 – 41, April-June 2004.

[29] Department of Automation and Computer-Aided Engineering. ACAE official homepage.
`http://www.acae.cuhk.edu.hk`.

[30] Department of Computer Science and Engineering. CSE official homepage.
`http://www.cse.cuhk.edu.hk`.

[31] The Chinese University of Hong Kong. CUHK official homepage.
`http://www.cse.cuhk.edu.hk`.

[32] Maxim Integrated Products. SOT23, 1.8V, Nanopower, Beyong-the-Rails Comparators With/Without Reference, 1999.
`http://pdfserv.maxim-ic.com/en/ds/MAX917-MAX920.pdf`.

[33] Maxim Integrated Products. DC-DC Convertor Tutorial, 2000.
`http://pdfserv.maxim-ic.com/en/an/AN710.pdf`.

[34] Maxim Integrated Products. DC/DC Conversion without Inductors, 2000.
http://pdfserv.maxim-ic.com/en/an/AN725.pdf.

[35] Maxim Integrated Products. 1.5μa i_Q, Step-Up DC-DC Converters, 2001.
http://pdfserv.maxim-ic.com/en/ds/MAX1722-MAX1724.pdf.

[36] Bob Nelson RFM. High Data Rate SAW-Stabilized ASK Transmitter, 2003.
http://www.rfm.com/products/apnotes/highdataratesaw.pdf.

[37] Jie Nie RFM. SAW Based Transmitter Design Notes, 2003.
http://www.rfm.com/products/apnotes/sawbasedtransmitter.pdf.

[38] Bjorn Rhoads. a general remote control program ver3.4, 1995.
http://www.rhoads.nu/bjorn/hp48/remote/remote.html.

[39] Mark Roberti. RFID Journal.
http://www.rfidjournal.com/.

[40] S.J. Roundy. *Energy Scavenging for Wireless Sensor Nodes with a Focus on Vibration to Electricity Conversion.* PhD thesis, May. 2003.
http://engnet.anu.edu.au/DEpeople/Shad.Roundy/paper/ShadThesis.pdf.

[41] Cotter W. Sayre. *Complete Wireless Design.* McGraw-Hill Professional, 2001.

[42] Cypress Semiconductor. Cypress Microsystems homepage, 2003.
http://www.cypressmicro.com.

[43] DALLAS Semiconductor. DS1620 digital thermometer and thermostat, 1999.
http://pdfserv.maxim-ic.com/arpdf/DS1620.pdf.

[44] National Semiconductor. National's New Revolutionary Microphone Amplifiers.
http://www.national.com/appinfo/amps/microphone.html.

[45] Leo Setian. *Practical Communication Antenna with Wireless Applications.* 1998.

[46] LINX technologies Ltd. LINX LC series transmitter datasheet, 1999.
http://www.rfdigital.com/pdf/rfd24003.pdf.

[47] UBICOM. SX20AC/SX28AC configurable communications controllers with EE/FLASH program memory, in-system programming capability and on-chip debug, 2001.
http://www.ubicom.com/pdfs/products/sx/processor/
SX-DDS-SX2028AC-16.pdf%.

[48] UCLA. WINS wireless integrated network sensors, 1993-1999.
http://www.janet.ucla.edu/WINS.

[49] Berkeley Univerisity of California. UC Berkeley Homepage, 2003.
http://www.berkeley.edu/.

[50] Berkeley University of California. Tiny OS, a component-based OS for the networked sensor regime, 2003.
http://webs.cs.berkeley.edu/tos/.

[51] LA University of California. UCLA homepage, 2003.
http://www.ucla.edu.

[52] Arie van Rhijn. Digital Microphones - Applications and System Partitioning, 2003.
http://www.national.com/nationaledge/apr03/article.html.

[53] Tony van Roon. Phase-Locked Loop Tutorial, 2001. `http://www.uoguelph.ca/~antoon/gadgets/pll/pll.html`.

[54] S. Vardhan, M. Wilczynski, G.J. Portie, and W.J. Kaiser. Wireless integrated network sensors (wins): distributed in situ sensing for mission and flight systems. In *Aerospace Conference Proceedings*, volume 7, pages 459–463, March 2000.

[55] C.B. Williams, C. Shearwood, M.A Harradinem, P.H. Meller, T.S. Birch, and R.B. Yates. Development of an electromagnetic microgenerator. In *Circuits, Devices and System, IEE proceedings*, volume 148, pages 1883–1884, Dec. 2001.

Publications

Full length conference paper

- Johnny M. H. Lee, Steve C. L. Yuen, Mimi H. M. Luk, Gordon M. H. Chan, Kin Fong Lei, Wen J. Li, Philip H. W. Leong, and Yeung Yam, "AA Size Power Cell for Wireless Applications Using Micro-Fabricated Resonators", *Asia-Pacific Conference of Transducers and Micro-Nano Technology (APCOT MNT 2004)*, July 2004, Japan.

- Steve Yuen, Johnny M. H. Lee, Mimi Luke, Gordon Chan, Philip HW Leong, Wen J. Li, and Yeung Yam, "AA size micro power conversion cell for wireless applications", *5th World Congress on Intelligent Control and Automation*, June, Hangzhou, China.

- Johnny M. H. Lee, Steve C. L. Yuen, Wen J. Li, and Philip H. W. Leong, "Development of an AA-Size Energy Transducer with Micro Resonators", *IEEE Int. Symp. on Circuit and Systems (ISCAS)*, Bangkok, Thailand, May 2003

- Johnny M. H. Lee, Steve C. L. Yuen, Wen J. Li, and Phillip H. W. Leong, "Micro Energy Converter for AA-Size Batteries", *The 1st Int. Mtg. on Microsensors and Microsystems (2003)*, January 12-14, 2003.

Magazine article (submitted)

- Steve C.L. Yuen, Johnny M.H. Lee, Wen J. Li and Philip H.W. Leong, "An AA-sized Micro Power Generator and its Application to a Wireless Sensor System v0.1", *IEEE pervasive computing magazine.*

Appendix A

Schematics

1. 2D input ring (transmitter section)

2. 2D input ring (receiver section)

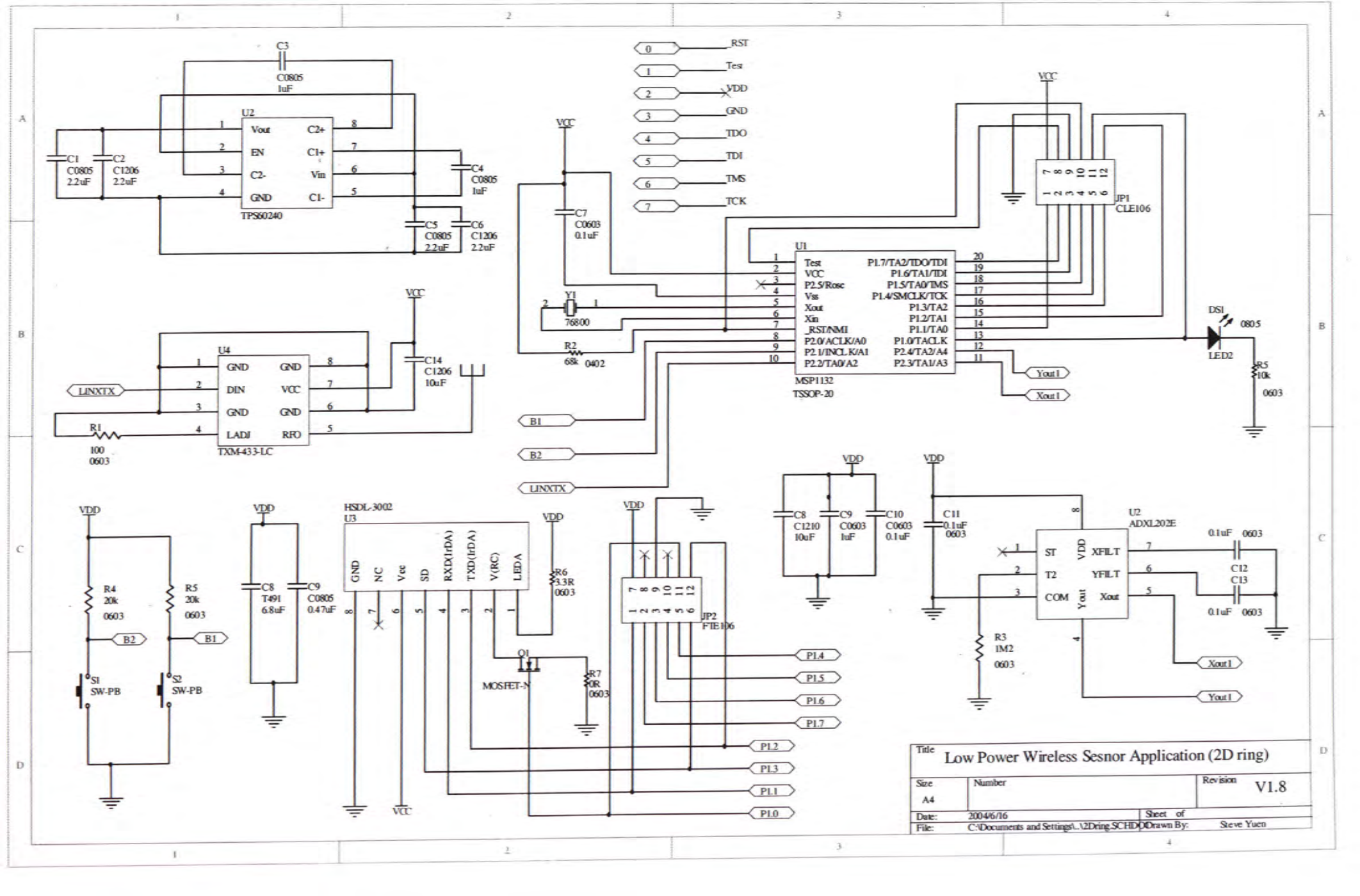
C3
C0805
1uF
U2
Vout
EN
C2-
GND
C2+
C1+
Vin
C1-
TPS60240
C1
C0805
2.2uF
C2
C1206
2.2uF
C4
C0805
1uF
C5
C0805
2.2uF
C6
C1206
2.2uF
RST
Test
VDD
GND
TDO
TDI
TMS
TCK
VCC
C7
C0603
0.1uF
U1
Test
VCC
P2.5/Rosc
Vss
Xout
Xin
_RST/NMI
P2.0/ACLK/A0
P2.1/INCLK/A1
P2.2/TA0/A2
P1.7/TA2/TDO/TDI
P1.6/TA1/TDI
P1.5/TA0/TMS
P1.4/SMCLK/TCK
P1.3/TA2
P1.2/TA1
P1.1/TA0
P1.0/TACLK
P2.4/TA2/A4
P2.3/TA1/A3
MSP1132
TSSOP-20
JP1
CLE106
Y1
76800
R2
68k
0402
Yout1
Xout1
DSI
0805
LED2
R5
10k
0603
U4
GND
DIN
GND
LADJ
GND
VCC
GND
RFO
TXM-433-LC
C14
C1206
10uF
LINXTX
R1
100
0603
B1
B2
LINXTX
C8
C1210
10uF
C9
C0603
1uF
C10
C0603
0.1uF
C11
0.1uF
0603
U2
ADXL202E
ST
T2
COM
VDD
Yout
XFILT
YFILT
Xout
0.1uF
0603
C12
C13
R3
1M2
0603
Xout1
Yout1
R4
20k
0603
R5
20k
0603
S1
SW-PB
S2
SW-PB
C8
T491
6.8uF
C9
C0805
0.47uF
HSDL-3002
U3
GND
NC
Vcc
SD
RXD(rDA)
TXD(rDA)
V(RC)
LEDA
R6
3.3R
0603
Q1
MOSFET-N
R7
0R
0603
JP2
FIE106
P1.4
P1.5
P1.6
P1.7
P1.2
P1.3
P1.1
P1.0
Title
Low Power Wireless Sesnor Application (2D ring)
Size
A4
Number
Revision
V1.8
Date:
2004/6/16
Sheet of
File:
C:\Documents and Settings\...\2Dring.SCHDOC
Drawn By:
Steve Yuen

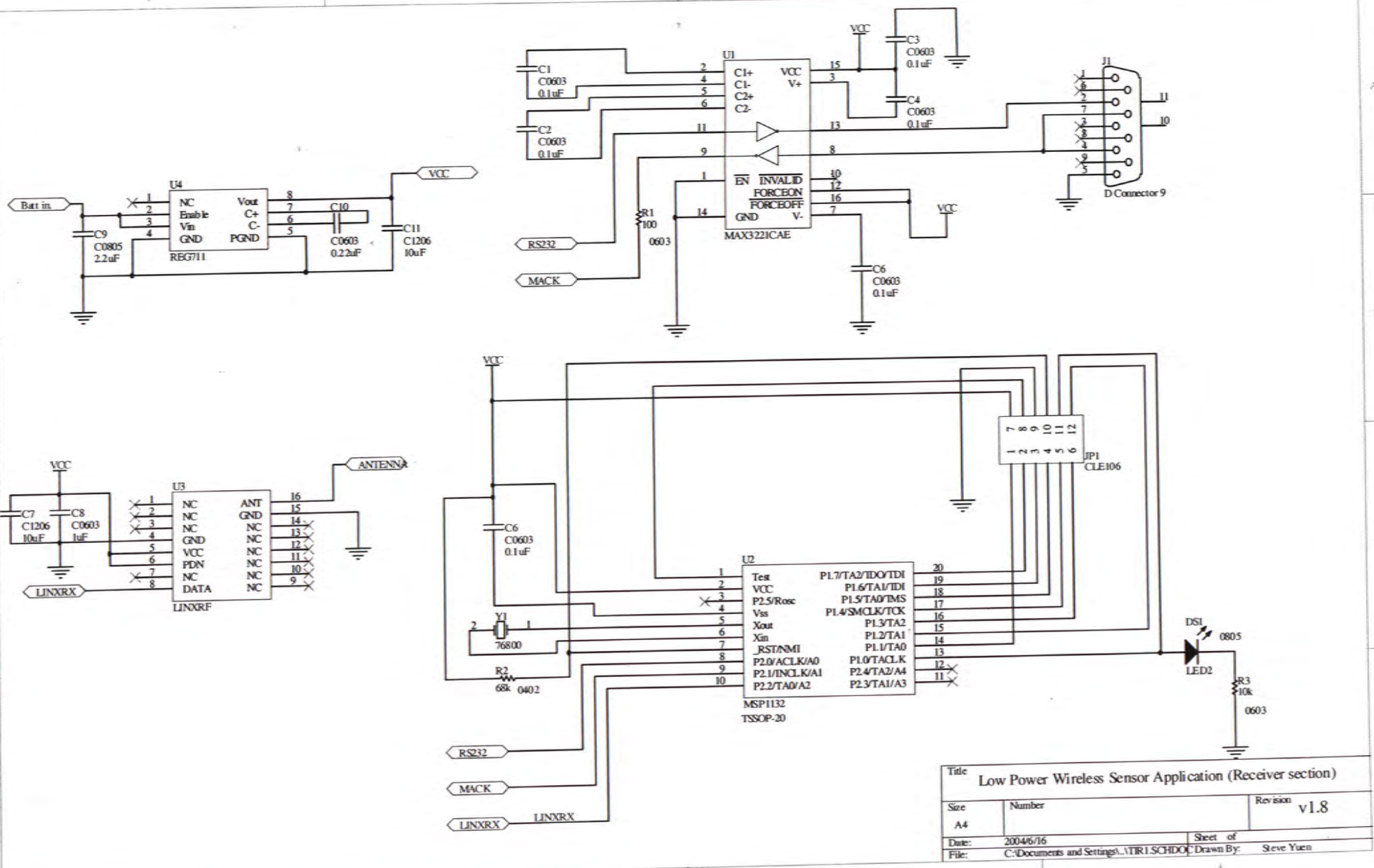
U1
MAX3221CAE
C1+
C1-
C2+
C2-
VCC
V+
EN
INVALID
FORCEON
FORCEOFF
GND
V-
C1 C0603 0.1uF
C2 C0603 0.1uF
C3 C0603 0.1uF
C4 C0603 0.1uF
C6 C0603 0.1uF
R1 100 0603
RS232
MACK
J1
D Connector 9
U4
REG711
NC
Enable
Vin
GND
Vout
C+
C-
PGND
Batt in.
C9 C0805 2.2uF
C10 C0603 0.22uF
C11 C1206 10uF
U3
LINXRF
ANT
GND
DATA
ANTENNA
C7 C1206 10uF
C8 C0603 1uF
LINXRX
U2
MSP1132
TSSOP-20
Test
P2.5/Rosc
Vss
Xout
Xin
_RST/NMI
P2.0/ACLK/A0
P2.1/INCLK/A1
P2.2/TA0/A2
P1.7/TA2/TDO/TDI
P1.6/TA1/TDI
P1.5/TA0/TMS
P1.4/SMCLK/TCK
P1.3/TA2
P1.2/TA1
P1.1/TA0
P1.0/TACLK
P2.4/TA2/A4
P2.3/TA1/A3
Y1 76800
R2 68k 0402
JP1 CLE106
DS1 LED2 0805
R3 10k 0603
Title
Low Power Wireless Sensor Application (Receiver section)
Size A4
Number
Revision v1.8
Date: 2004/6/16
Sheet of
File: C:\Documents and Settings\...\TIR1.SCHDOC
Drawn By: Steve Yuen